85

CRANFIELD INSTITUTE OF TECHNOLOGY

SCHOOL OF AUTOMOTIVE STUDIES

Ph.D THESIS

T. L. RICHARDS

# THE REDUCTION OF STRUCTURAL ACOUSTIC COUPLING IN CAR BODIES

APRIL, 1982

SUMMARY

The nature of sound in cars is discussed in the light of previous experimental and theoretical work, and the major contributions to interior noise are identified. The acoustic field inside a vibrating structure is analysed theoretically in terms of the acoustic cavity modes and the structural modes, and it is shown that reduction of structural-acoustic coupling could reduce the response for a wide variety of force inputs. Finite element analyses of prismatic acoustic cavities and two-dimensinal ring structures are described and these are combined in a simple theoretical model of ring-mode excitation of sound. By stiffening selected structural elements, the structural-acoustic coupling, and hence the acoustic response, are reduced.

ACKNOWLEDGEMENTS

I would like to express my gratitude to the following people:

Sunil Jha and Guy Tidbury, my supervisors, for their advice and encouragement during the project.

Various staff at the School of Automotive Studies and Cranfield Computer Centre for technical help - usually in getting my programs to work.

Angela Busby and Jeanette Reed, for typing the thesis.

I also acknowledge the financial support of the Science Research Council during this work.

# 1. INTRODUCTION

## 1.1 Background

In order to gain some insight into the general problem of noise reduction in cars, we first give consideration to the following relevant topics:-

1) The nature of sound in cars, in particular quantitative measurements of sound pressure levels and spectra.

2) The sources of excitation, their frequency characteristics, and the overall system parameters which influence the sound generation process.

3) The subjective and physiological response of human beings to sound, which in the final analysis is the only basis for any useful quantitative measure of noise.

Having identified the dominant contributions to car noise, the sound generation processes responsible may then be examined and preferably described in explicit mathematical form. In this way the effect of proposed remedial measures may be predicted. As will be shown later, the form of the governing equations and the numerical methods necessary for solution may themselves give clues as to the nature of desirable modifications, eliminating to some extent the need for a 'trial and error' approach.

## 1.2 The Nature of Sound in Cars

A number of experimental studies have been carried out in which interior sound levels have been measured, and the relative importance of the various sources of excitation assessed ((1), (2), (3)).

In general, high overall Sound Pressure Levels (referred to a pressure of $2 \times 10^{-5}$ $Nm^{-2}$ r.m.s.) of about 100 db are found. This overall level is dependent on speed, a doubling of which typically increases the SPL by 5-6 db, although local fluctuations of several db are observed which can be attributed to resonances occurring within the system. Thus, as Raff and Perry (2) point out, maximum levels are rarely encountered for long periods except during sustained high-speed driving on motorways.

A more detailed analysis can be made by examining the spectrum of Sound Pressure Level at a given speed. This is generally complex, consisting of a random background and a number of discrete frequency components. A typical spectrum is given by Jha (3), and this is shown in Figure 1. The measurements were made in a Hillman Imp saloon car, travelling at a constant 73 m.p.h., at which the engine speed was 4500 r.p.m. A number of features are apparent:-

1) An overall trend of decreasing SPL with frequency at a rate of roughly 15 db/decade.

2) Between 2Hz and 10Hz the level decreases from 103 db to 95 db with little local fluctuation. Such a uniform frequency distribution is typical of random noise.

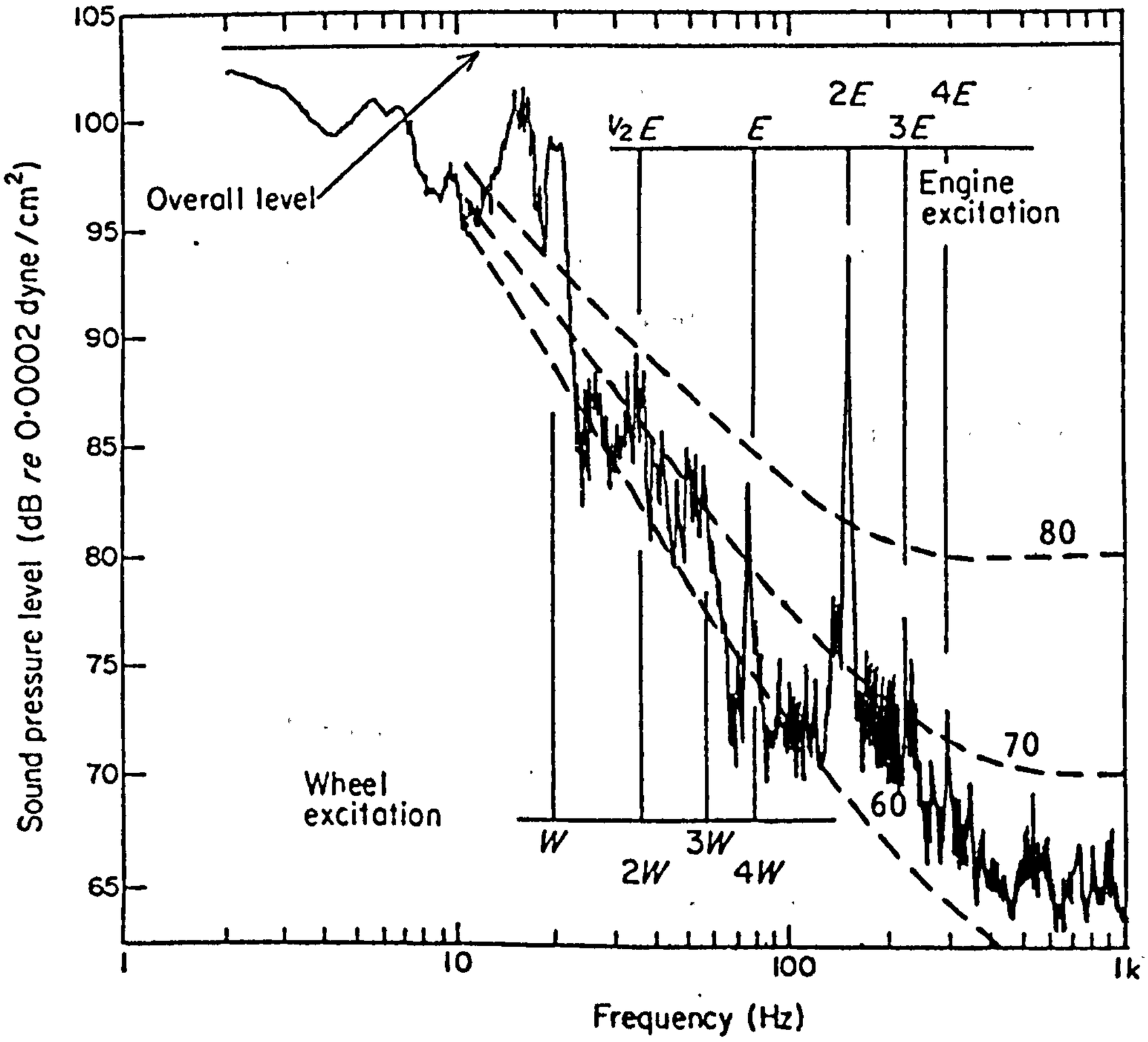


Fig. 1. Jha's Spectrum of Interior Car Noise (3)

— — — — — Equal Loudness Contours

3) At about 20 Hz the SPL has dropped to about 85 db, so it must be concluded that the major contribution to the overall SPL occurs below this frequency.

4) At higher frequencies the spectrum contains many discrete components, and some of the more distinct of these coincide with harmonics of the engine rotational frequency and the wheel rotational frequency. By far the highest of these peaks occurs at twice the engine rotational frequency (about 150Hz), with an increase of SPL from 75 db to 93 db. The effect of higher harmonics is considerably less.

Jha also measured the variation of some of the more important harmonic contributions to the overall SPL as the car accelerated from 20 m.p.h. to 65 m.p.h. The major contribution was at the wheel rotational frequency, and the overall level tended to follow this, but at some speeds either the fundamental or the first harmonic of the engine rotational frequency dominated. The engine harmonics fluctuated considerably with speed, possibly due to structural resonance.

Another class of sound commonly encountered is 'wind-throb' (6). This is caused by driving with one or more windows open, and results in very high overall Sound Pressure Levels of typically 120 db. The dominant components of wind-throb occur at low frequencies (below 20 Hz).

## 1.3 Sources of Excitation

Jha (3) has broadly classified the sources of interior sound excitation as follows:-

1) Excitation by the engine, transmission and accessories.

2) Road surface excitation.

3) Aerodynamic excitation.

The first of these consists of inlet and exhaust noise, forces due to impact during combustion, and forces due to unbalance of reciprocating and rotating components (1). Such excitation is periodic, and can be held responsible for the discrete frequency components in measured SPL spectra.

Road noise is characterised by spectra of a more continuous nature, due to the random irregularities of the road surface which cause vibration of the tyre casing. The levels of sound excited in this manner are dependent on the nature of the road surface, tread pattern and tyre construction (e.g. whether radial or cross-ply).

Aerodynamic noise is believed to be caused by the periodic shedding of vortices in the air-flow around the car (6). This is influenced greatly by small openings and leaks from the passenger compartment to the exterior, and the resulting tones are usually of fairly high frequency (of the order of 1000Hz). Some sound can be excited in a completely sealed car, as vortex shedding induces vibration of the body structure. Jha (3) states "The contribution of aerodynamic noise is not very great at moderate speeds and even at high speeds it seldom becomes a dominant source ...".

Aerodynamically excited wind-throb cannot be included by this statement as the resulting sound levels are so high. In this phenomenon the passenger compartment and open window have a low frequency acoustic resonance which is excited by the air-flow; the effect is akin to that found by blowing across the top of an empty bottle.

For all sources the path of the excitation is either through the structure (by vibration) or airborne (by excitation of sound) or a combination of both. Airborne transmission is influenced strongly by the degree of sealing of the passenger compartment from the engine compartment (affecting engine, fan and inlet noise) and the exterior (affecting aerodynamic and exhaust noise). Structure-borne transmission depends on response of the body to the exciting forces, while the interior sound levels resulting from any form of excitation depends on the acoustic properties of the passenger compartment.

At any point within the system the response is strongly dependent on resonances (either structural or acoustic) which amplify both sound and vibration levels. Jha (3) classifies the more important system resonances as:-

1) Rigid body vibration on suspension systems and wheels (0.5 - 10Hz).

2) Engine shake (11 - 17Hz).

3) Bending and torsional vibration of the car body as a whole (25 - 40Hz).

4) a) Ring mode vibration of the passenger compartment (following the vibration pattern of the side frames).

b) Bending vibration of the driveline (50 - 150Hz).

5) Acoustic resonances of the passenger compartment. The first of these occurs at about 90Hz, and there is usually a cluster of resonances around 150Hz. An open window completely alters these and the lowest resonance will now be in the wind-throb range (i.e. below 20Hz).

## 1.4 The Response of Humans to Sound

To relate noise to sound levels it is necessary to consider human response. Since noise is defined as unwanted sound then the only way of doing this is by asking subjects about it or by studying their behaviour and physiology during exposure. Although many such studies have been carried out, the data collected usually apply for either very simple or very specific types of sound, and their use in more general circumstances may not be justified.

The use of overall Sound Pressure Level can be of little use when attempting to assess subjective loudness; the sensitivity of the human ear is very much frequency dependent so subjective evaluation will be influenced by the nature of the SPL spectrum. Even having defined some measure of loudness, it cannot be assumed to have any bearing on other detrimental responses such as fatigue, annoyance, impaired performance, or possibly loss of hearing at high sound levels.

Beranek (4) gives an account of human hearing and the definitions of a number of measures of subjective loudness. One of these is Loudness Level, whose unit is the phon, and is defined as "the Sound Pressure Level of a 1000Hz tone that

sounds as loud as the sound under consideration". Loudness Level is measured using a 'jury' or people known not to have any obvious hearing defects, and it has been found that about ten subjects are usually sufficient to provide an accuracy of within 1 phon. (It is worth mentioning in this context that Apps (1) found that subjects were able to distinguish differences of 1db in overall SPL when asked to assess interior noise 'quality' of cars). Clearly it would be an impossible task to tabulate Loudness Levels for every conceivable kind of sound, and the most commonly used data (rightly or wrongly) are the Loudness Levels for single frequency tones (Fig. 2). By definition Loudness Level is equal to SPL at 1000Hz, while greatest sensitivity occurs at about 3000Hz. At lower frequencies Loudness Level is much less than SPL, although this effect is less marked at high levels (SPL = 80-100 db). This could be of considerable importance in car noise, because it means that changes of SPL at low frequencies will cause a greater increase in Loudness Level than at high frequencies. For example a change of SPL from 80 db to 90 db at 1000Hz causes a change in Loudness Level of 10 phon, while at 20Hz the corresponding change is 20 phon.

In an attempt to relate some measure of SPL to subjective loudness, the db (A), db (B) and db (C) weighting networks have been devised (7). The sound pressure amplitude is weighted with a frequency dependent function derived from the relation between SPL and Loudness Level for pure tones, and these in practice are found to be far more useful measures. The db(A) scale is based on the 40 phon contour (see Figure 2) and provides considerable attenuation at low frequencies; the db (B) scale is based on the 70 phon contour and there is less low-frequency attenuation; the db (C) scale is flat, reflecting the levelling out of contours above 100 db SPL.

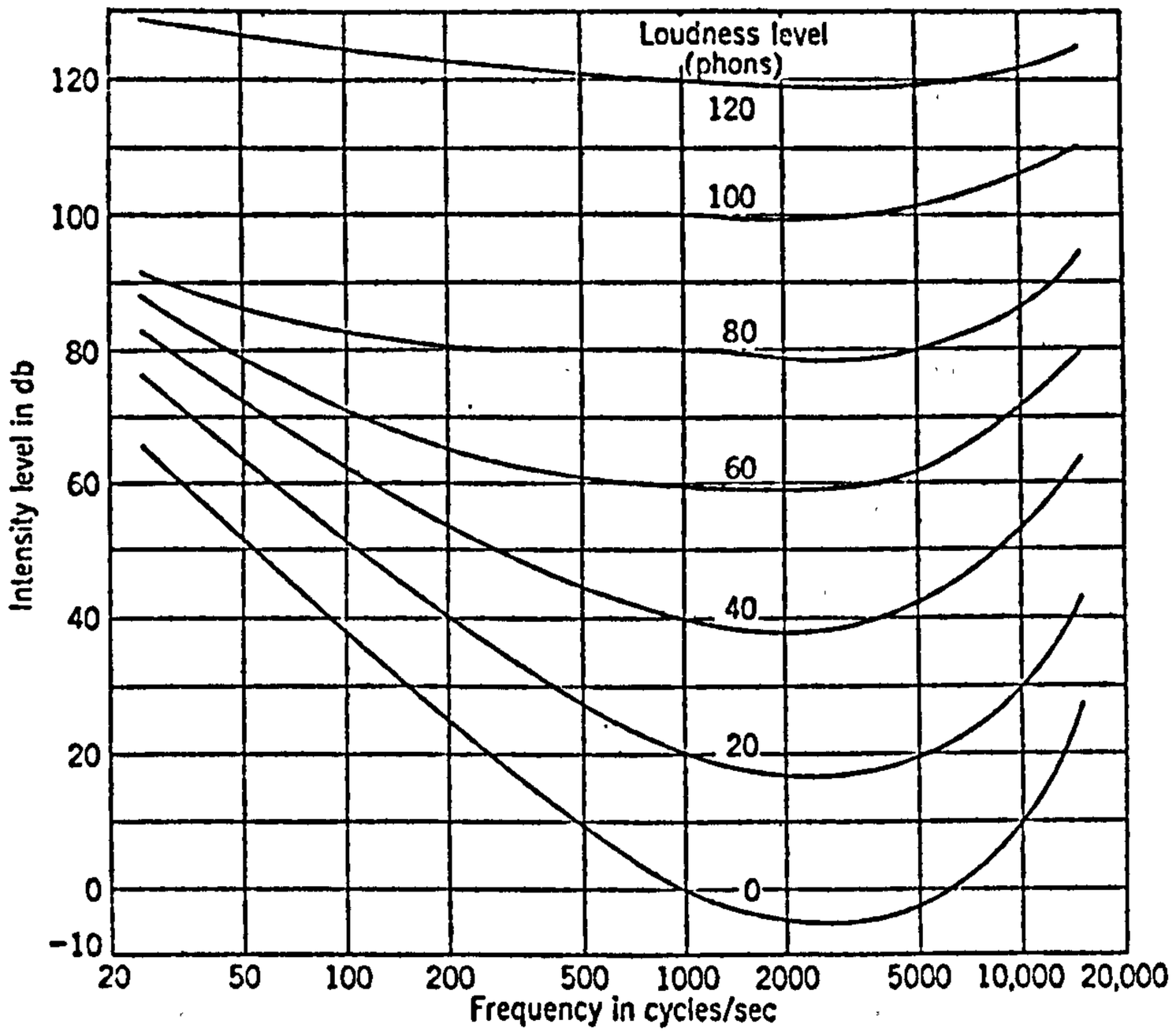


Fig. 2. Equal Loudness Contours for Pure Tones

The correct choice of weighting network depends on the overall SPL, and the recommended ranges are:-

| | |
|---|---|
| less than 55 db | db (A) network |
| 55-85 db | db (B) network |
| greater than 85 db | db (C) network |

The db (A) scale is by far the most commonly used, typically for external noise measurements in the vicinity of airports, motorways, industrial areas etc., and this popularity has probably led to its use at inappropriately high pressure levels. Certainly db (B) and db (C) measurements are comparatively rarely quoted.

The db (A) scale has been widely used for automotive applications, and Bryan (5) has suggested its use as an "interim" measure of car interior noise. Jha (3) found that the A-weighted overall level inside a car is considerably less than the overall SPL - typical values are in the region of 70 - 80 db (A). This is to be expected in view of the predominance of low frequency sound energy which is considerably attenuated. The use of the db (A) scale however must be treated with suspicion for the following reasons:-

1) The overall SPL inside a car is considerably higher than the limit of 55 db recommended for the db (A) scale.

2) It is insensitive to changes of level at low frequencies (in contrast to the human ear).

It is possible that the less commonly used B and C networks may be more suitable for car interior noise measurements because of their reduced attenuation at low frequencies.

As a result of these considerations an exercise was carried out in which contours of equal Loudness Level from Figure 2 were superimposed on Jha's SPL spectrum in Figure 1 in attempt to assess the importance of the various frequency regions. Since the value of the SPL spectrum at any particular frequency is not related to the overall level, this approach cannot be expected to provide any absolute measurement of subjective loudness, especially since the contours are only accurate for pure tones and not continuous spectra. However, it may allow some tentative judgement as to the more important frequency regions. In this case the 80 phon contour is exceeded by a band of noise at about 20Hz, and by the second harmonic of the engine rotational frequency at 150Hz. The 70 phon contour is exceeded in several places, although not at frequencies greater than 300Hz. As the engine speed for this example is fairly high (4500 r.p.m.), it seems unlikely that significant engine harmonics will occur at above 300Hz.

It is concluded, therefore, that although the major contribution to measured SPL lies in the frequency range below 20Hz, significant contributions (due mainly to harmonics of the engine speed) to the subjective assessment of noise are likely to exist at higher frequencies. There is some justification however for confining attention to frequencies below 300Hz. Further noise contributions may result from the high levels of low-frequency sound around 20Hz.

There is some evidence to suggest that high levels of low-frequency sound may have harmful effects in addition to their contribution to subjective loudness. While it is not intended to treat this topic in detail, it would appear that

levels in cars are sufficiently high to be of some concern. For example, the Department of Employment and Productivity in 1968 recommended that ear protection should be introduced if sound in the range 37.5 - 150Hz exceeds an overall SPL of 100 db, and at 90 db for sound between 150Hz and 300Hz (8). Evans and Tempest (9), in dealing specifically with vehicle interior noise, found that:

> "No level or frequency of infrasound in the 1-20Hz region caused any visual disturbance, but relatively low levels (115-120 db) cause a 30-40% increase on reaction time.
>
> Subjects commonly reported difficulty in performing these tasks due to feelings of lethargy and euphoria, described by some as being similar to slight intoxication".

## 1.5 Calculation of Sound Levels

Calculation of sound levels in a cavity due to the vibration of a surrounding structure requires knowledge of the acoustic characteristics of the cavity and the approach taken depends on the size of the cavity, as explained by Morse and Ingard (10). If the wavelength of the sound is considerably less than the cavity dimensions, then the problem can be approached statistically using 'geometrical acoustics'.

The basic assumption of geometrical acoustics is that the acoustic energy density is distributed uniformly throughout the room, and for this to be true there must be many acoustic resonances in the frequency range of interest to justify a statistical approach. The actual shape of the room is of no interest, the density of modes depending only on the volume. The geometrical approach is used widely in the design of large rooms whose acoustic characteristics are of importance, for example theatres, concert halls and lecture rooms.

If the wavelength of sound is greater than about one third of the shortest dimension of the room, then the assumptions of geometrical acoustics are no longer valid. This is because the number of acoustic resonances is small enough for each to have a significant effect on the sound level, so that the sound energy density is no longer uniformly distributed. The sound pressure is expressed as a summation over the normal modes of the cavity, and in practice only a few terms are necessary as the contribution of high frequency modes is small enough to be neglected. Since car passenger compartments usually have no more than about 15-20 modes below 300Hz, the normal mode approach is particularly applicable.

The normal modes and resonant frequencies for cavities of simple shape (for example, cylinders and perfect parallelepipeds) can usually be expressed explicitly, thus greatly simplifying the analysis. However if the cavity is of a complex shape (as car passenger compartments usually are) the resonances can only be found using numerical methods to solve the acoustic Helmholtz equation.

Jennequin (11) used a finite-difference method to obtain the two-dimensional modes of a car passenger compartment, and was able to calculate the sound field reasonably accurately using measured structural vibration data.

The use of finite differences, in this and other applications, has become less widespread in favour of finite element methods, probably because the conditions on irregular boundaries are more easily applied. Craggs (12), Shuku and Ishihara (13), Petyt et al (14) have all calculated the acoustic modes of vehicle passenger compartments using finite elements.

Wolf et al (15) considered the effect of finite wall rigidity by introducing an elastically mounted tailgate, and calculated modes for cavities with and without seats, and for a cavity with an open window. In (16) they introduced the concept of acoustic influence coefficients (in a manner similar to Jennequin's finite-difference approach (11)) on the surface of the cavity, which allowed portions of the boundary particularly sensitive to structural vibration to be pinpointed. By reducing vibration in one such region a 5 db reduction in SPL was achieved. Although this work used only two-dimensional solutions, this was probably justified because frequencies considered were less than 100Hz (the first three dimensional resonance being at about 150Hz in most cars).

In (17) full three-dimensional solutions were found using two-dimensional acoustic finite elements by taking advantage of the approximately prismatic shape of most car passenger compartments. The results compared well with those found experimentally in a model cavity. This work is described in detail in Chapter 3.

Nefske et al (37) give a comprehensive review of ways in which the finite element method has been applied to the structural-acoustic analysis of car bodies.

Jha and Cheilas (18) present a more experimental approach in which the acoustic response to boundary vibration is measured in a perspex model cavity. The response to any form of vibration was then found by summing contributions from each surface region.

## 1.6 Reduction of Noise

Broadly speaking, the reduction of interior car noise can be achieved either by control of the various excitation forces, or by control of the response of the system to these forces.

The excitation forces due to the engine depend on its own response to the forces generated by combustion and imbalance. Increasing the stiffness of the engine structure will tend to reduce this response, as this decreases the density of resonant frequencies (for example the use of five main bearings in a four-cylinder engine as opposed to three). The positioning of engine mounts affects the transmission of vibration to the body structure, and great improvements can be made by placing these at the nodes of any troublesome resonant modes. Generally, imbalance forces and impact forces can be reduced simply by demanding tighter tolerance during manufacture, but this in turn is limited by the requirements of mass-production.

Road noise can be reduced by improving the isolation between the suspension system and the body structure, but this invariably compromises the handling qualities of the vehicle. However, more sophisticated design methods have in recent years allowed the use of increasingly compliant suspension systems.

The noise response of the body structure can be improved in the following ways:

1) The use of structural damping.
2) Sound absorption within the passenger compartment.
3) Structural modification based on a knowledge of structural and acoustic resonant modes.

A bare car body shell is very poorly damped simply because steel itself has very little internal damping. Any dissipation that does occur is primarily due to friction between surfaces where the construction allows relative movement. Apps (1) reports that bolted construction results in greater damping than spot-welds while continuous welds provide the least damping, and cites the case of a manufacturer who encountered a significant increase in internal noise as a result of changing from bolted fabrication to welding. Because the structural damping is inherently so small, the addition of the usual trim has a considerable effect, but it is often necessary to employ materials in addition which specifically increase the damping. To be effective these have to be applied to fairly large areas, so their use is confined to panels rather than frame sections. The actual damping mechanism depends on the type of material used, and those in common use are:-

1) Mastic deadeners with an asphalt base, which are applied by brush or spray gun. Damping relies on flexure rather than overall movement of the panel.

2) Felt which is not continuously attached to the panel. Flexure causes friction at the interface, which can be increased by a loading septum on horizontal surfaces.

3) Loaded blankets. Relative motion due to inertia of the loading septum causes crushing of the damping material, so this mechanism relies on displacement rather than flexure of the panel.

The effectiveness of the various damping treatments can be measured in the laboratory by applying them to a standard steel plate (typically 50 cm square and 0.5 cm thick) which is excited electromagnetically at resonance. The excitation is abruptly removed, and the decay of the panel vibration is measured and expressed in units of db $sec^{-1}$. For a bare plate the decay rate is less than 1 db $sec^{-1}$, while loaded blankets can achieve rates in excess of 200 db $sec^{-1}$. The rate for mastic deadeners is more or less proportional to the amount applied, and a typical rate is about 25 db $sec^{-1}$ for a density of 0.8 $lb/ft^2$. These rates, while useful when assessing the relative performance of different damping materials, only apply in any absolute sense at the frequency at which the test was carried out, which is typically in the region of 150Hz. If we assume that a constant proportion of the vibration energy of a given mode is dissipated per cycle, then it is clear that the decay rate will be less at lower frequencies. Since car body vibration at low frequencies (below 100Hz) is influenced by the beams forming the frame of the structure, which have a small surface area compared with the panels, it seems that application of the damping treatments mentioned above will not provide any dramatic reduction of low frequency noise.

The mechanisms of sound absorption in commonly used materials has been described by Beranek (17) and Kosten (19). It has already been described how car passenger compartments are too small for the assumpions of geometrical acoustics to hold, and Beranek discusses these assumptions in relation to

different absorbing mechanisms, reporting that measured absorption coefficients for a given material are often strongly dependent on their environment even for rooms which would normally be considered acoustically 'large'.

In the next chapter the effect of absorbing boundaries will be considered in the context of modal analysis of acoustic cavities, and it will be shown that the damping of acoustic modes depends to a great extent on the positioning of the material in addition to its total area. The statistically derived coefficient of absorption will be thus of little use when considering specific applications, but is used in the following discussion which is concerned with the relative absorption of different types of construction, and its dependence on frequency. Kosten lists five fundamental absorption mechanisms:-

1) Rigid Porous material. This is uncovered so that the pores are totally accessible to the sound waves. High velocity gradients are set up in the air within the pores, and this results in viscous energy dissipation. The absorption coefficient for a typical material is high (about 75%) at frequencies above 1000Hz, but drops rapidly to less than 20% at frequencies lower than 100Hz.

2) Flexible with a non-porous surface. There is a certain amount of viscous absorption in the porous interior of the material, as well as structural damping. The mass of the surface layer should be kept as low as possible to prevent a fall in absorption at high frequencies. Absorption is typically good (greater than 50%) down to 200Hz, but below this performance is no better than 1).

3) Panels backed by an air layer. The combined system of the panel (mass) and the air layer (spring) has a resonance at which absorption will be greatest due to structural damping. Close to the resonant frequency (which may be in the range 50-700 Hz) absorption can be as high as 50%, but is poor elsewhere.

4) Perforated Panel. The panel itself is sufficiently heavy to remain effectively motionless, but the perforations in combination with the backing air layer act as a series of Helmholtz resonators, and the porous material within the air layer provides the absorption. The absorption coefficient can be greater than 50% at 100Hz, but falls at lower frequencies.

5) Single Helmholtz Resonator. This is included as a simplification of 4). The absence of absorbing material results in a sharper resonance, so absorption is confined to a narrow frequency band.

A common feature of all constructions is the fall in absorption at low frequencies, and it is unlikely that any such mechanism will greatly reduce the high levels of interior car noise below 50Hz. Improved performance at high frequencies may however affect subjective judgements, and Apps (1) reports how various damping and absorption treatments affect considerably people's impression of car quality, but make very little difference to measured sound levels. Further accounts of acoustic absorbing materials and related measurements are given in references (20), (21), (22), (23), and (24).

Particularly troublesome noise and vibration problems may be so severe that no reasonable amount of structural damping or acoustic absorption results in an acceptable reduction. When high vibration levels are confined to a narrow frequency range, they can usually be attributed to one or more structural resonances which are fortuitously subject to abnormally high levels of excitation. In such cases it is sometimes possible to effect drastic reductions by modifying the structure so that the offending resonances are shifted outside the frequency range of the excitation, or by moving the point of excitation to a node. If this approach is taken it is necessary to obtain quantitative knowledge of the mode or modes involved by experiment or theoretical analysis. It is quite possible that the modifications which eliminate one problem may result in another elsewhere, and an alternative remedy will be necessary.

Engine-shake and drive-line vibration are typical of problems which can be cured given a knowledge of the dominant resonances involved.

Control of acoustic resonances by means other than absorption has received very little attention, although the advent of the finite element analyses mentioned earlier will almost certainly stimulate interest in the subject, perhaps along the lines of the work of Wolf et al (16).

## 1.7 Conclusions

1) Interior Sound Pressure Levels in cars are typically 100 db. Most of the sound energy is confined to low frequencies (below 30Hz), but pronounced discrete frequency components, related to the engine speed, are found at higher frequencies around 100Hz.

2) Perceived loudness levels are dependent on the response of the human ear to sound, and the db (A) weighting scale has often been used to take this into account. However it has been argued that the use of the db (A) scale is perhaps inappropriate for measurements of interior car noise because of its excessive attenuation of low-frequency sound.

A simple comparison of equal loudness SPL contours with a measured spectrum suggests that the major contributions to noise are broad-band sound at about 20Hz and discrete engine harmonics above 50Hz. Sound above 300Hz has little or no effect.

3) The system resonances at the frequencies of maximum noise consist of bending and torsional vibration of the body as a whole (25 - 40Hz), ring mode vibration of the passenger compartment (50 - 150Hz) and acoustic cavity modes (90 and 150Hz). These will thus play a dominant role in the sound generation process.

4) In the absence of specific treatments, the structural damping and acoustic absorption inherent in the usual methods of car body construction will limit the amplitudes of the various resonances. Additional materials are commonly used to damp panel resonance and to provide some measure of sound absorption, but the efficacy of these is strongly dependent on frequency. While significant benefits can be obtained at higher frequencies (which perhaps owe more to the sensitivity of the human ear to small changes than to any great reduction in the absolute sound pressure level), the effects at frequencies below 100Hz will be slight if reasonable material quantities are to be used.

Consideration of these points has in part led to the approach adopted in this work. Attention is confined only to the vibrational and acoustical characteristics of the car body and passenger compartment, independently of any changes in the excitations due to engine, driveline or suspension. The effects of structural damping and acoustic absorption are considered, but will generally be assumed to be of comparable magnitude for different cases.

The essence of the problem may be expressed in the following way:-

> Given different car body designs which are quantitatively identical in terms of the excitation forces acting on them, structural damping and acoustic absorption characteristics, and total mass, while having at least a superficial qualitative resemblance in all other respects (for example, shape, strength, materials, construction),
>
> a) Is it likely that there will be significant differences in the nature of the sound generated in the passenger compartment?
>
> b) Can such differences be quantified in terms of easily identifiable parameters?
>
> c) Can design modification procedures be established which result in useful noise reductions?

The introduction of the finite element method means that dynamic analyses of complex structures and irregular acoustic cavities are now possible. In the early days the size of the problems that could be considered was limited by the computer time and storage required to obtain solutions to the matrix eigenvalue problem, which gives the resonant frequencies and modes of the system. Owing to this limitation, the task of input data preparation was relatively insignificant, and the resulting output data presented no difficulty in their interpretation or use, at least not because of their great volume.

The emphasis has now shifted. The speed and storage capacity of computing machinery have increased to such an extent that they no longer present any restriction for most practical applications. The real difficulties now lie firstly with the immense volume and detail of the input data now required. As a result considerable efforts have been made to automate the preparation process as far as possible by the use of mesh generation programs and other computer aided design techniques.

Even more of a problem is the interpretation of the vast quantities of output data. In the case of a car body, a complete structural-acoustic eigenvalue analysis up to, say, 300 Hz will (when achieved) result in several acoustic resonances and scores of structural resonances. Associated with each of these will be modes described in terms of thousands of degrees of freedom. In their own right, these results have a disproportionately small value, and serve only to identify essentially vague features of the system such as abnormally high modal densities.

An obvious next step would be to calculate the acoustic response to a set of structural force inputs closely approximating those that would be encountered in reality. However, quantifying these forces is likely to be a task of considerable magnitude, because both their amplitudes and frequency dependence have to be considered. This may be a feasible proposition for systems that operate under substantially steady-state conditions, for example stationary machinery and perhaps some aircraft, because the calculation could be carried out for a single forcing case. Road vehicles, on the other hand, encounter a wide variety of operating conditions encompassing variations in speed, road surfaces, engine loading and, to a lesser extent, alterations in specifications such as engine size, and tyre and suspension characteristics. Among this multiplicity of cases, the decision as to which have the most significance will necessary be somewhat arbitrary. Even if accurate predictions, as verified by experiment, are eventually made and regarded as successful for their own sake, no direct progress has been made towards the ultimate goal of noise reduction, except perhaps in the ability to compare the relative merits of differing designs.

Some progress, as mentioned earlier, has been made by adopting a semi-experimental approach in which measured vibration data are used to calculate the acoustic response in the passenger compartment. Such calculations give an indication of the relative importance of different portions of the vibrating surfaces, and thus any improvements that might result from structural modifications. While this approach stresses the important fact that the acoustic response depends on the pattern of vibration as well as its magnitude, its use as a design tool is severely limited by the need for laboratory experiments on an actual car body.

In Chapter 2 the acoustic response of a cavity due to the forced vibration of a surrounding structure is obtained in terms of the natural modes of the cavity and the structure. The resulting expression contains terms which represent the coupling between each acoustic mode and each structural mode. These terms have the following properties:-

a) They are readily computed using standard boundary integral methods from the acoustic and structural modal data.

b) They are intrinsic to the structural-acoustic system in that they do not depend on the distribution of external exciting forces nor on the position within the cavity at which the response is to be calculated.

c) Their magnitude depends on a surface integral over the interior of the structure, and the proximity of the acoustic and structural resonant frequencies. The surface integral may be small purely fortuitously, or may be zero because of symmetry of the structure. Terms for which the acoustic and structural resonant frequencies are well separated will also be comparatively small.

The smallest of these coupling terms will have a negligible effect on the acoustic response. In the case of a car body with symmetry about the centre-line roughly half of the coupling terms will be excluded because their surface integrals are identically zero. Because the structural resonances are considerably more numerous than acoustic resonances, many, and probably the vast majority, of the remaining terms will have a negligible effect in comparison with those having closely spaced structural and acoustic resonant frequencies. Thus we expect the acoustic response to be dependent chiefly on a few of the largest coupling terms, regardless of the forces acting on the structure.

The main value of this procedure is the considerable simplification it brings to the analysis of a large, complex structural problem.

The task of reduction of the acoustic response may now be attacked in two ways. Firstly structural modifications may be sought which reduce the largest coupling terms in the knowledge that this will almost invariably have a beneficial effect. In addition more conventional approaches are aided considerably because we now know precisely which structural modes have the most effect on the acoustic response. Thus additional damping treatment or the repositioning of the exciting forces can now be carried out with the aim of reducing the contribution of these particular modes. Conversely, no effort is wasted on the elimination of those modes which provide little or no acoustic excitation.

In Chapter 3 the finite element analysis of a simple car-shaped acoustic cavity is described, and the prismatic shape of the cavity is used to obtain full three-dimensional solutions from a single two-dimensional solution.

In Chapter 4 the resonances of a steel ring structure are determined experimentally and theoretically using the finite element method. It is found that the resonant frequencies of such structures occur naturally in pairs, and in the special case of a circular ring they are degenerate.

Finite element analyses of structural ring vibration and an acoustic cavity are combined in Chapter 5 to give a simple two-dimensional model of ring-mode excitation of sound. The coupling terms described in Chapter 2 were calculated for this case, and the acoustic response to a

harmonic exciting force was obtained. The effect of structural changes were treated as a linear perturbation of the element stiffness matrices, and by this means their effect on the structural-acoustic coupling could be assessed. The largest coupling terms were reduced by stiffening selected elements, and the modified acoustic response was significantly reduced at the most pronounced resonant peaks. The perturbation approach could be extended to give higher order approximations to the modified structural resonances, but the linear approximation gives particularly simple results because the combined effect of several changes is additive.

The choice of stiffened elements was arrived at somewhat crudely in Chapter 5 simply by visual inspection of the approximate changes. In the discussion in Chapter 6 the possibility of incorporating these techniques in a constrained optimisation scheme is considered. By this means it would appear that the complete process could be fully automated, which would be a significant achievement in the complex case of a real car-body structure.

# 2 THEORETICAL CONSIDERATIONS

## 2.1 Standing Waves in Cavities

Morse and Ingard (10) give a comprehensive analysis of sound in enclosed regions, and the results given in this chapter use their notation. The decision whether to adopt an analysis in terms of the normal modes of the enclosure, or to use geometric acoustics depends on the size of the cavity in relation to the wavelength of the sound. If the ratio of wavelength to cavity dimension is greater than about 1/3, normal mode analysis is to be preferred because the statistical assumptions of geometrical acoustics are not valid. In the case of sound in cars, it has been established in the previous chapter that the only significant contributions are at frequencies below 300Hz, that is, at wavelengths greater than about 1 metre. Since the largest dimension of a car passenger compartment is unlikely to exceed 3m, normal mode analysis must be used.

## 2.2 The Helmholtz Equation

The acoustic pressure field, p, in a homogeneous medium is governed by the wave equation:-

$$\frac{\partial^2 p}{\partial x^2} + \frac{\partial^2 p}{\partial y^2} + \frac{\partial^2 p}{\partial z^2} = \frac{1}{c^2}\frac{\partial^2 p}{\partial t^2} \qquad (2.1)$$

where c is the velocity of sound in the medium.

If the pressure is assumed to vary harmonically with time, such that $p = P \exp i\omega t$, substitution into equation 2.1 gives the Helmholtz equation:-

$$\frac{\partial^2 P}{\partial x^2} + \frac{\partial^2 P}{\partial y^2} + \frac{\partial^2 P}{\partial z^2} = -\frac{\omega^2}{c^2} P$$

or
$$\nabla^2 P = -\frac{\omega^2}{c^2} P. \qquad (2.2)$$

While such a harmonic variation of p with time will be assumed in all subsequent derivations, it should be noted that complete generality can be achieved by regarding $P(x,y,z,\omega)$ as the Fourier transform of $p(x,y,z,t)$. In this way arbitrary time variations may be considered.

In order to obtain solutions to equation 2.2 for an enclosed region, it is necessary to impose boundary conditions. These can be of two types:-

1. Specification of $\partial P/\partial n$, the component of grad P in (conventionally) the outward normal direction at the surface of the cavity.

2. Specification of P at the surface of the cavity.

For a given problem the boundary conditions may be of either type, or a combination of the two; the correct choice depends on the physical nature of the surface of the cavity.

## 2.3 Normal Modes of Rigid-Walled Cavities

If u is the vector of fluid velocity in an acoustic pressure field p, then

$$\rho \frac{\partial \underline{u}}{\partial t} = - \text{grad } p \qquad (2.3)$$

where $\rho$ is the density of the medium (10). If $p = P\exp i\omega t$ and $\underline{u} = \underline{U} \exp i\omega t$,

$$i\omega\rho \, \underline{U} = - \text{grad } P \; . \qquad (2.4)$$

$\underline{U}$ is the vector of fluid velocity amplitude, the normal component of which must be zero at a rigid wall. This implies that the normal component of grad P is also zero, that is:

$$\frac{\partial P}{\partial n} = 0 \; . \qquad (2.5)$$

For a region R completely enclosed by a rigid wall, equation 2.5 must hold everywhere on the surface S, and thus forms a suitable boundary condition for solution of equation 2.2, which results in a series of eigenfunctions $\phi_n$ and eigenvalues $\eta_n$, each of which obey the equations:

$$\nabla^2\phi_n + \eta_n^2 \phi_n = 0 \quad \text{in R} \qquad (2.6)$$

and $$\frac{\partial \phi_n}{\partial n} = 0 \quad \text{on S} \; . \qquad (2.7)$$

Physically, $\phi_n$ are the modes of the acoustic cavity resonances, with angular frequencies:

$$\omega_n = c\eta_n \quad . \tag{2.8}$$

Applying Green's second theorem (25) to two different eigenfunctions $\phi_i$ and $\phi_j$ gives:

$$\int_R (\phi_i \nabla^2 \phi_j - \phi_j \nabla^2 \phi_i)\, dV$$

$$= \int_S (\phi_i \frac{\partial \phi_j}{\partial n} - \phi_j \frac{\partial \phi_i}{\partial n})\, dS \quad . \tag{2.9}$$

Substituting equations 2.6 and 2.7 into equation 2.9 results in:

$$(\eta_i^2 - \eta_j^2) \int_R \phi_i \phi_j \, dV = 0 \quad .$$

Therefore if $\eta_i \neq \eta_j$ the modes are orthogonal, that is:

$$\int_R \phi_i \phi_j \, dV = 0 \quad . \tag{2.10}$$

Since any multiple of $\phi_i$ is itself a perfectly satisfactory solution to the Helmholtz equation, it is convenient to

normalise the eigenfunctions in the following way:

$$\int_R \phi_i^2 \, dV = 1 \, . \qquad (2.11)$$

Equations 2.10 and 2.11 allow considerable simplifications in subsequent derivations.

A problem that may arise is degeneracy, that is when two or more eigenfunctions have equal eigenvalues, which invalidates equation 2.10. In the simplest case of two-fold degeneracy, suppose there are two eigenfunctions $\phi_i$, $\phi_j$ for which:

$$\int_R \phi_i^2 \, dV = \int_R \phi_j^2 \, dV = 1,$$

$$\eta_i = \eta_j,$$

and $$\int_R \phi_i \phi_j \, dV \neq 0 \, .$$

Since $\eta_i = \eta_j$ any linear combination of $\phi_i$ and $\phi_j$ is itself a satisfactory eigenfunction provided it satisfies equation 2.11. If we define two new eigenfunctions $\phi_i'$ and $\phi_j'$ as substitutes for $\phi_i$ and $\phi_j$ such that:

$$\phi_i' = a_i\phi_i + a_j\phi_j$$

and $$\phi_j' = b_i\phi_i + b_j\phi_j$$

$a_i$, $a_j$, $b_i$, $b_j$ can be chosen to satisfy the three equations:

$$\int_R \phi_i'^2 \, dV = \int_R \phi_j'^2 \, dV = 1$$

and $$\int_R \phi_i' \phi_j' \, dV = 0 \, .$$

As the four coefficients have to satisfy only three equations, it is sufficient to change only one of the eigenfunctions. For example, $a_i = 1$ and $a_j = 0$ means $\phi_i' = \phi_i$, and because there are just two equations left to satisfy, $b_i$ and $b_j$ are uniquely determined.

Similar resoning can be applied to the general case of n-fold degeneracy which means, from a theoretical viewpoint, that the difficulty has been overcome. In practice, however, degeneracy or near-degeneracy will cause complications in, for example the experimental determination of mode shapes.

While it is often possible to obtain exact eigensolutions for cavities of simple shape, in most practical cases it will be necessary to resort to numerical methods. The use of finite elements for this purpose is described in detail in the next chapter.

## 2.4 The Green's Function

A more general problem is the solution of the Helmholtz equation for a given frequency $\omega$, and with arbitrary boundary conditions, that is:

$$\nabla^2 P(r) + k^2 P(r) = 0, \qquad (2.12)$$

where $k = \omega / c$ and r represents the position (x,y,z).

The Green's function satisfies the equation:

$$\nabla^2 G(r,r_o) + k^2 G(r,r_o) = -\delta(r-r_o) \qquad (2.13)$$

where $\delta(r-r_o)$ is defined by:

$$\delta(r-r_o) = 0, \quad r \neq r_o$$

$$= \infty, \quad r = r_o$$

$$\int_R \delta(r-r_o)\, dV = 1 \ . \qquad (2.14)$$

$G(r,r_o)$ is essentially the acoustic response to a unit source at $r_o$, although at this stage it is indeterminate because no boundary conditions have been specified.

Multiplying equation 2.13 by $P(r_o)$ and substituting 2.12 gives:

$$P(r_o)\, \nabla^2 G(r,r_o) - G(r,r_o)\, \nabla^2 P(r_o) = - P(r_o)\, \delta(r-r_o) \ .$$

Integrating with respect to $r_o$ over the region R, and then making use of equation 2.14 and Green's second theorem gives:

$$P(r) = \int_S \left(G(r,r_o) \frac{\partial P(r_o)}{\partial n_o} - P(r_o) \frac{\partial G(r,r_o)}{\partial n_o}\right) dS_o \qquad (2.15)$$

where the integration is carried out over the surface of the cavity.

The usefulness of this procedure lies in the fact that once a suitable Green's function has been specified, a variety of further solutions can be obtained using equation 2.15. In practice this may mean that numerical solution of the Helmholtz equation, by whatever means, will not be necessary in all cases.

A useful Green's function can be obtained by expressing it as a sum of the eigenfunctions of a rigid-walled cavity, that is:

$$G(r,r_o) = \sum_n a_n(r_o)\, \phi_n(r) \,.$$

This is substituted into equation 2.13, which with equation 2.6 gives:

$$\sum_n a_n \eta_n^2 \phi_n(r) - k^2 \sum_n a_n \phi_n(r) = \delta(r-r_o) \,.$$

This equation is multiplied by $\phi_i(r)$ and integrated over R, which gives, using equations 2.10 and 2.11:

$$a_i = \frac{\phi_i(r_o)}{\eta_i^2 - k^2} \quad .$$

The resulting Green's function is therefore given by:

$$G(r,r_o) = \sum_n \frac{\phi_n(r)\phi_n(r_o)}{\eta_n^2 - k^2} \quad . \qquad (2.16)$$

This form of the Green's function is particularly applicable for two reasons:

1) If the frequency range of interest covers only a few of the lowest resonant frequencies, terms for which $\eta_n^2 >> k^2$ contribute little to the summation and may therefore be omitted in practical calculations.

2) Since the rigid-walled boundary conditions mean that:

$$\frac{\partial \phi_n(r_o)}{\partial n_o} = 0,$$

the Green's function, which is a summation over $\phi_n$, also satisfies:

$$\frac{\partial G(r,r_o)}{\partial n_o} = 0 \quad . \qquad (2.17)$$

Thus the second term on the right-hand side of equation 2.15 vanishes, leaving:

$$P(r) = \int_S G(r,r_o) \frac{\partial P(r_o)}{\partial n_o} dS_o \quad . \qquad (2.18)$$

## 2.5 The Acoustic Pressure Inside a Cavity with a Vibrating Surface

In section 2.3 it has been described how the motion of the cavity surface is related to the boundary conditions imposed on the pressure field. Using equation 2.3, and assuming harmonic vibration of the surface, results in:

$$\frac{\partial P(r_o)}{\partial n_o} = \rho\omega^2 X(r_o) \qquad (2.19)$$

where $X(r_o)$ is the normal component of displacement amplitude. Equation 2.18 now becomes:

$$P(r) = \rho\omega^2 \int_S G(r,r_o)\, X(r_o)\, dS_o \qquad (2.20)$$

$$= \rho\omega^2 c^2 \sum_n \frac{\phi_n(r)}{\omega_n^2 - \omega^2} \int_S \phi_n(r_o)\, X(r_o)\, dS_o \qquad (2.21)$$

where $\omega_n = c\eta_n$ and $\omega = ck$. This expression for the pressure field shows that $P(r) \to \infty$ as $\omega \to \omega_n$, that is when the cavity is at resonance, which is to be expected when there is no energy loss at the surface.

At lower frequencies, as $\omega \to 0$, all the terms in the summation vanish unless $\omega_n = 0$. Since $\omega_n = 0$, $\phi_n^2 = 1/V$, where V is the volume of the cavity, is an admissible eigensolution (verified using equations 2.6, 2.7 and 2.11) equation 2.21 becomes:

$$P(r) = \frac{-\rho c^2}{V} \int_S X(r_o)\, dS_o$$

The integral essentially represents a small change $\Delta V$ in the volume of the cavity as a result of movement of the surface, and $P(r) = \Delta P$ is the corresponding change in pressure. This gives:

$$-\frac{1}{V}\frac{\Delta V}{\Delta P} = \frac{1}{\rho c^2}$$

which is the adiabatic compressibility of the medium (26).

## 2.6 The Effect of a Locally Reacting Absorbent Surface

The amplitude of the pressure field will in practice be limited by absorption due to the finite rigidity of the cavity surface. The absorbing mechanism can often be satisfactorily characterised by a locally reacting surface with a specific acoustic admittance $\beta$ (10). This is in general a complex quantity which varies with frequency. The resulting boundary condition is now:

$$\frac{\partial P}{\partial n} = -ik\beta P \qquad (2.22)$$

which must be added to those due to a vibrating cavity surface (equation 2.19). Equation 2.18 now becomes:

$$P(r) = \rho\omega^2 \int_S G(r,r_o)\, X(r_o)\, dS_o$$

$$- ik \int_S G(r,r_o)\, \beta(r_o)\, P(r_o)\, dS_o \,. \qquad (2.23)$$

This expression cannot now be evaluated directly because of the term containing $P(r_o)$, the unknown pressure field, on the right-hand side. However by expressing P(r) as a summation over the rigid-wall modes, that is:

$$P(r) = \sum_j a_j \phi_j(r), \qquad (2.24)$$

a set of simultaneous linear equations results which can be solved for the coefficients $a_j$. Since the contribution of high frequency modes is likely to small, the actual number of equations can be limited, thus speeding the computation.

Substituting equation 2.24 into 2.23 and using the expansion for $G(r, r_o)$ gives:

$$\sum_j a_j \phi_j(r) = \rho\omega^2 \sum_n \frac{\phi_n(r)}{\eta_n^2 - k^2} \int_S \phi_n(r_o)\, X(r_o)\, dS_o$$

$$- ik \sum_n \sum_j \frac{\phi_n(r)}{\eta_n^2 - k^2}\, a_j \int_S \phi_n(r_o)\, \beta(r_o)\, \phi_j(r_o)\, dS_o \,.$$

This equation is multiplied by $\phi_i(r)$ and integrated over the volume of the cavity, thus eliminating all terms with $n \neq i$. Use of equation 2.11 and some rearranging gives:

$$\eta_i^2 a_i + ik \sum_j a_j \int_S \phi_i(r_o)\, \beta(r_o)\, \phi_j(r_o)\, dS_o - k^2 a_i$$

$$= \rho\omega^2 \int_S \phi_i(r_o)\, X(r_o)\, dS_o \,. \qquad (2.25)$$

These are the simultaneous equations to be solved for $a_i$, which will in general be complex.

While equation 2.25 can be solved readily using a standard algorithm such as Gaussian elimination, further simplifications can be made when the acoustic admittance is small. In such a case the absorption will be small, and the response P(r) will exhibit pronounced peaks at resonance. This means that close to the ith resonance the coefficient $a_i$ will dominate, and the other coefficients may be ignored, that is:

$$\eta_i^2 a_i + ik\, a_i \int_S \phi_i(r_o)\, \beta(r_o)\, \phi_i(r_o)\, dS_o - k^2 a_i$$

$$= \rho\omega^2 \int_S \phi_i(r_o)\, X(r_o)\, dS_o,$$

giving

$$P(r) = a_i\, \phi_i(r)$$

$$= \rho\omega^2 \frac{\phi_i(r) \int_S \phi_i(r_o)\, X(r_o)\, dS_o}{\eta_i^2 + x - k^2}$$

where

$$x = ik \int_S \phi_i(r_o)\, \beta(r_o)\, \phi_i(r_o)\, dS_o \ .$$

The response at resonance is thus limited by the imaginary component of x, while in between resonances it will closely approximate the rigid-wall response, equation 2.21. In fact equation 2.21 can be used to give the overall response by allowing the resonant frequency $\omega_i$ a small imaginary component such that:

$$\omega_i \rightarrow \omega_i + i\,\gamma_i \ . \qquad (2.26)$$

Since it is only the real, or conductance, component of the acoustic admittance $\beta$ which limits the response at resonance, the imaginary component is ignored, and to a first approximation the damping factor $\gamma_i$ is given by:

$$\gamma_i = \frac{c}{2} \int_S \phi_i(r_o)\, \mathrm{Re}[\beta(r_o)]\, \phi_i(r_o)\, dS_o \ . \qquad (2.27)$$

It is apparent from equation 2.27 that the magnitude of the damping factor depends on the distribution of the absorbing material over the surface of the cavity, and that, for maximum effect at a given resonance, it should be placed where the pressure amplitude is highest rather than regions where nodal planes meet the surface.

While this analysis is accurate for small damping factors, it may prove to be a good approximation for fairly high degrees of absorption because the coefficients of $a_j$ ($j \neq i$) in equation 2.24 are likely to be quite small in comparison with the coefficient of $a_i$, that is the integral:

$$\int_S \phi_i \beta \phi_j \, dS$$

will usually be considerably larger for $i = j$ than for $i \neq j$. Clearly a diagonal form is desirable, and this topic is pursued in more detail in reference (27), where the performance of three different diagonal damping approximations are compared.

In some cases it may be necessary to lift the assumption of a locally reacting surface, and Craggs (28) gives such a formulation, based on finite elements, for rigid porous absorbing materials.

## 2.7 The Effect of Objects Inside the Cavity

The presence of large objects inside the cavity will affect the acoustic pressure field, and in a car passenger compartment these may include the seats and indeed human occupants.

The problem may be approached directly by taking such objects into account in the numerical solution of the Helmholtz equation, for example in reference (15) seats are included in some of the finite element meshes.

It is, however, possible to express the modified response in terms of the modes of the empty cavity, and this kind of analysis is given by Morse and Ingard (10) where they consider the more general problem of a change of cavity shape. Essentially extra integrals have to be added to equation 2.15 which are taken over the surfaces of the internal objects. Since the Green's function (equation 2.16) is known, an integral equation for P(r) results which can be approached in a similar manner to that used for equation 2.23, that is by obtaining a set of simultaneous equations for the unknown modal coefficients $a_i$.

## 2.8 Coupling of Structural and Acoustical Modes

In order to calculate the acoustic response inside the cavity, it is necessary to quantify the vibration of the surrounding structure, and experimental measurements are used for this purpose in references (11) and (16). In a fully theoretical analysis, the determination of the vibration of structures as complex as a car body has to be performed numerically. The most general cases can be handled using matrix structural analysis based on finite elements, and Zienkiewicz (29) gives a comprehensive account of this subject.

The structure is described by the matrix equation:

$$[K]\{u\} + [C]\{\dot{u}\} + [M]\{\ddot{u}\} = \{f\} \qquad (2.28)$$

where $[K]$ is the stiffness matrix, $[C]$ the damping matrix and $[M]$ the mass matrix, while $\{u\}$, $\{\dot{u}\}$ and $\{\ddot{u}\}$ list respectively the nodal displacements, velocities and accelerations. The

vector {f} lists the time dependent forces acting on the structure, and if these are harmonic, such that $\{f\} = \{F\} \exp i\omega t$ and $\{u\} = \{U\} \exp i\omega t$, equation 2.28 becomes:

$$[K]\{U\} + i\omega[C]\{U\} - \omega^2[M]\{U\} = \{F\} \; . \qquad (2.29)$$

The solution {U} will in general be complex, and it is convenient to express it in terms of the natural modes $\{U_i\}$ of the undamped structure, that is:

$$\{U\} = \sum_i b_i \{U_i\} \qquad (2.30)$$

where $\{U_i\}$ satisfies the equation:

$$[K]\{U_i\} - \omega_i^2 [M]\{U_i\} = 0 \qquad (2.31)$$

and the modes are orthogonal and normalised such that:

$$\{U_i\}^T[M]\{U_i\} = 1 \qquad (2.32)$$

$$\{U_i\}^T[M]\{U_j\} = 0 \quad i \neq j \qquad (2.33)$$

$$\{U_i\}^T[K]\{U_i\} = \omega_i^2 \qquad (2.34)$$

$$\{U_i\}^T[K]\{U_j\} = 0 \quad i \neq j \; . \qquad (2.35)$$

Equation 2.30 is substituted into equation 2.29, which is then pre-multiplied by $\{U_j\}^T$, which, making use of equations 2.32- 2.35, gives:

$$b_j\omega_j^2 + i\omega \sum_i b_i\{U_j\}^T[C]\{U_i\} - b_j\omega^2 = \{U_j\}^T\{F\} . \qquad (2.36)$$

These simultaneous equations can be solved for the coefficients $b_j$, and it is usually possible to neglect the contributions of higher frequency modes for which $\omega_j^2 >> \omega^2$.

As for acoustic absorption, a diagonal form of equation 2.36 leads to simplified solutions, that is when:

$$\{U_j\}^T[C]\{U_i\} = 0 \quad i \neq j, \qquad (2.37)$$

and the response can be obtained by allowing each resonant frequency the appropriate imaginary damping factor. The modal coefficients are now given by:

$$b_j = \frac{\{U_j\}^T\{F\}}{\omega_j^2 - \omega^2} . \qquad (2.38)$$

Since theoretical determination of the damping matrix [C] is often difficult, it is sometimes expressed as a linear combination of the stiffness matrix and the mass matrix, the proportion of each being determined by experiment (29). This approach automatically leads to a damping matrix which satisfies equation 2.37. Alternatively the work of Thomson et al (27), mentioned earlier in the context of acoustic absorption, is relevant here. If the damping is small,

equation 2.38 anyway gives a good approximation regardless of the form of the damping matrix.

The displacement amplitude $X(r_o)$ at the surface of the acoustic cavity may now be expressed as a sum over the structural resonances, that is:

$$X(r_o) = \sum_j b_j X_j(r_o) \tag{2.39}$$

where $X_j(r_o)$ is the surface displacement amplitude of the jth structural mode. Equation 2.39 is substituted into equation 2.21, and making use of equation 2.38 and the relationship $\Omega_i = c\eta_i$ (the acoustic resonant frequencies being expressed in this way in order to distinguish them from the structural resonant frequencies $\omega_j$) gives:

$$P(r) = \rho\omega^2 c^2 \sum_i \sum_j \phi_i(r) \frac{C_{ij}}{(\Omega_i^2 - \omega^2)(\omega_j^2 - \omega^2)} \{U_j\}^T\{F\}, \tag{2.40}$$

where

$$C_{ij} = \int_S \phi_i(r_o)\, X_j(r_o)\, dS_o, \tag{2.41}$$

and it is assumed that the acoustic absorption and structural damping characteristics are approximated by allowing $\Omega_i$ and $\omega_j$ the appropriate small imaginary damping factors. Further manipulation of equation 2.40 gives:

$$P(r) = \rho\omega^2 c^2 \sum_i \frac{\phi_i(r) \sum_j \{U_j\}^T\{F\} C'_{ij}}{(\Omega_i^2 - \omega^2)}$$

$$- \rho\omega^2 c^2 \sum_j \frac{\{U_j\}^T\{F\} \sum_i \phi_i(r) C'_{ij}}{(\omega_j^2 - \omega^2)} \qquad (2.42)$$

where

$$C'_{ij} = \frac{C_{ij}}{(\omega_j^2 - \Omega_i^2)} \; . \qquad (2.43)$$

Inspection of equation 2.42 shows that the first summation consists of a number of peaks coincident with the acoustic resonant frequencies, while the second has peaks corresponding to the structural resonances. Although a fortuitous cancellation of the terms in these summations may occur for particular force distributions, it is more likely that the amplitude of a given resonance will depend on the magnitude of the coefficients $C'_{ij}$.

In a typical car structure, where there are several force inputs with a great variety of frequencies and amplitudes, these coefficients can be expected to give some indication of where the most troublesome response will occur. In this way the acoustic response of a structure may be judged without having to consider particular forcing cases, as the coefficients $C'_{ij}$ are independent of these and the 'hearing' position, r.

Although the damping factor will in general be different for each resonance, we can expect damping among resonances of either kind (structural or acoustical) to be of a similar magnitude apart from any gross overall change with frequency. However it is not unlikely that the effects of sound absorption and structural damping will differ appreciably, and if the difference is great then either of the two summations in equation 2.42 will become relatively insignificant. For example if acoustic absorption dominates, the acoustic spectrum inside the cavity will exhibit peaks only at structural resonances which may lead to the erroneous deduction that acoustic modes are playing no part in the sound generation process.

Examination of equation 2.43 shows that the magnitude of a given coefficient $C'_{ij}$ depends on

a) The value of the surface integral in equation 2.41, which in turn depends on the shapes of the acoustic mode and the structural mode. Under certain circumstances it will be possible to predict that this will be zero for some combinations without actually evaluating the integral. For example a structure that is symmetric about some plane (as car bodies usually are) will have symmetric and antisymmetric modes, as will the acoustic cavity defined by the structure. The combination of two modes of different types in equation 2.41 thus results in $C_{ij} = 0$.

b) The proximity of the structural and acoustic resonant frequencies: if these differ greatly then the corresponding value of $C'_{ij}$ will be small.

The aim of any modifications to the structure would be to reduce the largest values of $C'_{ij}$ within the frequency range of interest, in the knowledge that this will amost certainly reduce the overall acoustic response for a wide variety of force inputs.

It is interesting to mention here the acceptance function proposed by Koopman and Pollard (30, 38), which is a closely related concept. This is probably more applicable when the excitation is at a single fixed frequency, as it is dependent both on frequency and force distribution.

The analysis so far has not included the possibility that the acoustic cavity has an effect on the structural vibration. To take this into account the acoustic pressure over the exterior of the cavity must be treated as an additional set of forces acting on the structure. Wolf (39) considers this topic and sets up a matrix eigenvalue equation in terms of the uncoupled structural and acoustic modes. He then proceeds directly to a numerical solution which gives the resonant frequencies of the coupled system, and its modes in terms of the uncoupled modes.

Dowell et al (40) treat the problem more generally by allowing abitrary time variations and arrive at a set of coupled differential equations for the time-dependent modal coefficients. They go on to derive approximate expressions for the acoustic response to sinusoidal excitation under a variety of resonant conditions. Some of these cases will be considered here in more detail.

The notation used in the previous parts of this chapter will be retained. Apart from symbolic differences, it should be noted that somewhat different normalisation conditions are used here and in both references (39) and (40). Beyond this, the formulations are equivalent. Dowell et al assume a diagonal form of structural damping from the outset, but do not initially assume this form for acoustic absorption. However, as their analysis proceeds they revert to the diagonal form implicitly by assuming a dominant acoustic mode near resonance, as in section 2.6. Diagonal forms for both structural damping and acoustic absorption with be assumed here by allowing the uncoupled resonant frequencies to be complex.

If, as before, $a_i$ and $b_j$ are the coefficients of the uncoupled acoustic and structural modes respectively, then the coupled equations are

$$\Omega_i^2 a_i - \omega^2 a_i = \rho\omega^2 c^2 \sum_j b_j C_{ij} \quad , \quad (2.44)$$

$$\omega_j^2 b_j - \omega^2 b_j = \sum_i a_i C_{ij} + \{U_j\}^T\{F\} \quad . \quad (2.45)$$

The summation on the right-hand side of equations 2.45 represents the acoustic pressure acting on the structure, and if this is omitted it may be verified that equations 2.44 and 2.45 lead to the acoustic response given by equation 2.42.

A number of near resonant special cases will now be examined following the approach given in reference (40).

(i) Exciting frequency close to a structural resonance ( $\omega \simeq \omega_j$).

In this case the jth structural mode is assumed to be dominant, and equations 2.44 simplify to

$$\Omega_i^2 a_i - \omega^2 b_j = \rho\omega^2 c^2 b_j \sum_i \frac{C_{ij}^2}{\Omega_i^2 - \omega^2} + \{U_j\}^T\{F\}. \quad (2.47)$$

If the first term on the right-hand side is very small then we have

$$b_j \simeq \frac{\{U_j\}^T\{F\}}{\omega_j^2 - \omega^2}.$$

This is the same as equation 2.38, and the acoustic response near resonance is given by equation 2.42 omitting all terms except that with $(\omega_j^2 - \omega^2)$ in the denominator. In this case the change in structural resonant frequency is negligibly small.

(ii) Structural resonant frequency changed by coupling with cavity modes.

In this case it will be assumed that the fractional change in resonant frequency is small, but not negligibly so as in the previous case. The modified resonant frequency is obtained from equation 2.47 by excluding the forcing term on the right-hand side. If in addition the change is small and none of the acoustic resonances are very close, so that

$$\frac{C_{ij}}{\Omega_i^2 - \omega^2} \simeq \frac{C_{ij}}{\Omega_i^2 - \omega_j^2} = -C'_{ij}$$

we have, after some manipulation,

$$\omega^2 \simeq \omega_j^2 \left(1 + \rho c^2 \sum_i C_{ij} C'_{ij}\right) \quad (2.48)$$

at resonance.

(iii) Exciting frequency close to an acoustic resonance ($\omega \cong \Omega_i$).

So far the results obtained are entirely equivalent to those given by Dowell et al (40). However, in this case there is a serious shortcoming in their analysis.

The ith acoustic mode is assumed to dominate, so that equations 2.45 simplify to

$$\omega_j^2 b_j - \omega^2 b_j = a_i C_{ij} + \{U_j\}^T \{F\}. \quad (2.49)$$

Eliminating $b_j$ and making use of 2.44 gives

$$a_i = \frac{\rho\omega^2 c^2 \sum_j \frac{C_{ij} \{U_j\}^T \{F\}}{\omega_j^2 - \omega^2}}{\Omega_i^2 - \omega^2 - \rho\omega^2 c^2 \sum_j \frac{C_{ij}^2}{\omega_j^2 - \omega^2}} \quad (2.50)$$

Dowell et al assume no acoustic absorption so that $\Omega_i$ is real. At this point they implicitly set $\omega = \Omega_i$ in order to obtain $a_i$, but this is unsatisfactory because the magnitude of this term is limited at resonance only by the imaginary part of the summation in the denominator, however small this might be. The acoustic resonant frequency has in fact been shifted by the coupling with the structure, and can be found by equating the denominator of 2.50 to zero. The acoustic response at the nearby position $\omega = \Omega_i$ is of little value because it bears no relation to that at the peak.

To simplify the algebra, a dominant structural mode will be assumed, whose resonant frequency however is not too close to the acoustic resonant frequency. Only a small change is assumed in

the latter. Under these circumstances we neglect all but a single term in the summations in 2.50, and the following approximations are applicable :

$$\frac{C_{ij}}{\omega_j^2 - \omega^2} \cong C'_{ij}$$

$$\mathrm{Im}\left(\frac{1}{\omega_j^2 - \omega^2}\right) \cong \frac{-2\omega_j \mathrm{Im}(\omega_j)}{(\omega_j^2 - \omega^2)^2}$$

$$\cong \frac{-2\omega_j \mathrm{Im}(\omega_j)}{(\omega_j^2 - \Omega_i^2)^2}$$

if $\mathrm{Im}(\omega_j) \ll |\omega_j - \omega|$.

At resonance equation 2.50 therefore becomes

$$a_i = \frac{\{U_j\}^T\{F\}}{2i\omega_j C'_{ij} \mathrm{Im}(\omega_j)} \qquad (2.51)$$

The response is limited by the ability of the acoustic mode to lose energy indirectly through damping of the structural mode, since there is no acoustic absorption. The extent to which this happens depends on the degree of coupling between the acoustic mode and the structural mode, and not suprisingly this is determined by the term $C'_{ij}$ in the denominator of 2.51.

If there is acoustic absorption which exceeds this indirect dissipation, and very little change in the acoustic resonant frequency, the summation in the denominator of 2.50 may be

ignored. The response is now the same as given by equation 2.42 when all terms but the ith acoustic term are neglected.

(iv) Exciting frequency close to an acoustic resonance and a structural resonance

$$(\omega \cong \Omega_i \cong \omega_j).$$

For this case a dominant acoustic mode and a dominant structural mode are assumed. Equations 2.44 and 2.45 therefore become

$$\Omega_i^2 a_i - \omega^2 a_i = \rho\omega^2 c^2 b_j C_{ij} \qquad (2.52)$$

$$\omega_j^2 b_j - \omega^2 b_j = a_i C_{ij} + \{U_j\}^T\{F\} \qquad (2.53)$$

Eliminating $b_j$ gives

$$a_i = \frac{\rho\omega^2 c^2 \{U_j\}^T\{F\} C_{ij}}{(\omega_j^2 - \omega^2)(\Omega_i^2 - \omega^2) - \rho\omega^2 c^2 C_{ij}^2} \qquad (2.54)$$

The last term in the denominator is real and has the effect of shifting the resonances. The behaviour of this expression is tricky and there are a variety of different limiting cases. If it is assumed that

$$|(\omega_j^2 - \omega^2)(\Omega_i^2 - \omega^2)| >> \rho\omega^2 c^2 C_{ij}^2$$

for all $\omega$, which implies a degree of both structural damping and acoustic absorption, then the response is that given by the equation 2.40 given a dominant single term.

The result in reference (40) assumes no acoustic absorption.

While these cases do not provide an exhaustive analysis of all conceivable possibilities, they do serve to illustrate

fundamental features of the interation between structure and cavity. These effects can have a varying degree of severity :

a) If the changes in the resonant frequencies of the system are very small when coupled (strictly speaking small in comparison with their spacing as well as absolute value) and there are not great changes in effective damping or absorption, then the uncoupled approximation (equation 2.42) will be satisfactory.

b) If the changes in frequency are somewhat larger but still small enough to be approximated by equation 2.48 (and a corresponding equation for the acoustic resonances) then equation 2.42 may still be adequate if these modified values are used.

c) Indirect damping or absorption may affect the imaginary parts of the resonant frequencies as in (iii), and these will have to be adjusted accordingly.

d) In the case of near-coincident structural and acoustic resonances the result is uncertain and cases must be treated individually. If the structural acoustic interaction is small, however, and there is sufficient damping and absorption, the uncoupled approximation is sufficient.

e) If the changes as calculated by these approximate methods turn out to be large, then it is unlikely that they are adequate. It would then be necessary to resort to a coupled numerical eigenvalue analysis of the type given by Wolf (39).

It has been shown that coupling effects between the structure and cavity can significantly affect the acoustic response. However, it is clear that the terms $C'_{ij}$ play a large part in determining the nature of this coupling, despite the fact that equation 2.42 may no longer be valid. Thus the original concept of trying to reduce the $C'_{ij}$ still seems sensible even when the system is strongly coupled. The only conceivable circumstance in which a large value may actually reduce the response is the extreme case when a lightly damped mode dissipates most of its energy indirectly through another mode.

Because it is possible that the damping or absorption characteristics of the system may be altered significantly by coupling, it would be desirable to take this into account in an analysis of the type described by Wolf. This could be done by allowing complex values for the uncoupled resonant frequencies in the usual way, and then performing a more general complex eigensolution for the coupled equations. The resulting resonances would then have the appropriate modified damping properties.

# 3 CALCULATION OF ACOUSTIC CAVITY RESONANCES USING FINITE ELEMENTS

## 3.1 Acoustic Finite Elements

In the previous chapter it has been established that the rigid-wall modes are of central importance in the calculation of the pressure field inside an acoustic cavity. Exact solutions for the modes of general irregular cavities cannot be obtained, but good numerical approximations may be obtained using finite elements.

A completely general finite element formulation for acoustic cavity resonance, based on variational methods, is given in appendix 3.I and this results in a matrix equation:

$$[K]\{P\} - \frac{\omega^2}{c^2}\,[M]\{P\} = 0 \qquad (3.1)$$

The vector $\{P\}$ lists the values of pressure amplitude at the nodes of the finite element mesh, and the exact form of the matrices $[K]$ and $[M]$ depends on the type of element used. Equation 3.1 is an eigenvalue problem, the solution of which gives N eigenvectors $\{\phi_i\}$ and their corresponding eigenvalues $\omega_i$, where N is the total number of nodes in the mesh.

Many algorithms for use with digital computers have been devised which solve matrix eigenvalue problems, and this large subject is not discussed here. It should be noted, however, that equation 3.1 has certain characteristics, associated with physical reality, which affect the choice of the most economical solution routine. These are:

a) The matrices $[K]$ and $[M]$ are symmetric.

b) The matrix $[K]$ is positive semi-definite, that is $\{P\}^T[K]\{P\} \geq 0$ for any vector $\{P\}$. Physically this corresponds to the fact that the total kinetic energy of the medium must be at least zero.

c) The matrix $[M]$ is positive definite, that is $\{P\}^T[M]\{P\} > 0$ for any non-zero vector $\{P\}$, meaning that the potential energy of any pressure distribution is always greater than zero.

These features mean that negative eigenvalues cannot exist, so that a less complex and more economical solution algorithm can be used than that necessary for a completely general eigenvalue problem. The popular NAG subroutine library contains a selection of such routines, and these have been used to obtain all the finite element solutions described later in this chapter.

Equation 2.10, which describes the orthogonality of the modes, can be expressed in terms of the finite element eigensolutions in the following way:-

$$\{\phi_i\}^T[M]\{\phi_j\} = 0 \qquad i \neq j \tag{3.2}$$

Equation 2.11, which normalises the modes, thus becomes:

$$\{\phi_i\}^T[M]\{\phi_i\} = 1 \tag{3.3}$$

and these last two equations can be used to obtain:

$$\{\phi_i\}^T[K]\{\phi_j\} = 0 \qquad i \neq j \tag{3.4}$$

$$\{\phi_i\}^T[K]\{\phi_i\} = \frac{\omega_i^2}{c^2} \tag{3.5}$$

The solution routines used provide such normalisation, and also ensure orthogonality of degenerate modes.

## 3.2 Prismatic Cavities

In many physical problems the geometry and material properties do not vary along one co-ordinate direction, and if the co-ordinate system is Cartesian we are therefore dealing with prismatic structures or volumes. Zienkiewicz (29) gives an account of how the finite element solution of such problems can be made far more economical than that of general three dimensional problems. If the problem is described in the co-ordinate system (x, y, z) with geometry and material properties not changing in the z-direction, then a two-dimensional finite element subdivision is made in the x-y plane, with variation of the unknown quantity in the z direction being expressed as a sum of Fourier components. Thus, instead of having a single degree of freedom at each node, there are now as many degrees of freedom as there are Fourier components.

At first sight it appears that the number of degrees of freedom required will still be approximately equal to that required for a full three-dimensional subdivision, hence requiring the same amount of computing effort. However, because of the mutual orthogonality of some of the Fourier components, the matrix equation describing the whole system often decouples into a number (usually equal to the number of Fourier components) of smaller matrix equations, which can then be solved separately. For most solution routines the storage and time required are proportional to the square and the cube of the number of degrees of freedom respectively, so the advantages of the procedure outlined above become immediately apparent. Craggs and Stead (41) give an analysis of this sort for a combined plate/cavity problem.

If this method is applied to acoustic cavity resonance, it is found that not only does the overall matrix equation decouple into a number of smaller problems, but that each of these is very simply related to the others. This makes it necessary to solve a single two-dimensional problem only, from which all the three-dimensional modes may be calculated.

While this derivation is not particularly difficult, it is not included here as the same result can be obtained rather more directly by assuming a separated solution of the form $P_o(x,y)\ Z(z)$ to the Helmholtz equation (equation 2.2). It is then found that if a two-dimensional eigenfunction (i.e. pressure amplitude distribution) $P_o(x,y)$ and resonant $\omega_o$ are found which satisfy equation 2.2, then $P_n(x,y,z)$ and $\omega_n$ are also admissible solutions if:

$$\omega_n = c\sqrt{\frac{n^2\pi^2}{a^2} + \frac{\omega_o^2}{c^2}} \qquad n = 1,2,3,... \qquad (3.6)$$

$$P_n = P_o \cos \frac{n\pi z}{a} \qquad n \text{ even}$$

$$P_n = P_o \sin \frac{n\pi z}{a} \qquad n \text{ odd} \tag{3.7}$$

where the plane z=0 lies midway across the cavity, which is bounded by rigid walls at z = -a/2 and z = +a/2. The use of eqn. (3.6) in this way is suggested in reference (41).

The two-dimensional solutions $P_o(x,y)$ described later will be obtained using the finite element method, although there is no reason in principle why they should not be evaluated using some other method. In most applications it will be desirable to normalise the modes in the manner of equation 2.11. Integrating $P_n^2(x,y,z)$ over the volume of the cavity for even n gives:

$$\int_R P_n^2 \, dV = \int_R P_o^2 \cos^2 \frac{n\pi z}{a} \, dV$$

$$= \int_{-a/2}^{a/2} \cos^2 \frac{n\pi z}{a} \, dz \cdot \int P_o^2 \, dxdy$$

$$= \frac{a}{2} \int P_o^2 \, dxdy,$$

where the remaining integral is taken over the two-dimensional section normal to the z-axis. Exactly the same result is obtained for odd n. If the two-dimensional solution is normalised, that is:

$$\int_R P_o^2 \, dV = a \int P_o^2 \, dxdy = 1$$

then

$$\int_R P_n^2 \, dV = \tfrac{1}{2}$$

Thus suitably normalised three-dimensional modes can be obtained by multiplying equation 3.7 by $\sqrt{2}$.

An example of three-dimensional finite element analysis of an acoustic cavity is given by Petyt et al (14). The case considered was that of a model van body, whose resonances were also investigated experimentally. The finite element analysis used eight twenty-noded isoparametric elements, only half of the cavity being modelled due to the symmetry about the centre-line. This approach yields first a series of modes which are symmetric about the centre-line, and another consisting of antisymmetric modes. It was observed that the nodal patterns of the antisymmetric modes were virtually identical to those of the symmetric modes apart from a longitudinal nodal plane along the centre-line. Although this cavity was not exactly prismatic due to its slightly sloping sides, these features are apparent in equation 3.7, where even n results in symmetric modes and odd n gives antisymmetric modes.

## 3.3 Linear and Quadratic Triangular Elements

Since it has been shown how full three-dimensional solutions can be obtained from the two-dimensional solutions of a prismatic cavity, the finite element analyses described here used only two-dimensional elements. Although the choice of element shape is more or less arbitrary, and can be made to suit specific problems, triangular elements have been used because they can be made to fit the most general of two-dimensional regions (unlike, for example, rectangular elements).

The simplest triangular element has nodes only at the vertices, and is usually referred to as a 'linear triangle' because the variation of the unknown quantity P(x,y) is a linear function of the spatial co-ordinates. Thus P(x,y) is specified uniquely everywhere within the triangle by the three nodal values, and contours are always straight lines.

Triangular elements of higher orders can also be devised (29). For example, a quadratic in two dimensions needs six parameters to define it, so a quadratic triangle has six nodes (three at the vertices and three at the mid-sides), while a cubic triangle has ten nodes.

Although the linear triangle requires the simplest formulation, the quadratic triangle is probably capable of a better representation of the pressure amplitude distribution P. The boundary conditions require that $\partial P/\partial n$ is zero at the surface of the cavity, and this means that contours of P must be normal to the surface where they meet it. In some cases, for example when two sides of an element lie on the boundary, the linear triangle will give a poor approximation because contours within it are necessarily straight lines. It is also

widely held that, for a given number of degrees of freedom, subdivision into a few complex elements gives better results than a larger number of simple elements (29).

In the following analyses, all the cases considered were analysed using both linear and quadratic triangles in order to compare the performances of the two types. Details of these elements are given in appendix 3.II, along with the element matrices which are assembled to form equation 3.1. McRae (42) gives a more detailed comparison of this sort.

## 3.4 Test Case Results

In all the problems analysed subsequently, solutions were obtained using both linear and quadratic triangular elements. In order to make a fair comparison, equal numbers of degrees of freedom were used for the two types, and furthermore the nodes were positioned identically. This was achieved simply by placing four linear elements in the position alternatively occupied by a single quadratic element. In the mesh diagrams given, only the quadratic element subdivision is shown.

The zero-frequency modes, for which the pressure amplitude is constant, are not shown in the results although of course they are valid solutions, and as such will be computed by many eigen solution routines (including the one used here). It has been described in section 2.5 how normalisation gives $\phi^2 = 1/V$, where $\phi$ is the pressure amplitude of the zero frequency mode, and V is the volume of the cavity. Since the volume is readily calculated by hand, this relationship provides a useful preliminary check of the program and the mesh input data.

The accuracy of programs was assessed by comparing their results with some exact solutions to the two-dimensional Helmholtz equation. The first case considered was a rectangular cavity of 3m x 2m, with c, the velocity of sound, equal to 250 $ms^{-1}$. The resonant frequencies for such a two-dimensional cavity are given by:

$$f = \frac{c}{2}\sqrt{\left(\frac{n_x}{l_x}\right)^2 + \left(\frac{n_y}{l_y}\right)^2} \qquad (3.8)$$

where $n_x$, $n_y$ are integers, and $l_x$, $l_y$ are the dimensions of the cavity in the x and y directions respectively (31). Two finite element subdivisions were used, and these are shown in figure 3.1. The coarser mesh has 25 nodes, giving 32 linear elements or 8 quadratic elements, while the finer mesh has 81 nodes with 128 linear elements or 32 quadratic elements. The computed resonant frequencies are given in table 3.1, and illustrate the increased accuracy of the finer mesh. In all cases except one (where the exact frequency is 131.8Hz and the fine mesh is used), for a given number of degrees of freedom the quadratic elements yield better results than the linear elements.

Also considered was the case of resonance of a cylindrical cavity. Exact results can be obtained fairly simply by treating the axisymmetric modes only, such that the pressure amplitude is a function only of the radial distance r from the axis of the cylinder, and these solutions and the necessary normalisation are dealt with in appendix 3.III. The modes are given by:

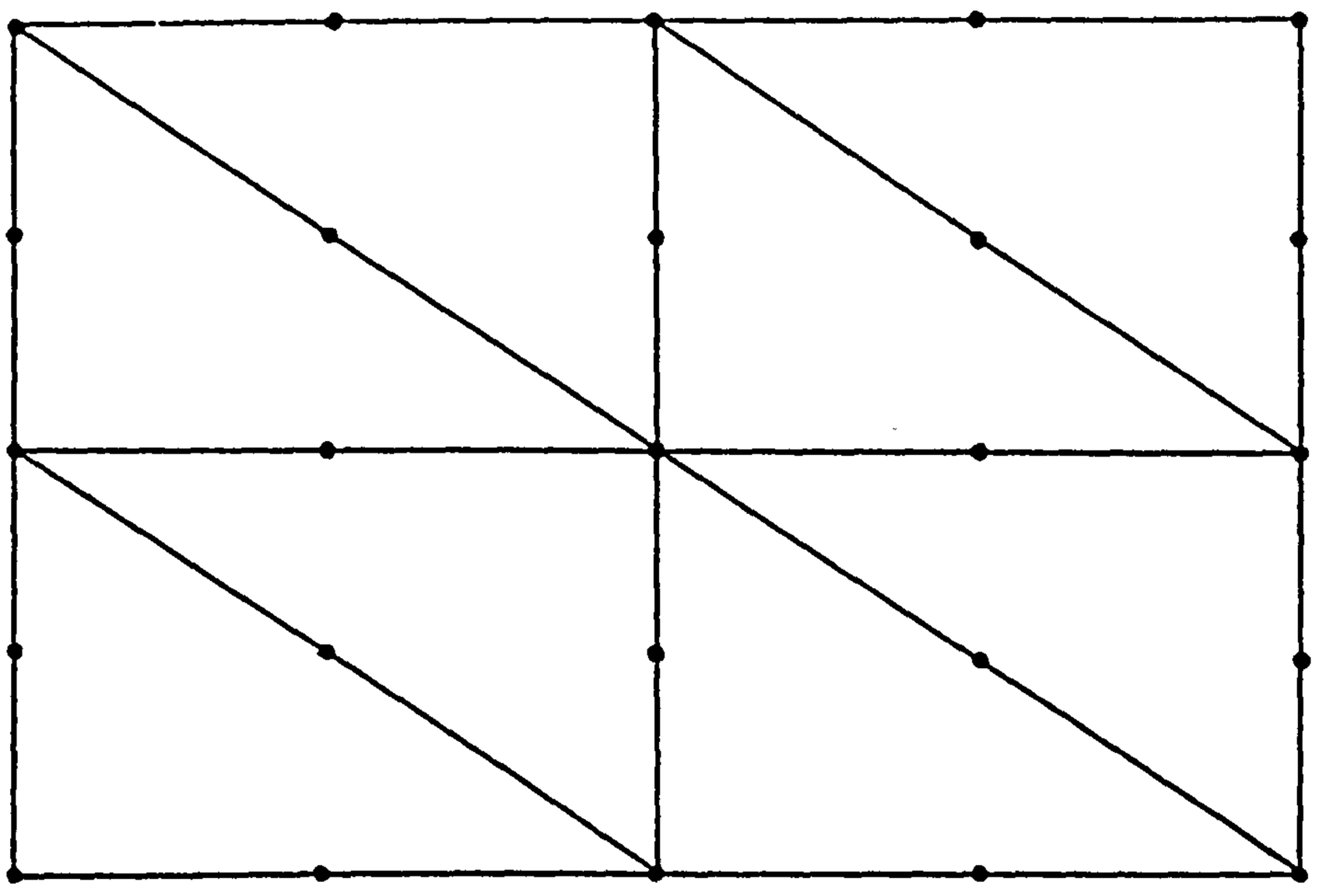


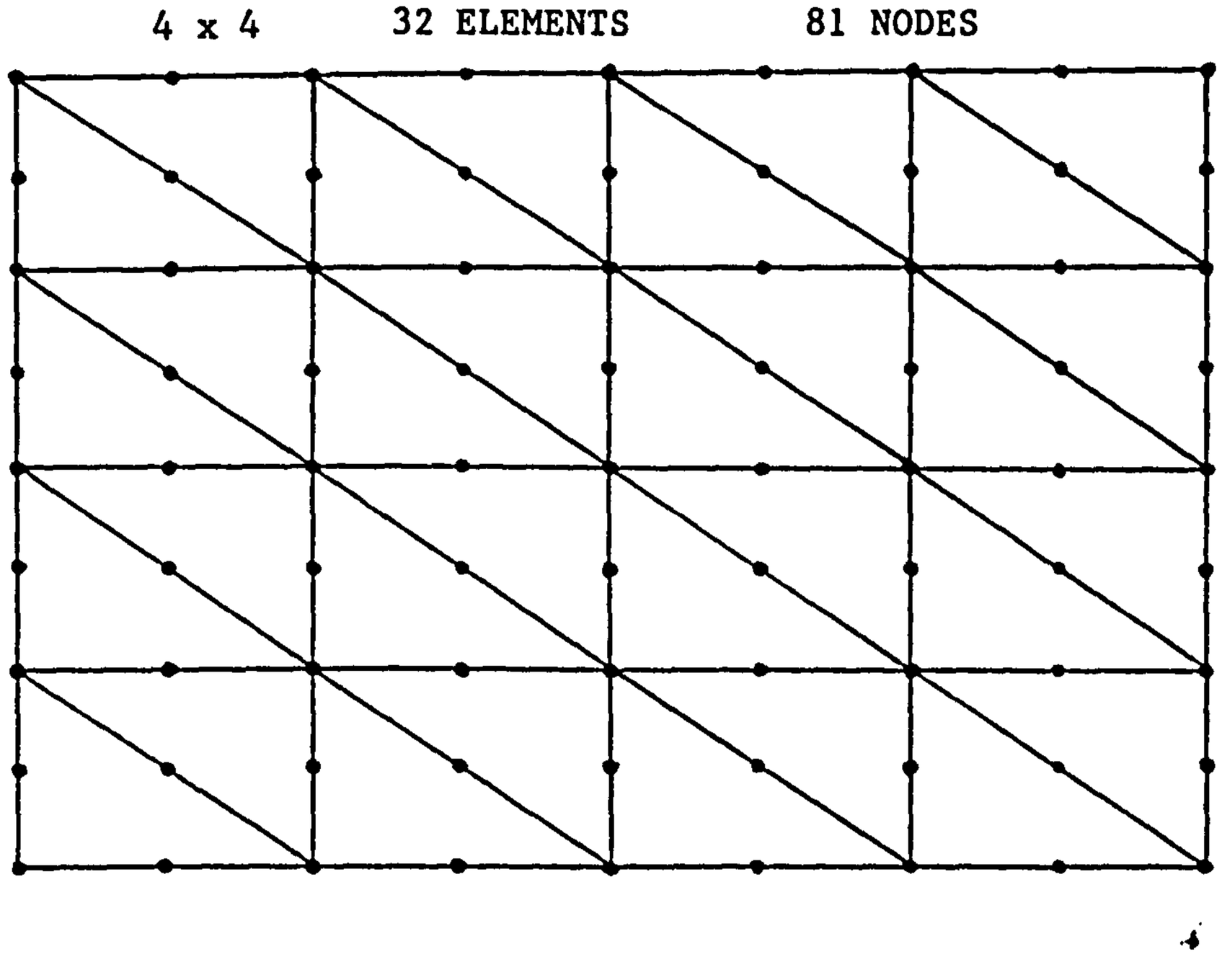


Fig. 3.1 Finite Element Meshes for the 3m x 2m Rectangular Cavity

Table 3.1 The Acoustic Resonant Frequencies of a 3m x 2m Rectangular Cavity ($c = 250\ ms^{-1}$)

| Mode | | Resonant Frequencies (Hz) | | | | |
|---|---|---|---|---|---|---|
| | | Coarse Mesh | | Fine Mesh | | |
| $n_x$ | $n_y$ | Linear | Quadratic | Linear | Quadratic | Exact |
| 1 | 0 | 42.7 | 41.8 | 41.9 | 41.7 | 41.7 |
| 0 | 1 | 64.0 | 62.7 | 62.9 | 62.5 | 62.5 |
| 1 | 1 | 80.5 | 76.4 | 76.5 | 75.2 | 75.1 |
| 2 | 0 | 91.5 | 91.0 | 85.5 | 83.6 | 83.3 |
| 2 | 1 | 121.4 | 110.8 | 108.8 | 105.0 | 104.2 |
| 0 | 2 | 136.8 | 135.1 | 128.1 | 125.4 | 125.0 |
| 1 | 2 | 148.2 | 141.3 | 132.2 | 132.7 | 131.8 |

$$\phi_n(r) = \frac{J_o(\beta_n r/R)}{RJ_o(\beta_n)} \sqrt{\frac{1}{\pi a}} \qquad (3.9)$$

and the corresponding resonant frequencies by:

$$f_n = \frac{1}{2\pi} \cdot \frac{c}{R} \cdot \beta_n \qquad (3.10)$$

$J_o$ is the Bessel function of the first kind of order zero, R and a are respectively the radius and depth of the cavity, and $\beta_n$ are the roots of $J_1(\beta)$, the Bessel function of the first kind of order one.

The dimensions R=0.4m and a=2m were used in the finite element analysis, and the mesh, consisting of 57 nodes and 88 linear elements or 22 quadratic elements, is shown in figure 3.2. Because only axisymmetric modes are considered, the problem is adequately modelled by any radial segment of the cylinder, and in this case a segment of $60^o$ was arbitrarily chosen. However the volume of the segment is only a sixth of that of the true cylinder, and because of this the finite element modes must be divided by $\sqrt{6}$ to achieve correct normalisation.

Table 3.2 shows the computed resonant frequencies for C=343 $ms^{-1}$, along with the exact results according to equation 3.10. The corresponding mode shapes are plotted in figures 3.3-3.6, using the values along the edge of the $60^o$ segment.

It can be seen that the accuracy of the first two resonant frequencies is good, while the second two results are rather poor. This decrease in accuracy is to be expected

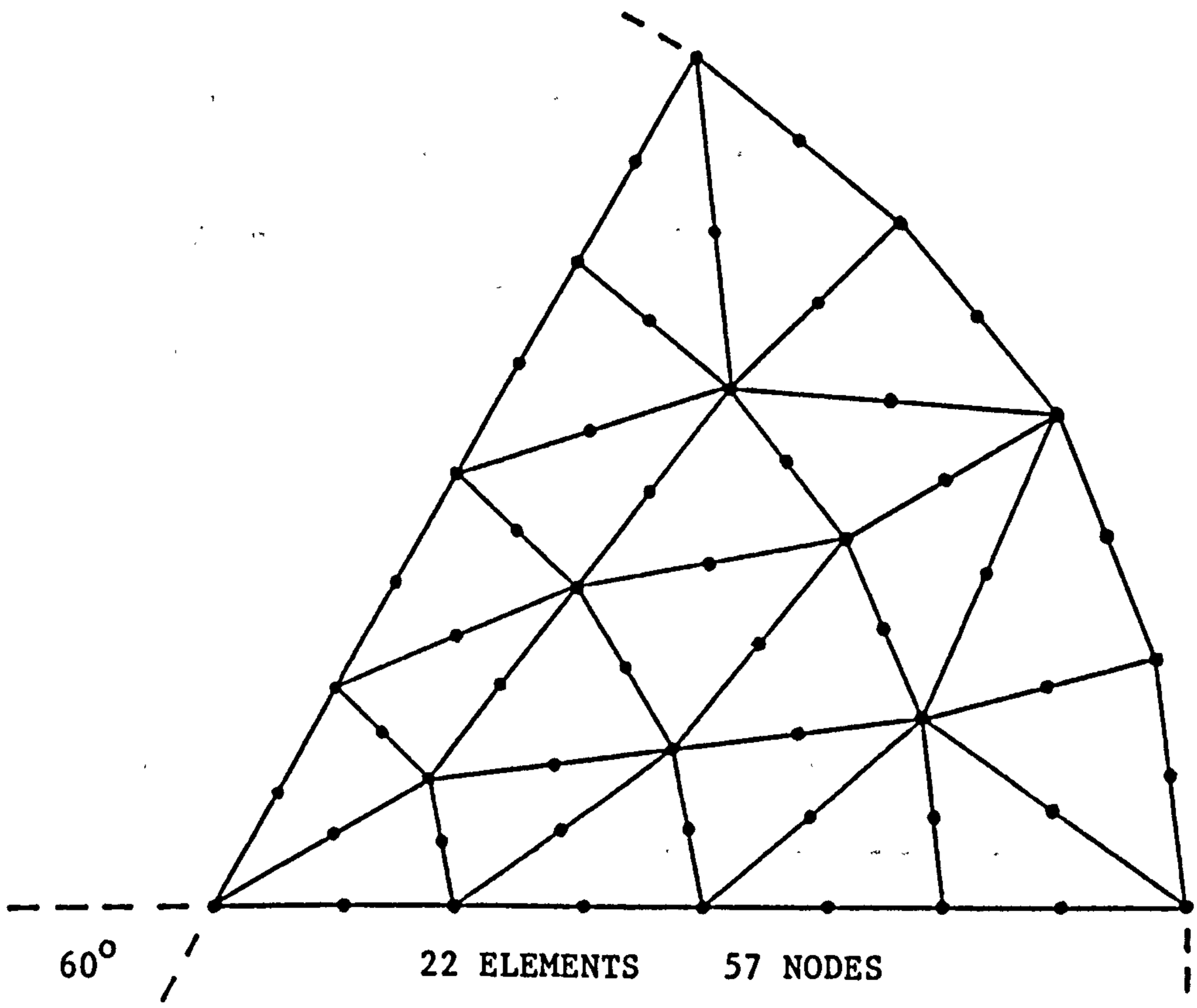


Fig. 3.2 Finite Element Subdivision
for the Cylindrical Cavity

Table 3.2 The Axisymmetric Resonant Frequencies of a Cylindrical Cavity.

(Radius = 0.4m; c = 343 $ms^{-1}$)

| Resonant Frequencies (Hz) | | |
|---|---|---|
| Linear | Quadratic | Exact |
| 529.6 | 526.1 | 522.9 |
| 988.2 | 966.8 | 957.5 |
| 1476.6 | 1414.8 | 1388.4 |
| 2009.9 | 1982.8 | 1818.4 |

Table 3.3 The Two-Dimensional Resonant Frequencies of a Car-Shaped Cavity (c = 343 $ms^{-1}$)

| Resonant Frequencies (Hz) | | |
|---|---|---|
| Linear | Quadratic | Measured (32) |
| 175.7 | 175.1 | 175 |
| 312.6 | 309.6 | 309 |
| 332.8 | 330.2 | 322 |
| 433.7 | 427.3 | 426 |
| 464.7 | 455.1 | 452 |

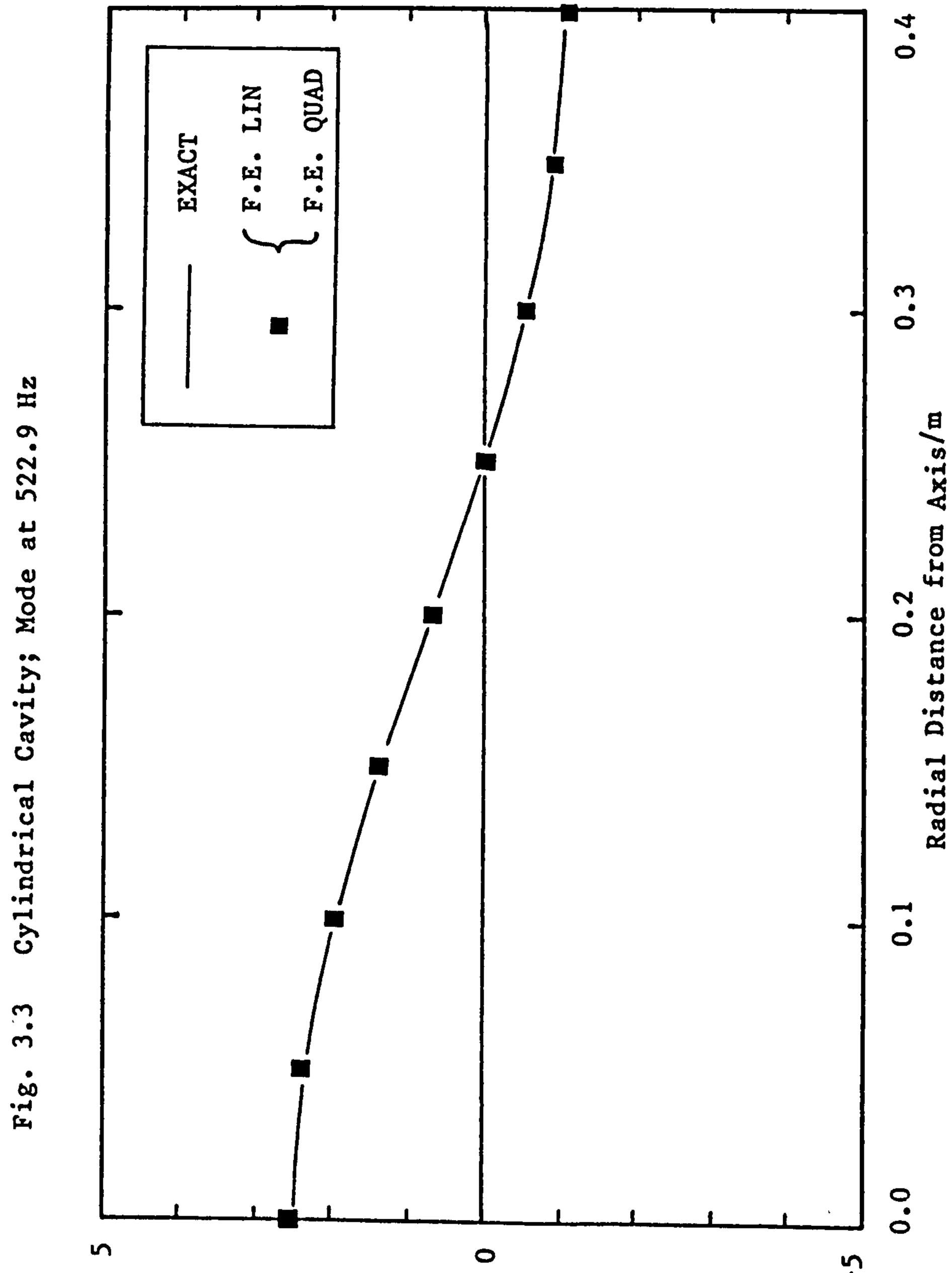


Fig. 3.3 Cylindrical Cavity; Mode at 522.9 Hz

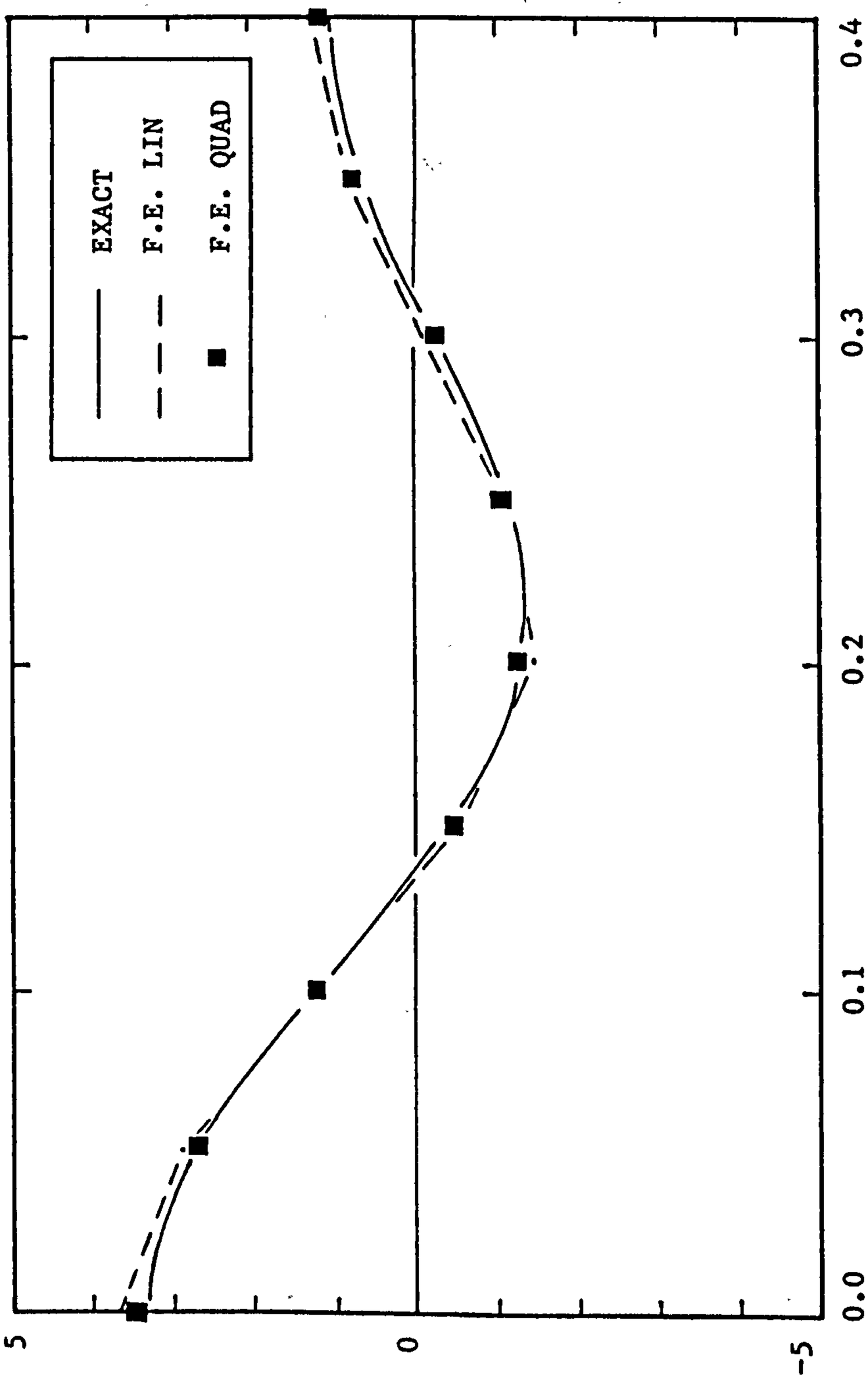


Fig. 3.4. Cylindrical Cavity; Mode at 957.5 Hz

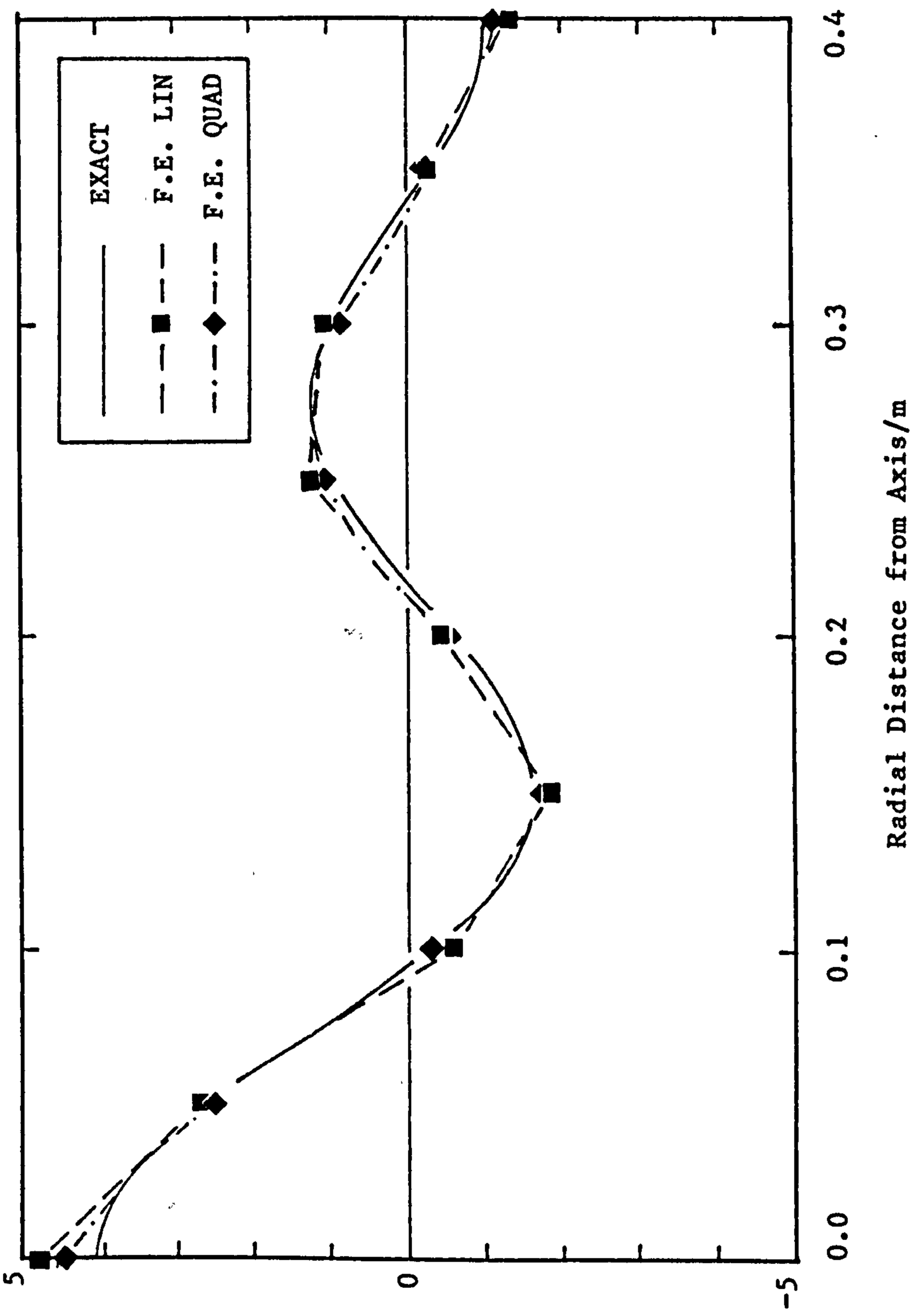


Fig. 3.5. Cylindrical Cavity; Mode at 1388.4 Hz

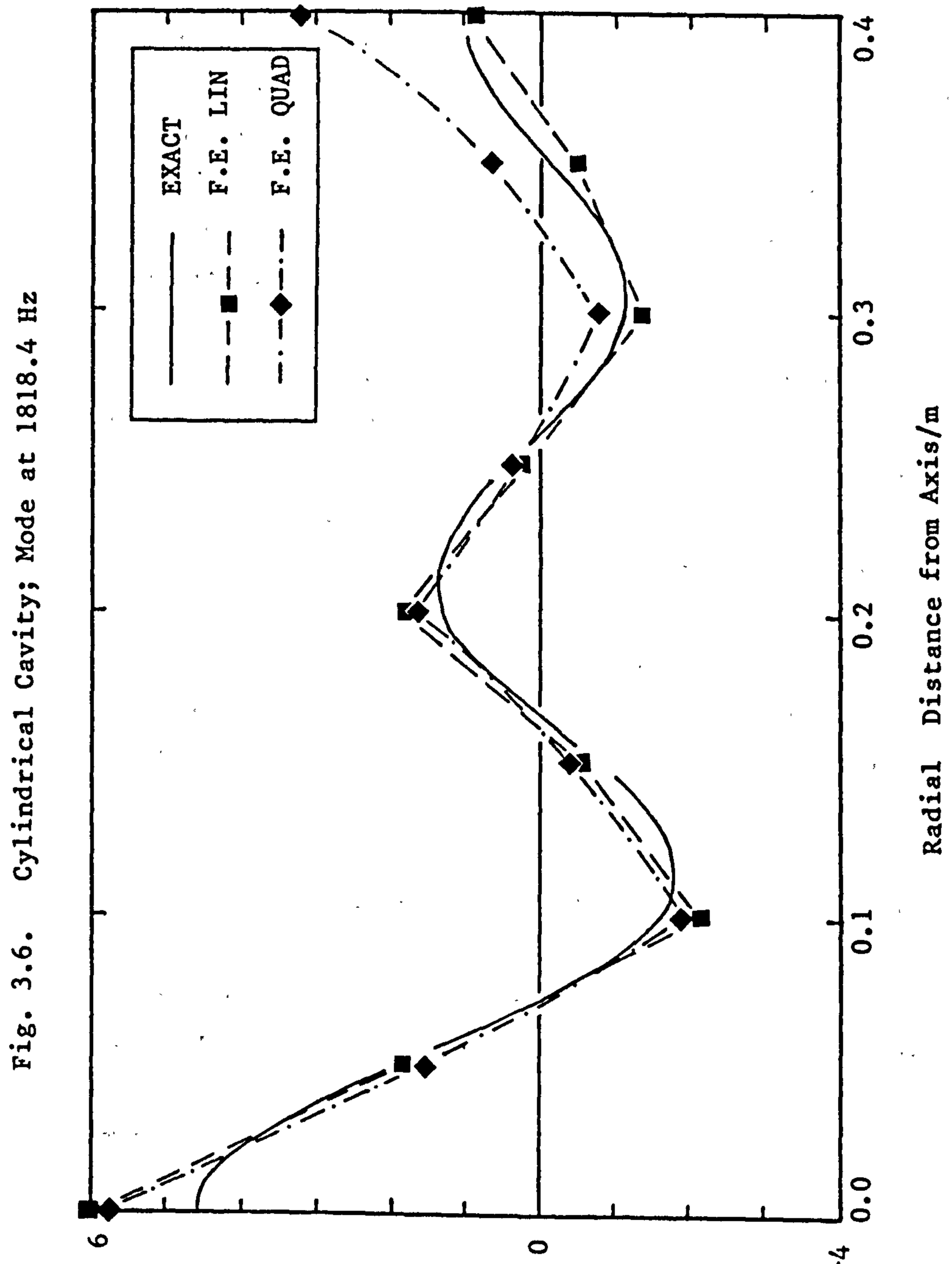


Fig. 3.6. Cylindrical Cavity; M

because the modes invariably become more complicated with increasing frequency, and the finite element mesh is less able to provide a good approximation. When this happens the computed mode shapes tend to exhibit sharp discontinuities at the boundaries between elements, and a poor approximation to the boundary conditions at the surface. Thus by inspecting these modes it is usually possible to gain some idea of the validity of the solution, and if it is suspect a finer mesh must be used.

The finite element analyses give only as many resonances as there are degrees of freedom, while in theory any cavity has an infinite number of resonances (Morse and Ingard (10) discuss average modal densities when relating wave acoustics to geometrical acoustics). If the mesh is sufficiently fine, it will be possible by inspection to establish a one-to-one correspondence between computation and exact theory for a few of the lowest frequency modes, but at higher frequencies the correspondence becomes less distinct and eventually disappears.

In all cases, excepting the one instance for the rectangular cavity mentioned earlier, the quadratic element provides more accurate resonant frequencies than the linear element thus reinforcing the prevalent view that a few high order elements are usually better than many low order elements.

## 3.5 Analysis of a Model Car Cavity

Jha and Cheilas describe experimental measurements of the resonant frequencies of a half-scale perspex model of a car passenger compartment in references (18) and (32). This cavity was prismatic, and is thus capable of being theoretically analysed using the procedures described in section 3.2.

The two-dimensional subdivision of the cavity is shown in figure 3.7, and this has 109 nodes. Again the finite element solutions were carried out using both linear and quadratic elements (numbering 176 and 44 respectively). The first five of the resulting two-dimensional resonant frequencies are shown in table 3.3, along with the measured results. As in the previous examples, quadratic elements give the better results.

The two-dimensional mode shapes for the quadratic element analysis are shown in figures 3.8-3.12 as contour plots of pressure amplitude. The scaling is arbitrary and chosen to give a suitable visual representation, so the modes are not normalised. On the plot for the mode at 175.1 Hz, the measured position of the nodal plane is shown.

The three-dimensional resonant frequencies were calculated using equation 3.6 and these are listed in table 3.4 showing their relationship to the two-dimensional resonances. The width of the cavity, a, was 0.65m. The zero-frequency mode must be included, and the three-dimensional modes resulting from this consist of plane standing waves across the width of the cavity.

The resonant frequencies were placed in ascending order, and these are compared with the measured values in table 3.5.

The frequencies for the full-scale case will be half those of the model. The two lowest resonances therefore occur at about 86 Hz and 132 Hz. A point of some interest is the closely spaced resonances at about 155Hz, 158Hz and 165Hz.

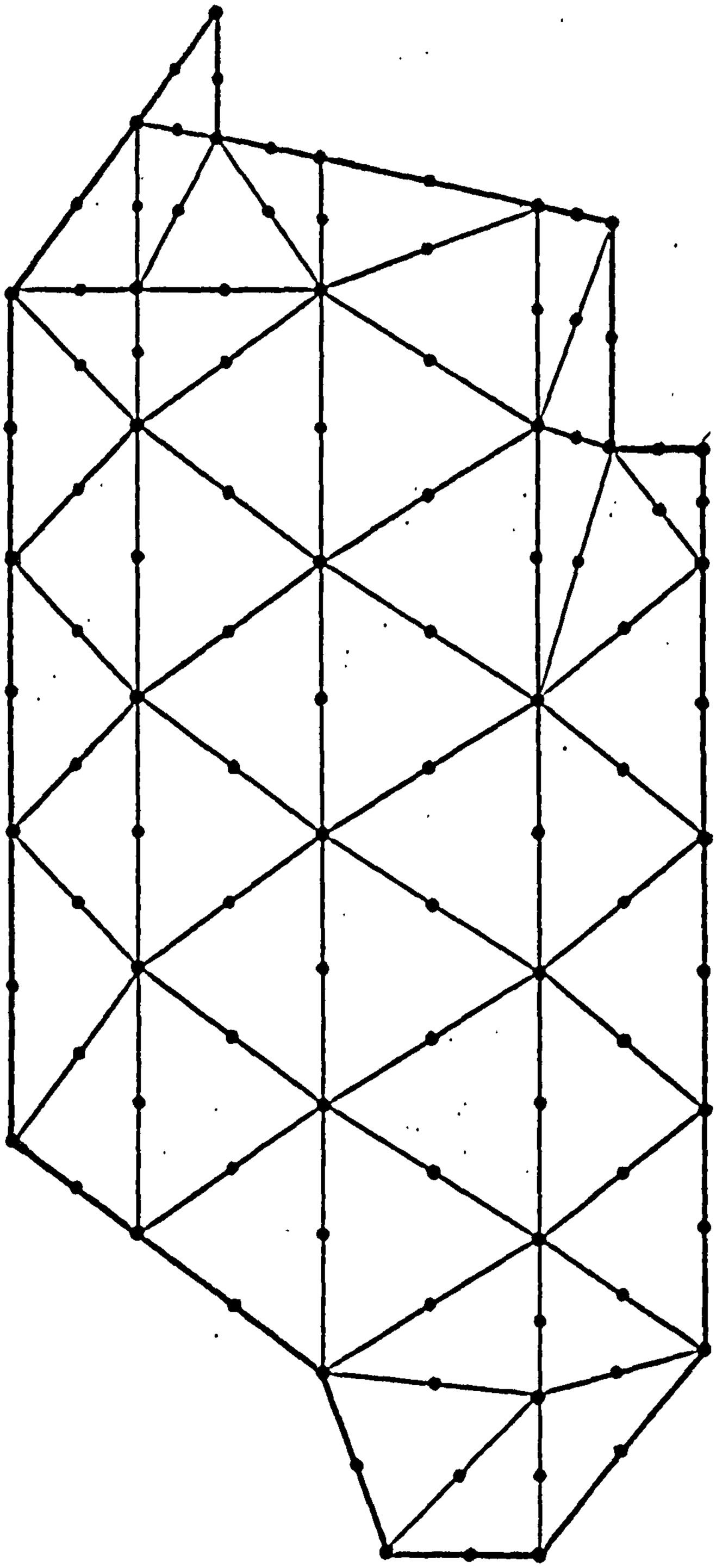

44 ELEMENTS 109 NODES

Fig. 3.7 Finite Element Subdivision of the Cube Car Cavity

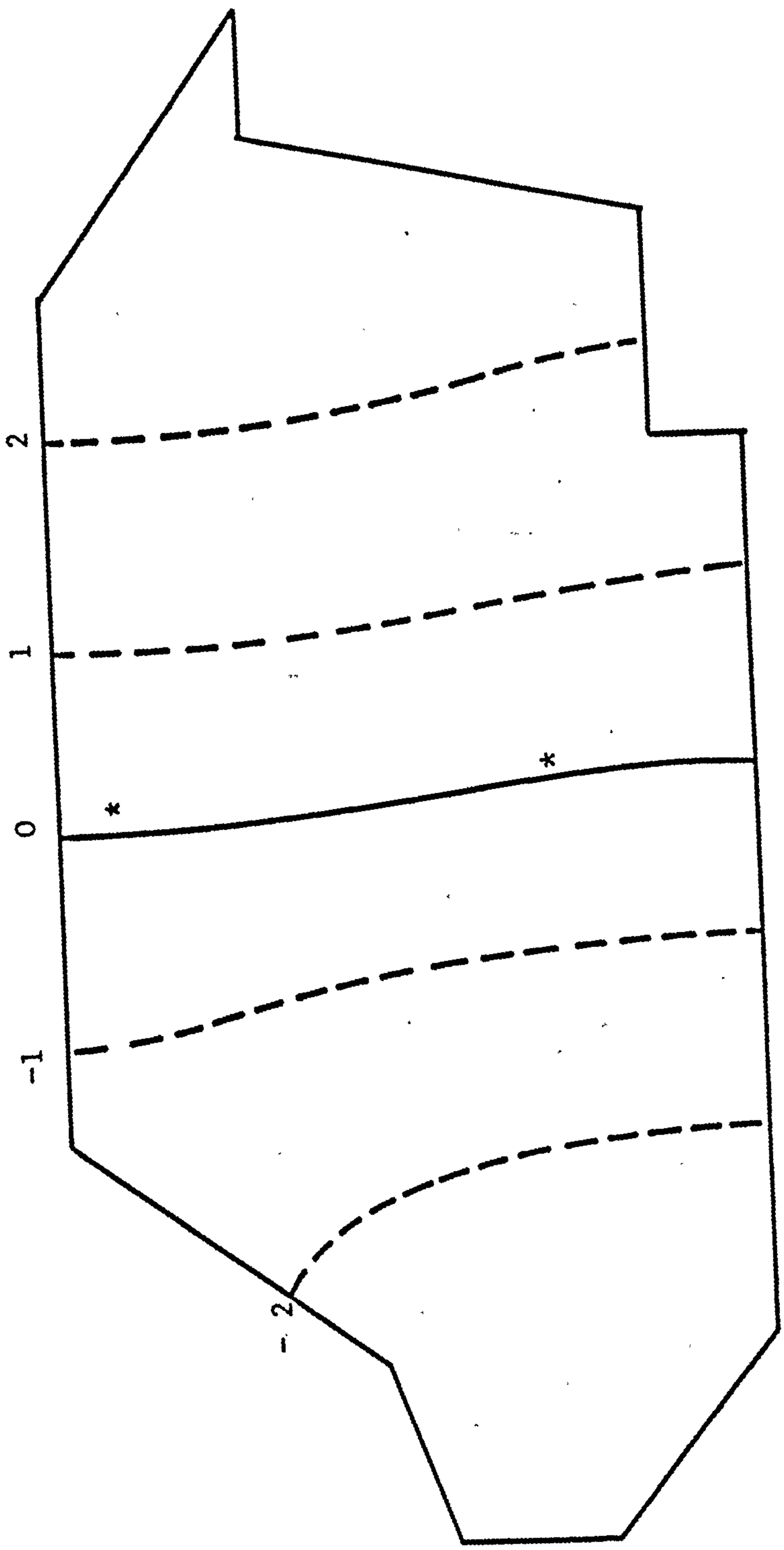


Fig.3.8 Mode @ 175.1 Hz

* Measured position of nodal plane.

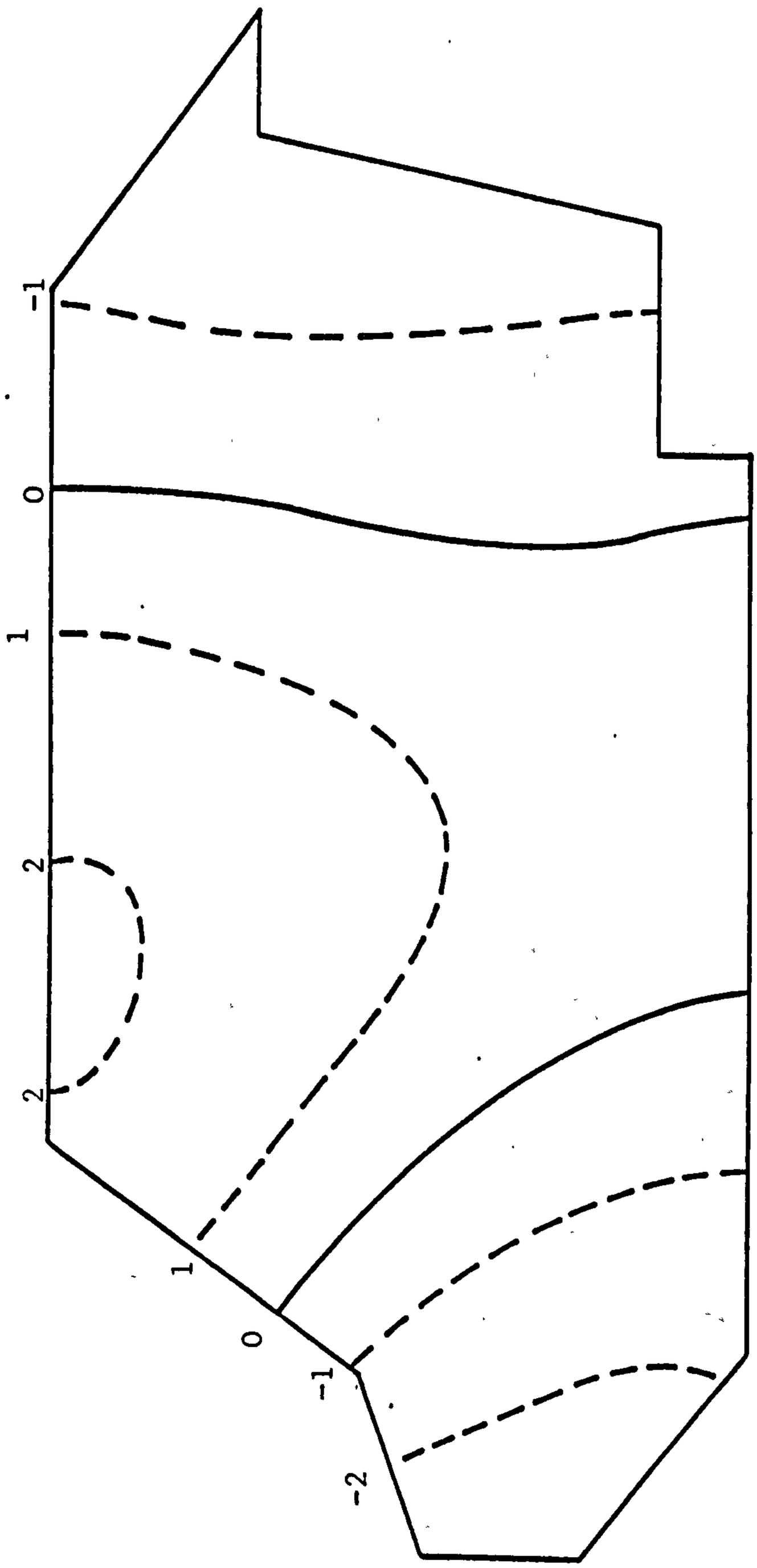


FIG. 3.9 Mode at 309.6Hz

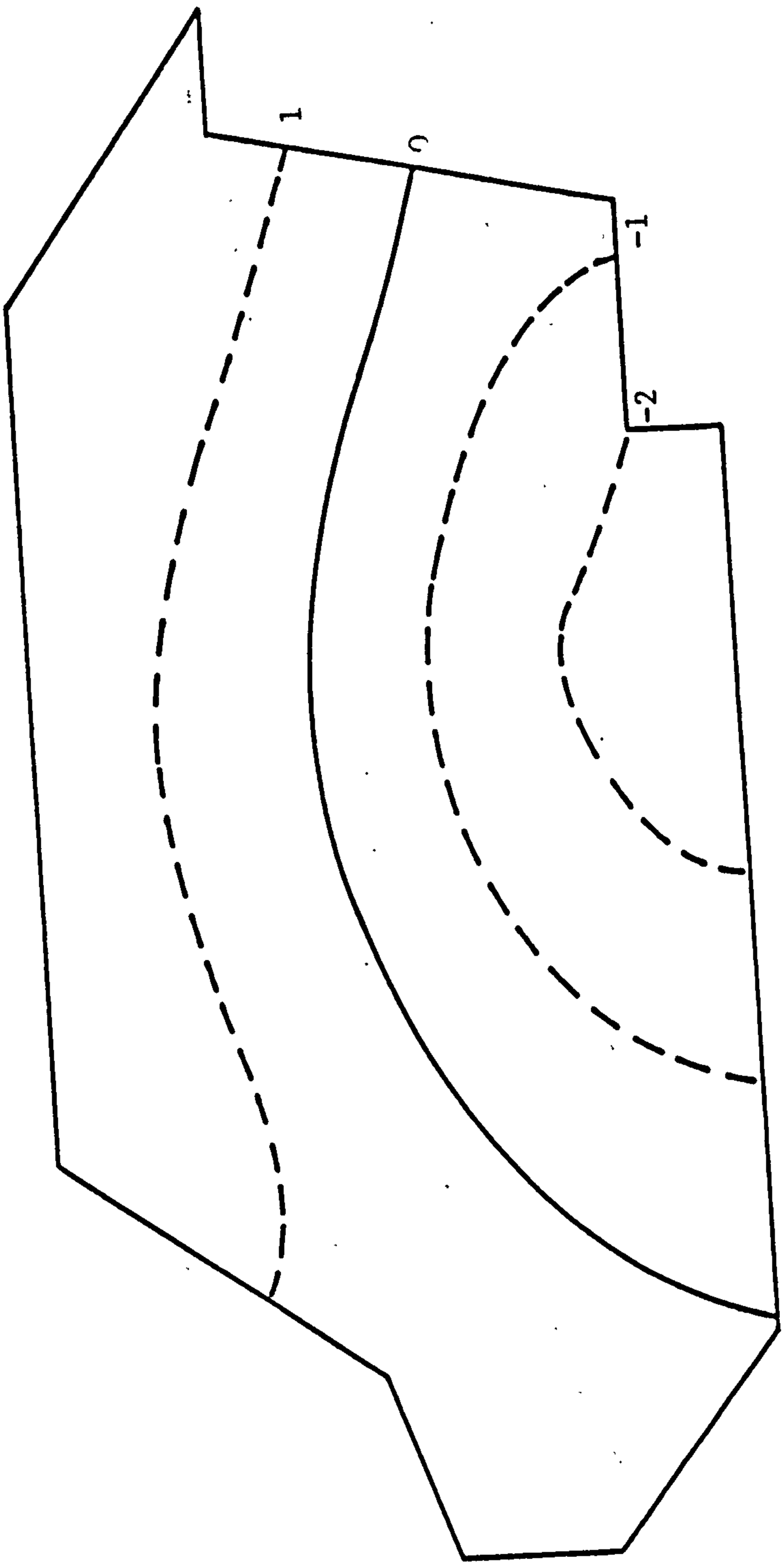


FIG. 3.10 Mode at 330.2Hz

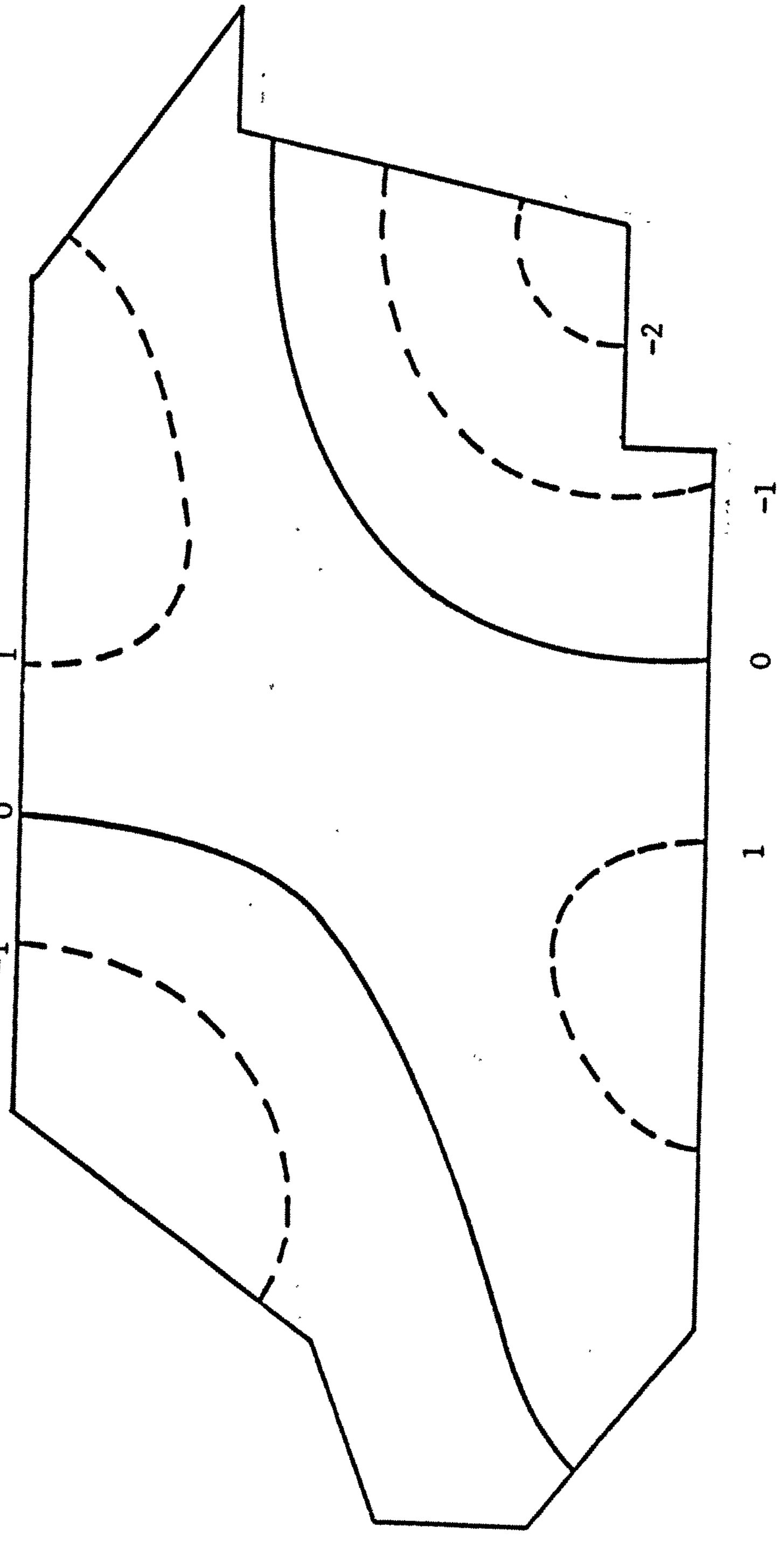


Fig. 3.11 Mode at 427.3Hz

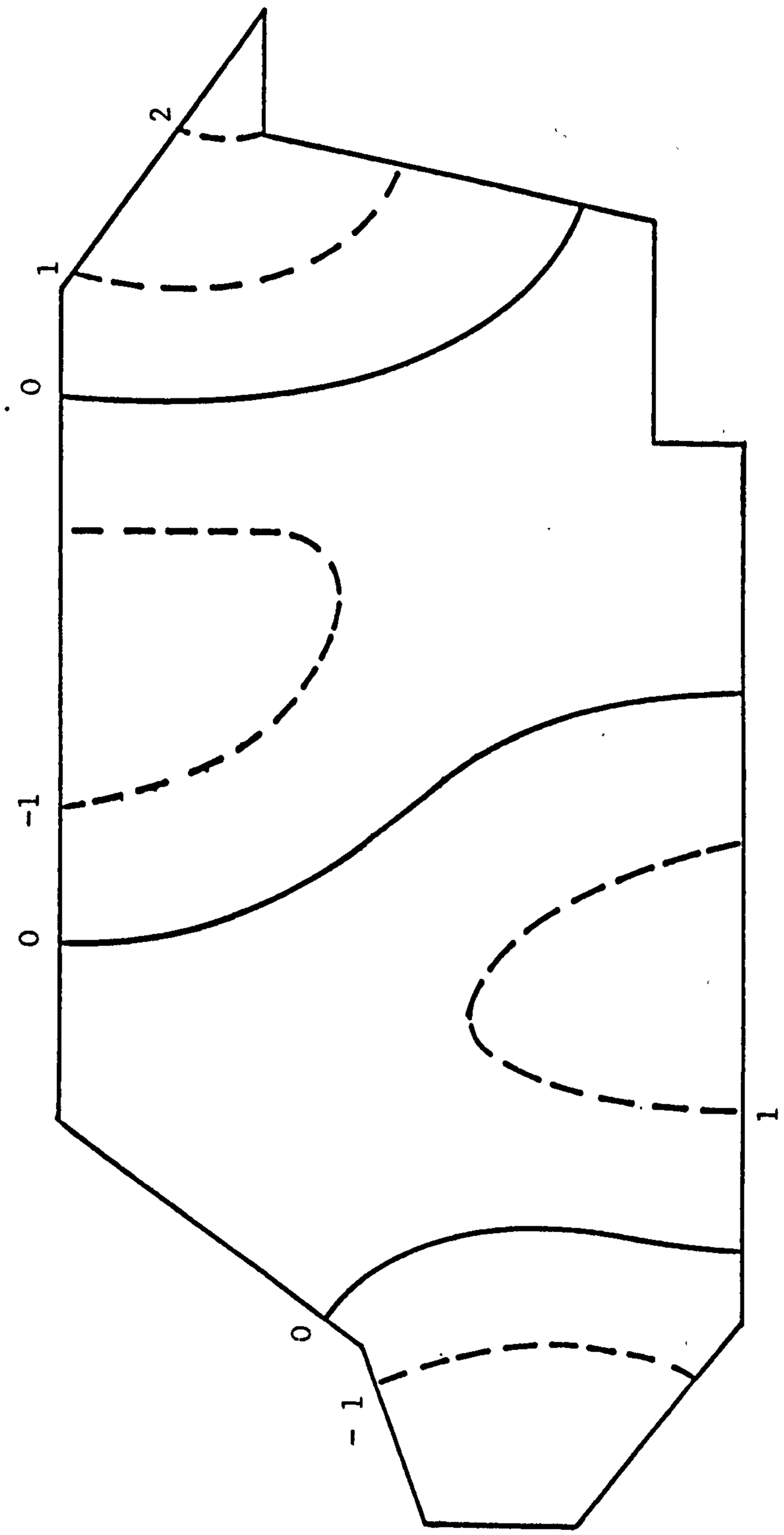


Fig. 3.12 Mode at 455.1 Hz

Table 3.4 The Two-Dimensional Resonant Frequencies of the Car Cavity and the Calculated Three-Dimensional Resonances

| n | $f_n$(Hz) |
|---|---|
| 0 | 0.0 * |
| 1 | 263.8 |
| 2 | 527.7 |
| 0 | 175.1 * |
| 1 | 316.7 |
| 2 | 556.0 |
| 0 | 309.6 * |
| 1 | 406.8 |
| 2 | 611.8 |
| 0 | 330.2 * |
| 1 | 422.7 |
| 2 | 622.5 |
| 0 | 427.3 * |
| 1 | 502.2 |
| 2 | 679.0 |
| 0 | 455.1 * |
| 1 | 526.1 |
| 2 | 696.8 |

* Two-Dimensional Resonances

Table 3.5 Comparison of Calculated and Measured Resonant Frequencies of the Car Cavity

| Computed (Hz) | Measured (Hz) |
|---|---|
| 175.1 | 175 |
| 263.8 | 264 |
| 309.6 | 309 |
| 316.7 | 317 |
| 330.2 | 322 |
| 406.8 | 407 |
| 422.7 | 421 |
| 427.3 | 426 |
| 455.1 | 452 |
| 502.2 | 500 |
| 526.1 | 522 |

## Appendix 3.I The Finite Element Formulation for Acoustic Cavity Resonance

Acoustic cavity resonance is governed by the Helmholtz equation:

$$\frac{\partial^2 P}{\partial x^2} + \frac{\partial^2 P}{\partial y^2} + \frac{\partial^2 P}{\partial z^2} + k^2 P = 0, \qquad (3.I.1)$$

where P is the pressure amplitude and $k = \omega/c$, being the frequency and c the velocity of sound.

Since the surface of the cavity is assumed to be rigid, then the normal component of the particle velocity here must be zero. The amplitude of the particle velocity is proportional to the vector grad P, and if $\partial P/\partial n$ is the normal component,

$$\frac{\partial P}{\partial n} = 0 \qquad (3.I.2)$$

everywhere on the surface of the cavity. This boundary condition has to be obeyed by any solution to equation 3.I.1.

## Euler's Theorem of Variational Calculus

The relevant details of the proof of this theorem are given by Zienkiewicz (33). The theorem states that for a given volume V bounded by a surface S with:

$$\chi = \int_V f(x,y,z,\phi,\phi_x,\phi_y,\phi_z)\, dV$$

$$+ \int_S (q\phi + \alpha\phi^2)\, dS \qquad (3.I.3)$$

where

$$\phi_x = \frac{\partial \phi}{\partial x}\ , \text{ etc.,}$$

then if $\chi$ is a minimum f obeys the equations:

$$\frac{\partial f}{\partial \phi} - \frac{\partial}{\partial x}\left(\frac{\partial f}{\partial \phi_x}\right) - \frac{\partial}{\partial y}\left(\frac{\partial f}{\partial \phi_y}\right) - \frac{\partial}{\partial z}\left(\frac{\partial f}{\partial \phi_z}\right) = 0 \qquad (3.I.4)$$

everywhere in the volume V, and

$$l_x \frac{\partial f}{\partial \phi_x} + l_y \frac{\partial f}{\partial \phi_y} + l_z \frac{\partial f}{\partial \phi_z} + q + \alpha\phi = 0 \qquad (3.I.5)$$

everywhere on the surface S. $l_x$, $l_y$, $l_z$ are the direction cosines of the normal to S with the co-ordinate axes.

With $\phi$=P, it is now necessary to find a function f such that equations 3.I.4 and 3.I.5 become equations 3.I.1 and 3.I.2 respectively. It can be verified that a suitable function is:

$$f = \left(\frac{\partial P}{\partial x}\right)^2 + \left(\frac{\partial P}{\partial y}\right)^2 + \left(\frac{\partial P}{\partial z}\right)^2 - k^2P^2 \qquad (3.I.6)$$

with $q=\alpha=0$. Note that:

$$l_x \frac{\partial P}{\partial x} + l_y \frac{\partial P}{\partial y} + l_z \frac{\partial P}{\partial z} \equiv \frac{\partial P}{\partial n}$$

The functional $\chi$ to be minimised is now given by:

$$\chi = \tfrac{1}{2} \int_V \left[\left(\frac{\partial P}{\partial x}\right)^2 + \left(\frac{\partial P}{\partial y}\right)^2 + \left(\frac{\partial P}{\partial z}\right)^2\right] dV$$

$$- \tfrac{1}{2} k^2 \int_V P^2 \, dV \qquad (3.I.7)$$

and with the problem stated in this way it is now suitable for solution by finite element techniques.

## The Finite Element Formulation

The volume V is divided into a number of finite elements, with the pressure amplitude distribution P(x,y,z) defined by the finite number of values at the nodes of the elements. If N is the number of nodes, then the nodal values of P can be listed in the vector:

$$\{P\} = \begin{Bmatrix} P_1 \\ P_2 \\ \cdot \\ \cdot \\ \cdot \\ P_N \end{Bmatrix}$$

It is with respect to this vector that the functional $\chi$ is to be minimised, and this is achieved if:

$$\frac{\partial \chi}{\partial P_i} = 0 , \quad i = 1, 2 \ldots N \qquad (3.I.8)$$

Because $\chi$ takes the form of an integral over the volume V, it can be expressed as a sum of contributions $\chi_e$ obtained by integration over each element individually, that is:

$$\chi = \Sigma \chi_e \qquad (3.I.9)$$

A typical equation 3.I.8 becomes:

$$\frac{\partial \chi}{\partial P_i} = \Sigma \frac{\partial \chi_e}{\partial P_i} = 0 \qquad (3.I.10)$$

where the summation is carried out over all the elements (although normally $\partial\chi_e/\partial P_i = 0$ for elements not sharing the ith node).

Because P(x,y,z) within each element can be expressed in terms of the nodal values then the contribution $\chi_e$ and hence the terms $\partial\chi_e/\partial P_i$ can be determined.

If P(x,y,z) is a linear combination of the nodal values, then it can be written as:

$$P = N_1P_1 + N_2P_2 + \ldots.$$

$$= \begin{bmatrix} N_1 & N_2 & N_3 & \ldots. \end{bmatrix} \begin{Bmatrix} P_1 \\ P_2 \\ \cdot \\ \cdot \\ \cdot \end{Bmatrix}$$

or
$$P = [N] \{P\}_e \qquad (3.I.11)$$

where $\{P\}_e$ is a vector listing the values of P at the nodes of the element under consideration. The matrix $[N]$ is a function of the spatial co-ordinates, and its form depends on the type of element used, although in most cases it will be a polynomial. Clearly

$N_i = 1$ at the ith node

and $N_i = 0$ at all other nodes.

The contribution $\chi_e$ to the functional is given by:

$$\chi_e = \tfrac{1}{2} \int_V \left[ \left(\frac{\partial P}{\partial x}\right)^2 + \left(\frac{\partial P}{\partial y}\right)^2 + \left(\frac{\partial P}{\partial z}\right)^2 \right] dV$$

$$- \tfrac{1}{2} k^2 \int_V P^2 \, dV$$

where the integration is now carried out over the volume of the element. Differentiating with respect to $P_i$ gives:

$$\frac{\partial \chi_e}{\partial P_i} = \int_V \left[ \frac{\partial P}{\partial x} \frac{\partial}{\partial P_i}\left(\frac{\partial P}{\partial x}\right) + \frac{\partial P}{\partial y} \frac{\partial}{\partial P_i}\left(\frac{\partial P}{\partial y}\right) + \frac{\partial P}{\partial z} \frac{\partial}{\partial P_i}\left(\frac{\partial P}{\partial z}\right) \right] dV$$

$$- k^2 \int_V P \frac{\partial P}{\partial P_i} \, dV \qquad (3.I.12)$$

Using equation 3.I.11 we obtain:

$$\frac{\partial P}{\partial x} \frac{\partial}{\partial P_i}\left(\frac{\partial P}{\partial x}\right) = \frac{\partial N_i}{\partial x}\left[\frac{\partial N}{\partial x}\right]\{P\}_e \quad \text{etc.}$$

and

$$P \frac{\partial P}{\partial P_i} = N_i \, [N]\{P\}_e \ ,$$

and these equations can be rewritten as:

$$\frac{\partial P}{\partial x}\ \frac{\partial}{\partial P_i}\left(\frac{\partial P}{\partial x}\right) = \sum_j \frac{\partial N_i}{\partial x}\ \frac{\partial N_j}{\partial x}\ P_j \qquad \text{etc.}$$

and

$$P\ \frac{\partial P}{\partial P_i} = \sum_j N_i\ N_j\ P_j$$

Substitution into equation 3.I.12 gives:

$$\frac{\partial \chi_e}{\partial P_i} = \sum_j \left[\int_V \left(\frac{\partial N_i}{\partial x}\ \frac{\partial N_j}{\partial x} + \frac{\partial N_i}{\partial y}\ \frac{\partial N_j}{\partial y} + \frac{\partial N_i}{\partial z}\ \frac{\partial N_j}{\partial z}\right) dV\right] P_j$$

$$- k^2 \sum_j \left[\int_V N_i\ N_j\ dV\right] P_j$$

and these equations can be rewritten in matrix form as:

$$\frac{\partial \chi}{\partial \{P\}_e} \equiv \begin{Bmatrix} \frac{\partial \chi_e}{\partial P_1} \\ \frac{\partial \chi_e}{\partial P_2} \\ \cdot \\ \cdot \\ \cdot \end{Bmatrix} = [k]_e \{P\}_e - k^2 [m]_e \{P\}_e \qquad (3.I.13)$$

where the elements of the matrices $[k]_e$ and $[M]_e$ are given by:

$$k_{ij} = \int_V \left( \frac{\partial N_i}{\partial x} \frac{\partial N_j}{\partial x} + \frac{\partial N_i}{\partial y} \frac{\partial N_j}{\partial y} + \frac{\partial N_i}{\partial z} \frac{\partial N_j}{\partial z} \right) \, dV \qquad (3.I.14)$$

and

$$m_{ij} = \int_V N_i \, N_j \, dV \qquad (3.I.15)$$

Equations 3.I.10 may also be written as a matrix equation:

$$[K]\{P\} - k^2[M]\{P\} = 0 \, , \qquad (3.I.16)$$

an eigenvalue problem which may be solved numerically to fund the natural frequencies and modes of the cavity.

The matrices $[K]$ and $[M]$ are obtained as an assembly of the element matrices $[k]_e$ and $[m]_e$, the positioning of which depends on the relation between the local nodal numbering in each element and the numbering in the overall system.

Normalisation

It will be desirable in many cases to obtain normalised modes such that:

$$\int_V \phi_i^2 \, dV = 1 \qquad (3.I.17)$$

The finite element approximation to the mode $\phi_i(x,y,z)$ is defined by $\{\phi_i\}$ which is an eigenvector of equation 3.I.16, and within a given element:

$$\phi_i (x,y,z) = [N]\{\phi_i\}_e$$

Squaring this equation gives:

$$\phi_i^2 = [N]\{\phi_i\}_e \, [N]\{\phi_i\}_e$$

$$= \{\phi_i\}_e^T \, [N]^T \, [N]\{\phi_i\}_e$$

and the contribution of the element to the integral in equation 3.I.17 is equal to:

$$\{\phi_i\}_e^T \left( \int_V [N]^T [N] \, dV \right) \{\phi_i\}_e$$

Using equation 3.I.15 gives:

$$\int_V [N]^T [N] \, dV = [m]_e$$

so the element contribution becomes:

$$\{\phi_i\}_e^T [m]_e \{\phi_i\}_e^T$$

Summation of these terms over all the elements gives the required integral, and this procedure is identical to the assembly which forms equation 3.I.16. Therefore correct normalisation is achieved if:

$$\{\phi_i\}^T [M] \{\phi_i\} = 1 \qquad (3.I.18)$$

# Appendix 3.II Derivation of Linear and Quadratic Triangular Element Matrices; The Finite Element Computer Program

## The Linear Element

This type of triangular element has three nodes (one at each vertex) which are, by convention, numbered in an anti-clockwise fashion. The variation of the pressure amplitude P(x,y,z) is expressed as a linear combination of the nodal values, that is:

$$P = N_1P_1 + N_2P_2 + N_3P_3$$

$$\text{or} \quad P = [N]\{P\}_e \qquad (3.II.1)$$

$N_1$, $N_2$, $N_3$ are functions of position, and it is necessary that:

$N_i = 1$ at the ith node

and $N_i = 0$ at all other nodes.

While a suitable $[N]$ matrix could be found in terms of the x and y co-ordinates of the element plane, it is more convenient to define a new set of co-ordinates which are particularly suitable for triangular elements (33). The triangle is divided into three areas $A_1$, $A_2$, $A_3$ as follows:

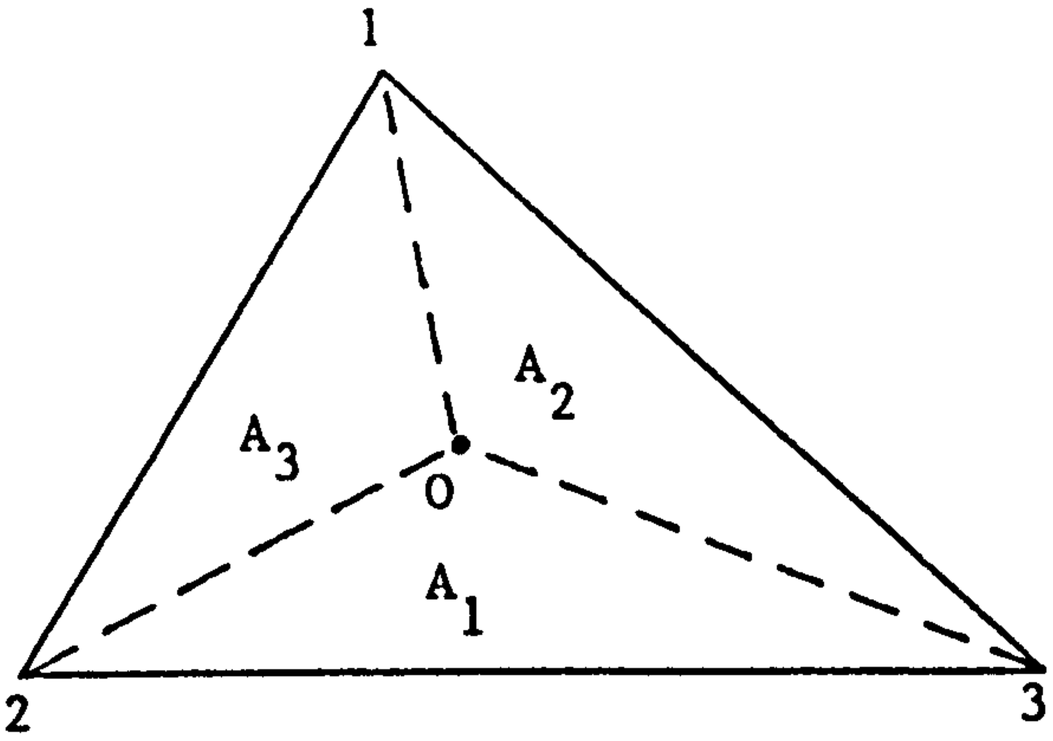


The position of the point 0 may be defined in terms of the three 'area co-ordinates' $L_1$, $L_2$, $L_3$ where:

$$L_1 = \frac{A_1}{\Delta}$$

$$L_2 = \frac{A_2}{\Delta}$$

$$L_3 = \frac{A_3}{\Delta}$$

and $\Delta$ is the area of the triangle.

The area co-ordinates are linearly related to the x and y co-ordinates, and it can be shown that:

$$L_1 = (a_1 + b_1x + c_1y) \;/\; 2\Delta$$

$$L_2 = (a_2 + b_2x + c_2y) \;/\; 2\Delta \qquad (3.II.2)$$

$$L_3 = (a_3 + b_3x + c_3y) \;/\; 2\Delta$$

where

$$a_1 = x_2y_3 - x_3y_2$$

$$b_1 = y_2 - y_3 \qquad (3.II.3)$$

$$c_1 = x_3 - x_2 \quad \text{etc.} \qquad (3.II.4)$$

and $x_1, y_1$ etc. are the co-ordinates of the vertices of the triangle.

The area of the triangle, $\Delta$, is given by:

$$\Delta = \tfrac{1}{2} \det \begin{vmatrix} 1 & x_1 & y_1 \\ 1 & x_2 & y_2 \\ 1 & x_3 & y_3 \end{vmatrix} \qquad (3.II.5)$$

It is important to adhere to the anti-clockwise numbering scheme, because otherwise equation 3.II.5 yields a negative value for the area of the triangle.

It can be easily verified that the area co-ordinates themselves are suitable shape functions for the linear triangle, so that:

$$P = L_1P_1 + L_2P_2 + L_3P_3, \qquad (3.II.6)$$

that is, $N_1 = L_1$ etc.

Taking into account the fact that there is no variation of P in the z direction, the expressions for the element matrices in appendix 3.I become:

$$k_{ij} = a \int\int \left( \frac{\partial N_i}{\partial x} \frac{\partial N_j}{\partial x} + \frac{\partial N_i}{\partial y} \frac{\partial N_j}{\partial y} \right) \, dx \, dy \qquad (3.II.7)$$

and

$$m_{ij} = a \int\int N_i \, N_j \, dx \, dy \qquad (3.II.8)$$

where a is the width of the cavity in the z direction and the integrations are carried out over the plane of the element. Noting that:

$$\frac{\partial L_i}{\partial x} = \frac{b_i}{2\Delta} \qquad (3.II.9)$$

and

$$\frac{\partial L_i}{\partial y} = \frac{c_i}{2\Delta} \qquad (3.II.10)$$

and making use of the integration formula for area co-ordinates given by Zienkiewicz (33), namely:

$$\iint L_1^{\,p}\, L_2^{\,q}\, L_3^{\,r}\ \ dxdy = \frac{p!q!r!}{(p+q+r+2)!}.2\Delta\ , \qquad (3.II.11)$$

the element matrices may now be evaluated, resulting in:

$$k_{ij} = \frac{a}{4\Delta}\,(b_i b_j + c_i c_j) \qquad (3.II.12)$$

and

$$m_{ij} = \frac{a\Delta}{6} \qquad \text{for } i = j$$

$$= \frac{a\Delta}{12} \qquad \text{for } i \neq j \qquad (3.II.13)$$

The Quadratic Element

This more complex element has six nodes, the extra three nodes being situated at the mid-sides. The following numbering scheme has been chosen:

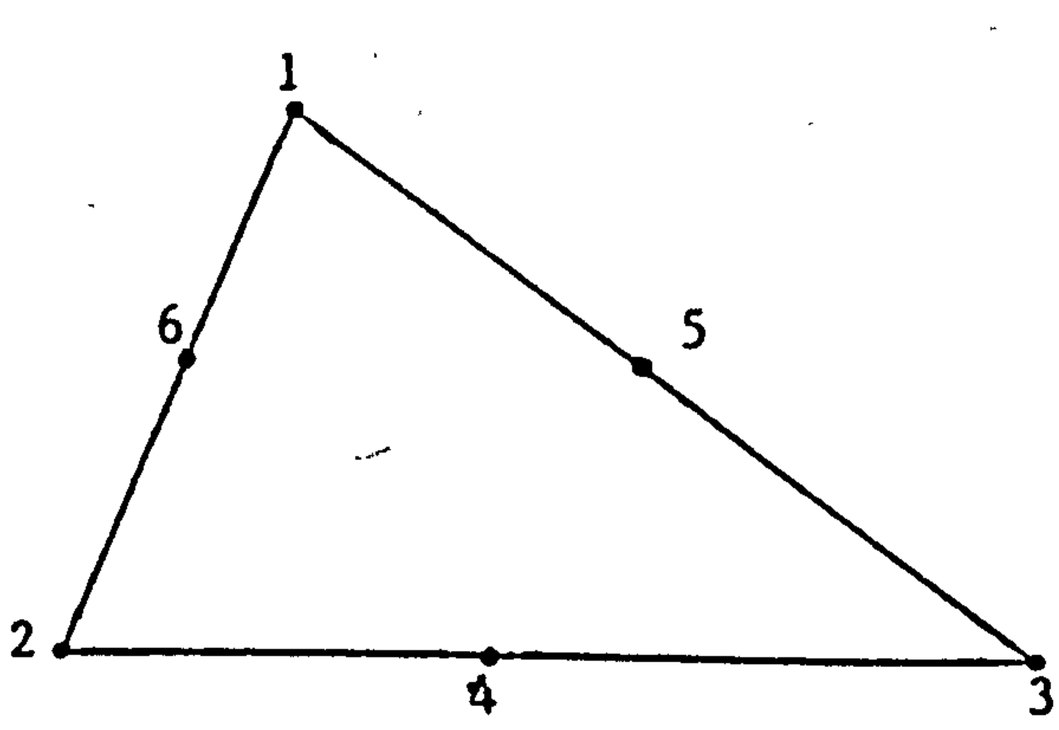

Suitable shape functions for the quadratic triangle are:

$$N_1 = 2L_1^2 - L_1$$

$$N_2 = 2L_2^2 - L_2$$

$$N_3 = 2L_3^2 - L_3$$

$$N_4 = 4L_2L_3$$

$$N5 = 4L_3L_1$$

$$N_6 = 4L_1L_2 \quad ,$$

and these equations, along with equations 3.II.7 to 3.II.11 are used to evaluate the element matrices. These manipulations are straightforward but rather tedious, so they are not included here.

The matrix $[k]_e$ can be split into two separate matrices, such that:

$$[k] = [k_x]_e + [k_y]_e$$

and the $[k_x]_e$ matrix is given by equation 3.II.14. The $[k_y]_e$ matrix has exactly the same form, but the entries are expressed in terms of $c_1$ etc. rather than $b_1$ etc.

The $[m]_e$ matrix is given by equation 3.II.15.

$$\left[k_x\right]_e = \frac{aA}{4}$$

| | | | | | |
|---|---|---|---|---|---|
| $b_1^2$ | $-1/3\ b_1b_2$ | $-1/3\ b_1b_3$ | 0 | $4/3\ b_1b_3$ | $4/3\ b_1b_2$ |
| $-1/3\ b_2b_1$ | $b_2^2$ | $-1/3\ b_2b_3$ | $4/3\ b_2b_3$ | 0 | $4/3\ b_2b_1$ |
| $-1/3\ b_3b_1$ | $-1/3\ b_3b_2$ | $b_3^2$ | $4/3\ b_3b_2$ | $4/3\ b_3b_1$ | 0 |
| $4/3\ b_1b_2$ | $4/3\ b_2b_1$ | 0 | $4/3(b_2b_3+b_1b_2^2+2b_1b_3)$ | $4/3(b_1b_3+b_2b_1^2+2b_2b_3)$ | $8/3(b_1^2+b_1b_2+b_2^2)$ |
| $4/3\ b_1b_3$ | 0 | $4/3\ b_3b_1$ | $4/3(b_3b_2+b_1b_3^2+2b_1b_2)$ | $8/3(b_3^2+b_3b_1+b_1^2)$ | $4/3(b_1b_2+b_3b_1^2+2b_3b_2)$ |
| 0 | $4/3\ b_2b_3$ | $4/3\ b_3b_2$ | $8/3(b_2^2+b_2b_3+b_3^2)$ | $4/3(b_3b_1+b_2b_3^2+2b_2b_1)$ | $4/3(b_2b_1+b_3b_2^2+2b_3b_1)$ |

Equation 3.II.14

Equation 3.II.15

$$[m]_e = a\Delta \begin{bmatrix} 1/30 & -1/180 & -1/180 & -1/45 & 0 & 0 \\ -1/180 & 1/30 & -1/180 & 0 & -1/45 & 0 \\ -1/180 & -1/180 & 1/30 & 0 & 0 & -1/45 \\ -1/45 & 0 & 0 & 8/45 & 4/45 & 4/45 \\ 0 & -1/45 & 0 & 4/45 & 8/45 & 4/45 \\ 0 & 0 & -1/45 & 4/45 & 4/45 & 8/45 \end{bmatrix}.$$

## The Finite Element Computer Programs

The computer programs using linear and quadratic elements were written in FORTRAN and run on an ICL 1903T computer in batch mode. A flow chart for the program using quadratic elements is shown in figure 3.II.1. The necessary input data are:

NVERT — The number of nodes at triangle vertices.

NELEM — The number of elements.

NPTS — The total number of nodes (equal to NVERT when using linear elements).

A — The width of the cavity in the z direction.

C — The velocity of sound.

NRES — The number of resonant modes to be output (it will usually be somewhat wasteful and unnecessary to output all the modes especially for large problems).

X(I) — The x co-ordinate of the Ith vertex.

Y(I) — The y co-ordinate of the Ith vertex.

NOD(J,K) — The node number in the overall system of the Kth node of the Jth element. (K = 1,3 for linear elements; K = 1,6 for quadratic elements).

The flow chart up to point 10 deals with the input section of the program.

It is then necessary to set up the overall system matrices [K] and [M], which is done by taking each element in turn, calculating its element matrices and adding them to the overall matrices. The triangle parameters $b_i$, $c_i$,$\Delta$ are first computed according to equations 3.II.3 - 3.II.5, which enables the $[k]_e$ and $[m]_e$ matrices to be calculated using equations 3.II.12 and 3.II.13 for linear elements, or equations 3.II.14 and 3.II.15 for quadratic elements. The entries in the element matrices are then individually added to the appropriate positions in the overall matrices. The array NOD(J, K) determines this positioning: the entry at the position (K,L) in the Jth element matrix is added to the overall matrix in the position (NOD(J,K), NOD(J,L)).

When assembly is complete the solution routine is called, and this was selected from the NAG subroutine library. NRES resonant frequencies and modes are then output on a lineprinter.

The size of the problem that can be handled by such a program is limited by the storage required, which is chiefly occupied by the [K] and [M] matrices. Considerable economies could be made by taking advantage of the inherent sparsity of finite element matrices, although this was not done here. It should be noted in this context that matrices obtained using high order elements will be less sparse than those derived from low order elements, simply because the higher order element shares more nodes. Thus, if the solution routine takes advantage of sparsity, and the same number of degrees of freedom are used for each case, a high order solution will require more storage and time than that for low order elements. This may to some extent offset the gains in accuracy usually expected when using high order elements.

Figure 3.II.1 Flowchart for the Finite Element Program

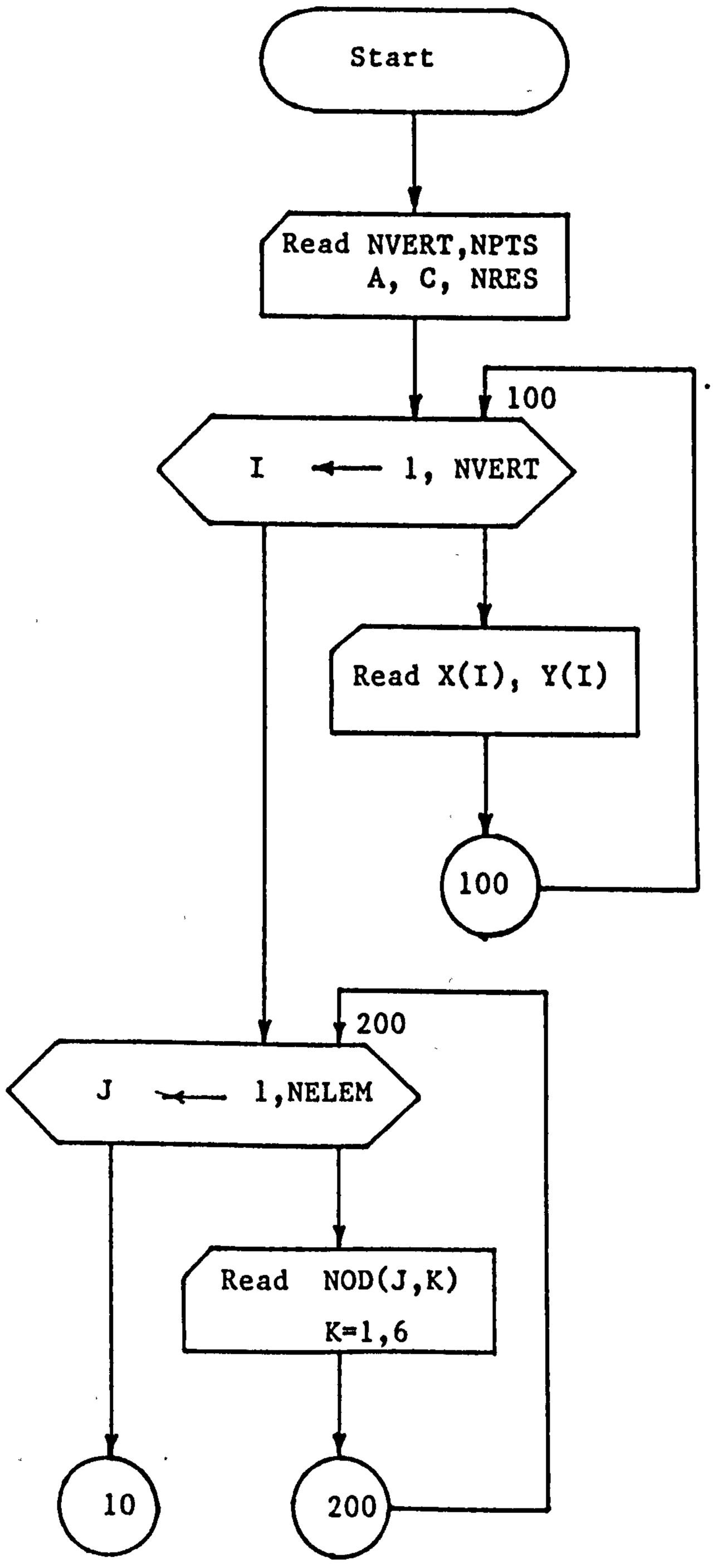


Cont.

Figure 3.II.1 cont.

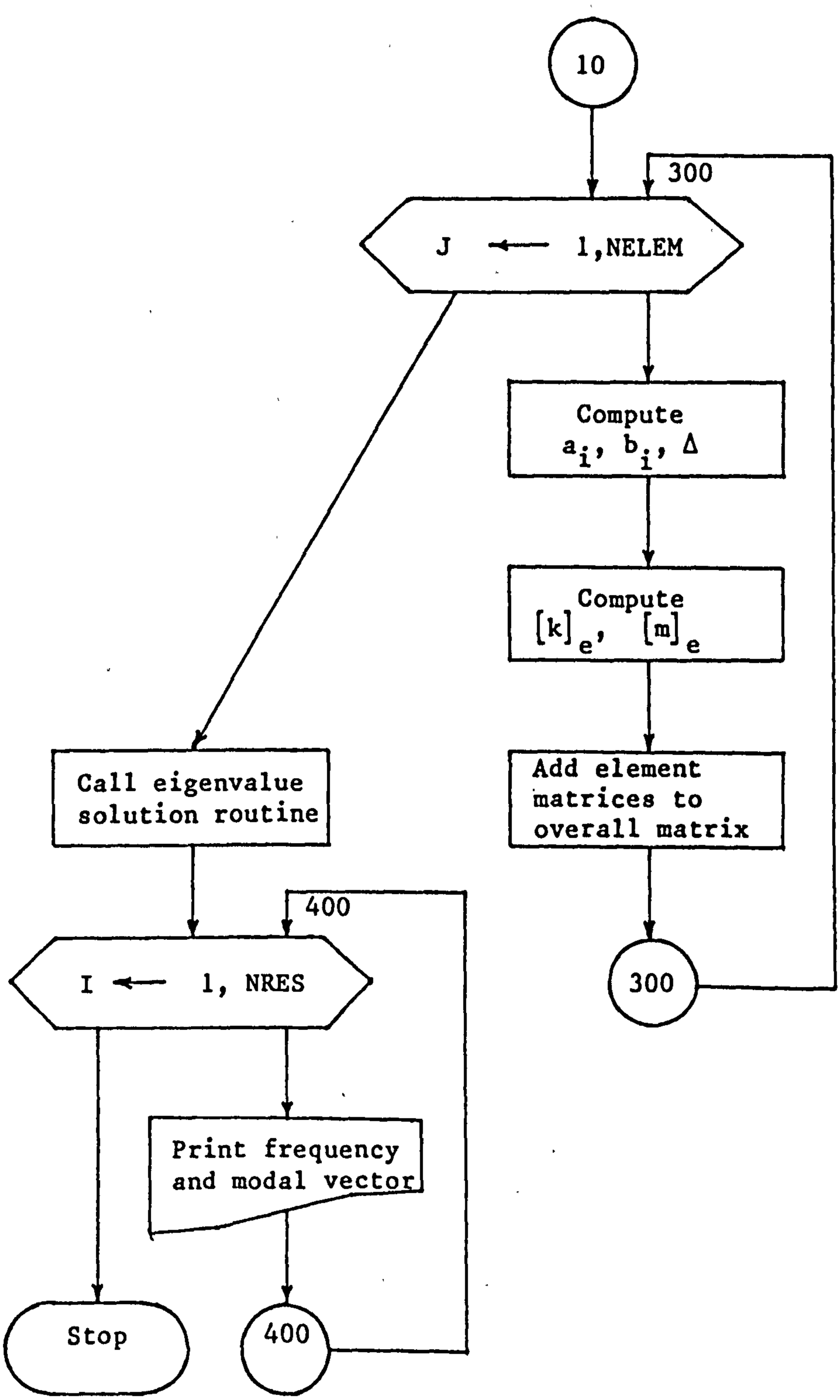

## Appendix 3.III Axisymmetric Resonance of Cylindrical Cavities

Exact solutions for the resonances of a cylindrical cavity can be obtained fairly simply by treating the axisymmetric modes only, such that the pressure amplitude is a function only of the distance r from the axis of the cylinder. For these modes the Helmholtz equation becomes:

$$\frac{d^2P}{dr^2} + \frac{1}{r}\frac{dP}{dr} + k^2P = 0 \qquad (3.III.1)$$

where $k = \omega/c$. This equation can be re-written as:

$$\beta^2 \frac{d^2P}{d\beta^2} + \beta\frac{dP}{d\beta} + \beta^2P = 0 \qquad (3.III.2)$$

where $\beta = kr$.

The only satisfactory solution to equation 3.III.2 is $J_o(\beta)$, the Bessel function of the first kind of order zero. Other solutions have singularities at $\beta=0$ (34).

If the radius of the cavity is R, then the boundary conditions require that:

$$\frac{dP}{dr} = 0 \quad \text{at } r=R$$

that is $kJ_o'(\beta) = 0$ at $\beta=kR$.

However $J_o'(\beta) = -J_1(\beta)$, where $J_1(\beta)$ is the Bessel function of the first kind of order one, so if $\beta_n$ are the roots of $J_1(\beta)$, the resonant frequencies of the cavity are given by:

$$k_n = \frac{\beta_n}{R}$$

that is

$$\omega_n = \frac{c}{R}\beta_n \qquad (3.III.3)$$

To achieve the required normalisation it is necessary to evaluate the integral

$$I = \int_V P^2 \, dV$$

$$= 2\pi h \int_o^R r J_o^2(kr) \, dr$$

where h is the axial length of the cylinder.

Substituting $\beta=kR$ gives:

$$I = \frac{2\pi h}{k^2} \int_0^{kR} \beta \, J_o{}^2(\beta) \, d\beta.$$

Successive manipulations of equation 3.III.2 shows that:

$$\beta J_o{}^2 = \tfrac{1}{2} \frac{d}{d\beta} \left( \beta^2 J_o{}^2 + \beta^2 J_o{}'^2 \right)$$

and integrating this over the given limits, noting that $J_o'(kR) = 0$ at resonance, results in:

$$I = \pi h R^2 J_o{}^2(k_n R)$$

Thus it is necessary to divide $J_o(k_n r)$ by $\sqrt{I}$, resulting in the normalised modes:

$$\phi_n(r) = \frac{J_o(k_n r)}{R J_o(k_n R)} \sqrt{\frac{1}{\pi h}} \qquad (3.III.4)$$

# 4 STRUCTURAL RING MODE VIBRATION

## 4.1 Experimental Determination of the Modes of a Simple Two-Dimensional Ring Structure

It has been described in chapter 1 how the two-dimensional 'ring-modes' about the periphery of the frame surrounding the car passenger compartment contribute significantly to the vibration of the body structure.

In order to investigate this kind of vibration an experimental determination of the modes of a simple steel ring structure was carried out. The shape chosen was that of a longitudinal section through the passenger compartment of a Hillman Avenger car body. The steel used was of section 6" x 0.5".

The ring was suspended from a steel support frame by rubber cords, and this arrangement is shown in figure 4.1, along with the measuring apparatus which was based on rack-mounted equipment made by Spectral Dynamics.

An electro-mechanical vibrator was attached to the underside of the steel ring via an impedance head, which gave outputs proportional to the acceleration and the force applied to the structure.

The system was driven by a variable frequency oscillator, and the sinusoidal output of this was fed to a servo unit which provided control of the signal amplitude. The resulting output was then applied to the vibrator via a power amplifier.

Fig. 4.1. The Steel Ring and Vibration Measurement Apparatus

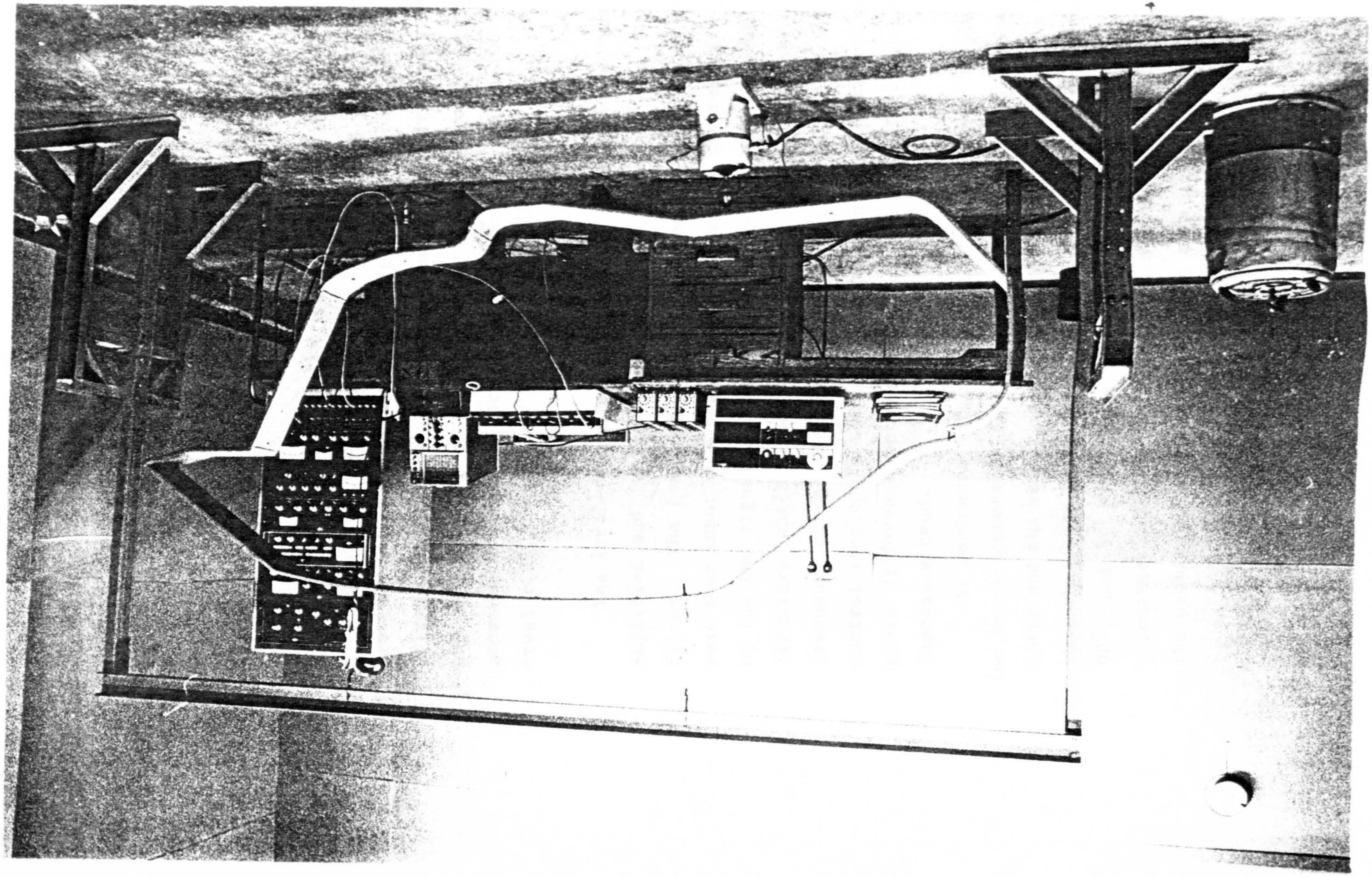

The output of the variable frequency oscillator was also fed into a carrier generator, in which the input signal was used to modulate a 100 kHz carrier. The upper sideband of the resulting signal (at 100 kHz + oscillator frequency) was then used as a reference for a tracking filter.

The force output of the impedance head was amplified and then input to one channel of the tracking filter, which provided as outputs both the filtered signal and a D.C. voltage proportional to its amplitude. The latter was fed to the servo unit, thus completing the control loop which provided a constant force amplitude at the connection to the steel ring.

The acceleration signal from the impedance head was also amplified and fed to the remaining channel of the tracking filter. The resulting signal and the filtered force signal were then input to a phasemeter, which gave the relative phase of the two signals. The phasemeter contained resonant dwell circuitry which produced a voltage used to control the frequency of the oscillator over a small range. This second control loop could then be used to maintain a constant preset phase difference between the force and acceleration at the impedance head.

At resonance, provided there is a dominant single mode, (no near-degeneracy) there is no phase difference between the force and the velocity at the point of excitation. This means that the phase between the force and the acceleration must be $90^{o}$, and by presetting the dwell circuitry to this figure resonance could be accurately maintained. The frequency of the oscillator was measured using a digital counter.

Small accelerometer mounting points were positioned at 44 points around the periphery of the steel ring, so that a single accelerometer could be moved quickly from one point to another. The output of the accelerometer was amplified and then measured using an A.C. digital voltmeter.

The complete apparatus is shown schematically in figure 4.2.

The procedure adopted was to sweep the oscillator frequency from a preset lower limit (about 5 Hz) to the upper limit (about 110 Hz). Careful observation of the acceleration level and its phase with the force acting on the ring allowed the resonant frequencies to be noted. The oscillator frequency was then returned to the lower limit, and the accelerometer was attached to the first point on the structure. The frequency was increased, stopping in the vicinity of each resonance. At these points the resonant dwell circuit was switched on and the system was allowed to stabilise. The accelerometer output as measured by the digital voltmeter was then recorded. On completion of the frequency sweep the oscillator was returned to the lower limit, and the accelerometer was moved to the next position. The process was then repeated for all the points remaining.

To check replication from sweep to sweep, a number were repeated at random throughout the whole series. No significant changes were observed between these and the original measurements.

The results obtained are shown later in comparison with those determined theoretically using finite elements.

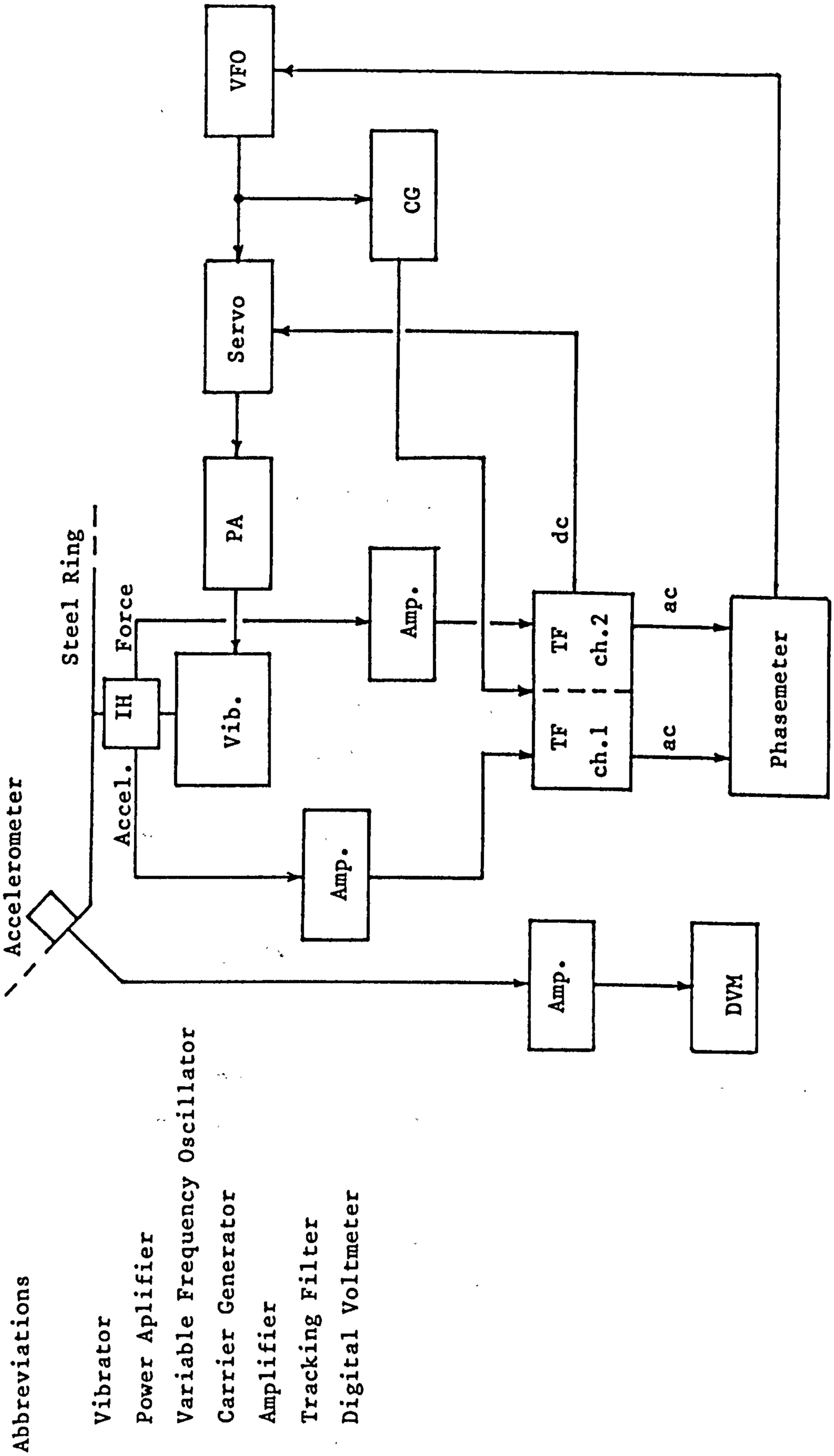


Key to Abbreviations

| | |
|---|---|
| Vib. | Vibrator |
| PA | Power Aplifier |
| VFO | Variable Frequency Oscillator |
| CG | Carrier Generator |
| Amp. | Amplifier |
| TF | Tracking Filter |
| DVM | Digital Voltmeter |

Fig. 4.2. Diagram of the Vibration Measurement Apparatus

## 4.2 Calculation of Ring Modes Using Finite Elements

Zienkiewicz (33) describes how the finite element formulation for the reponse of a linear structure in general results in a matrix equation of the form:

$$[K]\{x\} + [C]\{\dot{x}\} + [M]\{\ddot{x}\} = \{f\} \qquad (4.1)$$

$[K]$, $[C]$ and $[M]$ are respectively the stiffness, damping and mass matrices and $\{x\}$, $\{\dot{x}\}$, $\{\ddot{x}\}$ are the vectors of nodal displacements, velocities and acceleratoins. The vector $\{f\}$ lists the time dependent forces acting on the structure.

In chapter 2 it was described how the response of such a system is often usefully expressed a sum over the normal modes of the free, undamped case, that is the eigensolutions to the matrix equation:

$$[K]\{X\} - \omega^2 [M]\{X\} = 0 \qquad (4.2)$$

The vector $\{X\}$ lists the nodal displacement amplitudes arising from the assumption of a harmonic variation with time such that $\{x\} = \{X\} \exp i\omega t$.

Ring mode vibration has been analysed here using two-dimensional beam elements of the type described by, for example, Livesley in reference (35). These elements have two nodes, one at each end of the beam, and there are two translational and one rotational degree of freedom at each node. It is convenient initially to described the

displacement of each element in its own local co-ordinate system where the x-axis lies along the length of the beam. The displacement, u, in this longitudinal direction is a linear function of x which is uniquely defined by the two nodal values. The transverse displacement v normal to the x-axis is assumed to be independent of u, while the angular rotation $\theta$ at any point is equal to dv/dx. The two nodal rotations along with the two transverse displacements mean that a cubic variation of v, requiring four coefficients, is uniquely defined.

The transformation from the overall co-ordinate system to the local system is effected adequately by a rotation through the angle between the overall, or global, x-axis and the local axis along the element. This transformation can be expressed by the matrix equation:

$$\{X\}'_e = [T]\ \{X\}_e \qquad (4.3)$$

where $\{X\}'_e$ and $\{X\}_e$ list the element nodal displacements and rotations in the local system and the global system respectively. The global element stiffness matrix $[K]_e$ may now be expressed in terms of the local matrix $[K]'_e$ and the matrix of direction cosines $[T]$ as follows:

$$[K]_e = [T]^T[K]'_e\ [T] \qquad (4.4)$$

The global element mass matrix is obtained in the same manner, and this and the stiffness matrix are assembled into the overall system matrices forming equation 4.2.

It is common for the matrix multiplications in equation 4.4 to be carried out explicitly before any numerical computation is carried out, but in this work they were performed numerically. The extra time required for this is not great, and in the examples of structural-acoustic coupling given in the next chapter the matrix [T] is in any case required to calculate the normal displacement amplitudes of the beam elements.

As in the case of acoustic cavity resonance, the propoerties of the matrices in equation 4.2 affect the choice of an economical solution routine. The stiffness matrix is positive semi-definite because the potential energy of the displaced structure must be at least zero, and the mass matrix is positive definite because the kinetic energy of the structure for non-zero displacement velocities must be greater than zero. Both matrices are symmetric. These features are identical to those encountered in the acoustical problem, and exactly the same NAG solution routines were used.

The element matrices are given in appendix 4.I, as are the details of the computer program.

## 4.3 Test Case Results

Physically, there must be three allowable solutions to equation 4.2 for which the resonant frequency is zero. These modes consist of the two rigid body displacements and a single rigid body rotation in which there are no deformations of the structure. Correct finite element analysis gives these modes, so their existence provides a useful check of the program and the input data.

Finite element analyses were made of elliptical rings of differing eccentricity, each having the same circumferential length as the car-shaped ring which was 259 inches. The same beam section was also assumed, that is 6 inches wide and 0.5 inch thick. The material properties used were those of steel (Young's modulus equal to $30 \times 10^6$ psi and density equal to 0.283 lb $in^{-2}$). Five cases were considered, with the ratio of the minor axis to the major axis taking the values 0.2, 0.4, 0.6, 0.8 and 1.0, the last being the special case of a circle. Twenty-five elements were used in each example, giving a total of 75 degrees of freedom.

The exact resonant frequencies of a circular ring are given by Arnold and Warburton (43):

$$f_n = \frac{n(n^2-1)}{\sqrt{n^2+1}} \cdot \frac{1}{2\pi} \sqrt{\frac{EI}{\mu R^4}} \qquad n = 2,3... \qquad (4.5)$$

where E is Young's modulus, I is the second moment of area of the cross-section, $\mu$ the mass per unit length and R the radius of the circle. The order n of the mode is equal to the number of complete wavelengths around the circumference. For a rectangular section, the second moment of area is given by:

$$I = \frac{at^3}{12} ,$$

where a is the width and t is the thickness.

Because of the circular symmetry, a given mode must be able to exist at any angular orientation about the circumference. This can be achieved by allowing any combination of two such shapes displaced from one another by a quarter wavelength (this ensures orthogonality). The resonances are therefore two-fold degenerate, that is two modes exist at each resonant frequency.

The finite element results are shown in table 4.1 along with the exact results for a circle. The derivation of equation 4.5 assumes that elongation of the ring is negligible, a case that would result for very thin beams. Although the finite element analysis allows longitudinal deformation of the elements, inspection of the modal data for the cases considered showed that such displacements were indeed small (about a hundred times less than typical transverse deformations).

The results for the ellipses show the expected splitting of the resonances as the shape departs from that of a circle. An interesting feature is the relatively small splitting for odd order modes. This matter is discussed further in Appendix 4.II.

## 4.4 Comparison of Experimental and Theoretical Results

The dimensions of the car-shaped ring were determined with reasonable accuracy by superimposing a photograph of it on graph paper. From this a 25 element subdivision was made for the finite element analysis.

A post-processing computer program was written which provided a graphical plot of the deformed structure for each mode. The measured results were plotted by hand, and the

theoretical and experimental mode shapes are shown in figures 4.3-4.12. These plots are scaled arbitrarily to give a suitable visual representation.

The resonant frequencies are compared in table 4.2. These occur in pairs, as in the cases of the circle and the ellipse, and the order of each can be established with a reasonable degree of certainty by examination of the modal data.

During the measurements there was some evidence of a resonance at 23.6 Hz, but the response was insufficient to allow the resonant dwell to stablise. This is thought to be due to the existence of a node close to the point of excitation (marked by an arrow on the experimental plots) and this view is supported by the shape of the finite element mode at 22.9 Hz. Similar difficulties were encountered with the resonance at 82.6 Hz, although a reasonable measurement of the mode shape was made, and again the point of excitation is close to a node.

Table 4.1 Resonant Frequencies of Ellipses (Hz)

| n | Circle (exact) | b/a * 1.0 | 0.8 | 0.6 | 0.4 | 0.2 |
|---|---|---|---|---|---|---|
| 2 | 7.35 | 7.4 | 7.3 | 7.1 | 6.7 | 6.4 |
| 2 | | 7.4 | 7.5 | 7.8 | 8.9 | 12.0 |
| 3 | 20.8 | 20.9 | 20.7 | 20.0 | 18.9 | 17.6 |
| 3 | | 20.9 | 20.7 | 20.1 | 18.9 | 17.7 |
| 4 | 39.9 | 40.1 | 39.8 | 38.9 | 37.0 | 34.7 |
| 4 | | 40.1 | 39.8 | 39.1 | 38.1 | 39.3 |
| 5 | 64.5 | 64.9 | 64.6 | 63.6 | 61.1 | 57.6 |
| 5 | | 64.9 | 64.6 | 63.6 | 61.3 | 57.9 |
| 6 | 94.6 | 95.3 | 95.1 | 94.0 | 91.1 | 86.3 |
| 6 | | 95.3 | 95.1 | 94.1 | 91.8 | 89.8 |

n = order of mode

* b/a = ratio of ellipse minor axis to major axis.

Table 4.2 Resonant Frequencies of the Car-Shaped Ring Structure

| Order of Mode | Measured (Hz) | Calculated (Hz) |
|---|---|---|
| 2 | 8.2 | 6.9 |
| 2 | 11.1 | 10.2 |
| 3 | 20.7 | 19.4 |
| 3 | 23.6 | 22.9 |
| 4 | 36.6 | 34.3 |
| 4 | 42.1 | 40.0 |
| 5 | 52.0 | 49.1 |
| 5 | 62.3 | 59.0 |
| 6 | 82.6 | 78.0 |
| 6 | 95.8 | 91.2 |

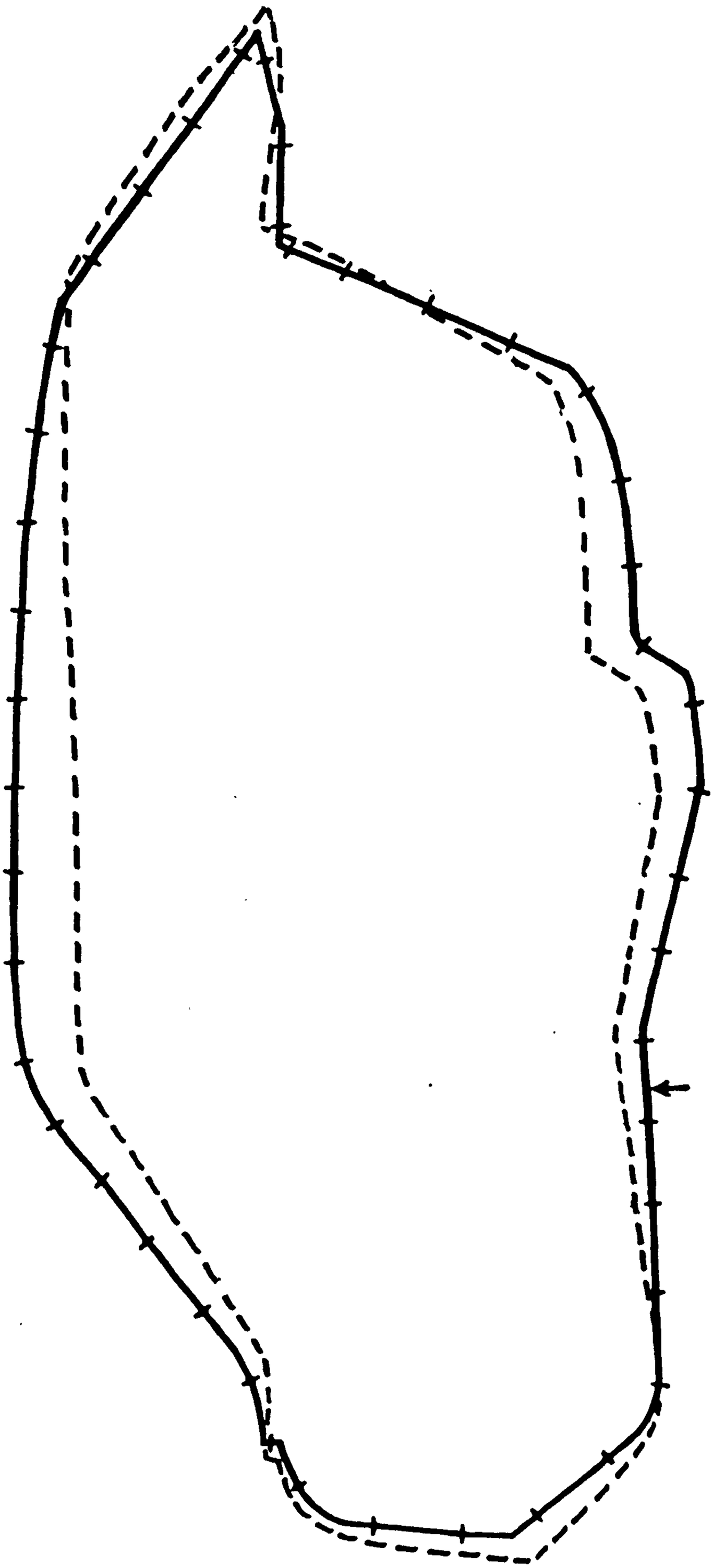

Fig. 4.3a Measured Mode at 8.2 Hz

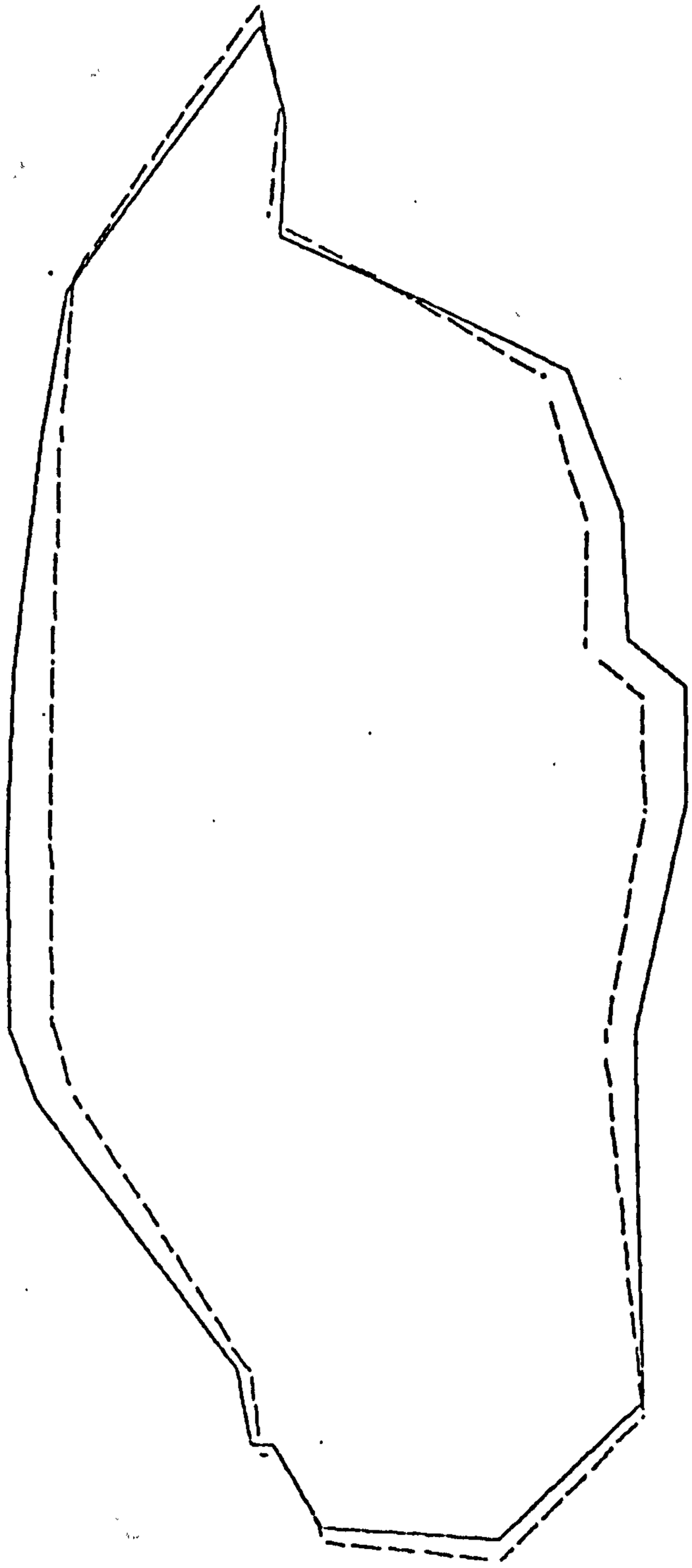

Fig. 4.3b Calculated Mode at 6.9 Hz

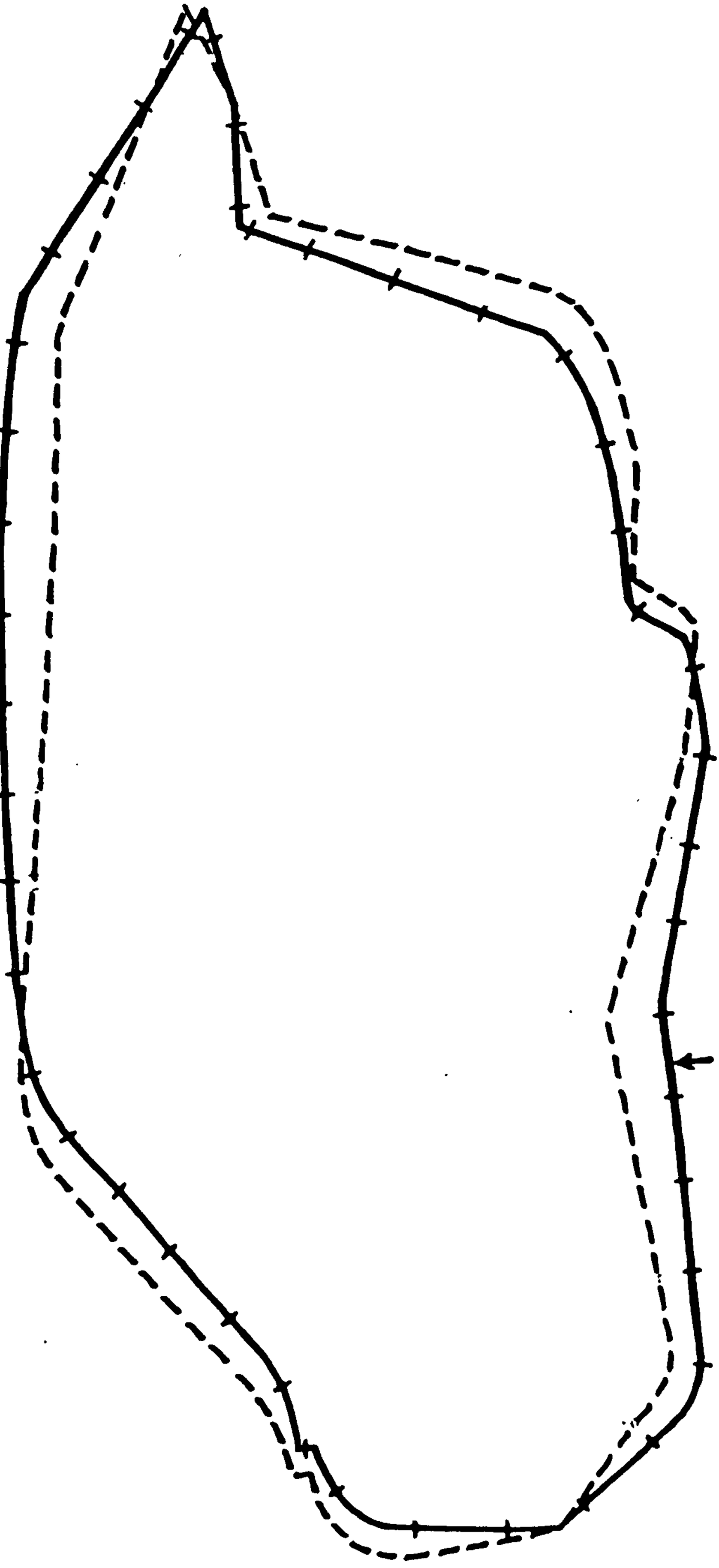

Fig. 4.4a Measured Mode at 11.1 Hz

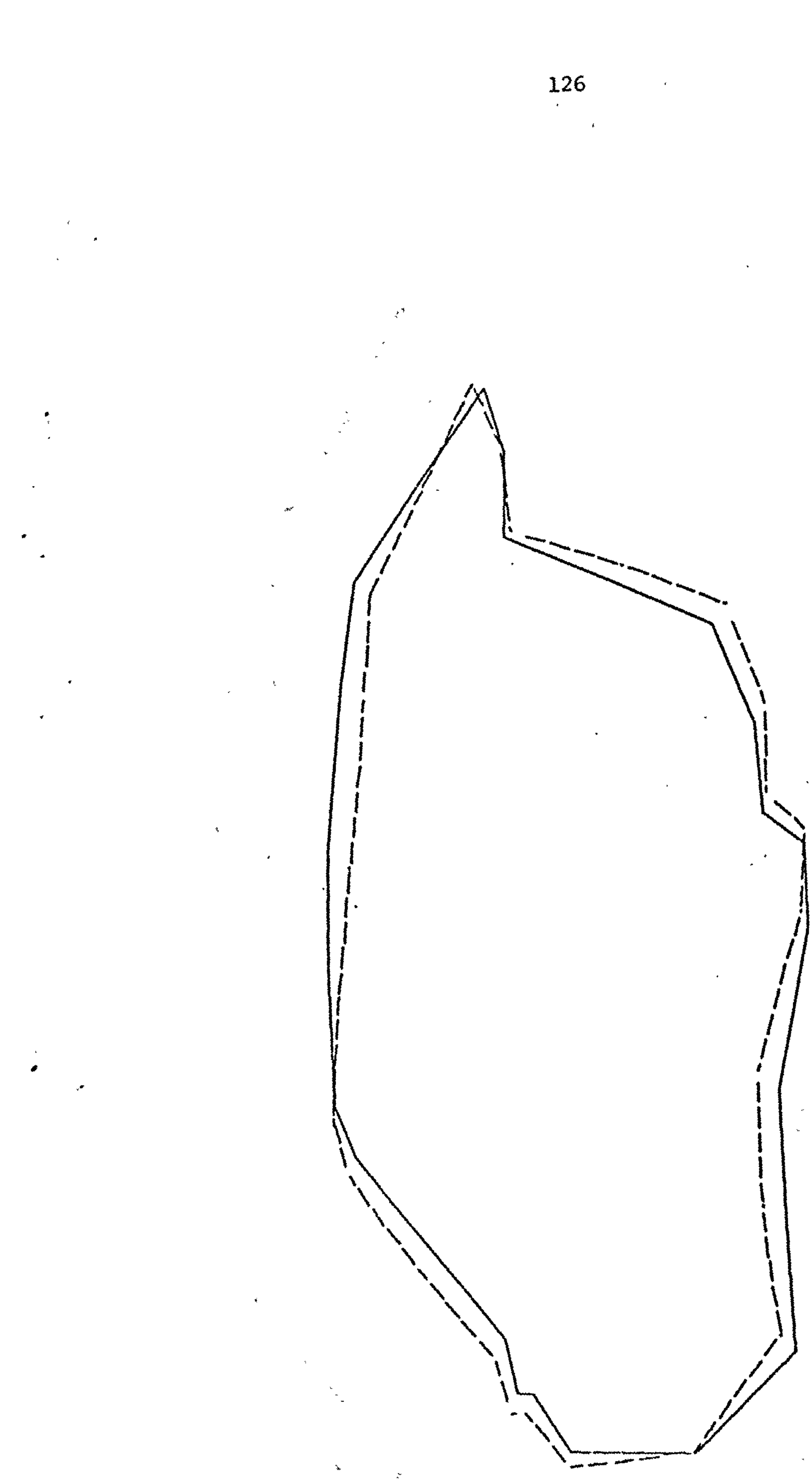

Fig. 4.4b Calculated Mode at 10.2 Hz

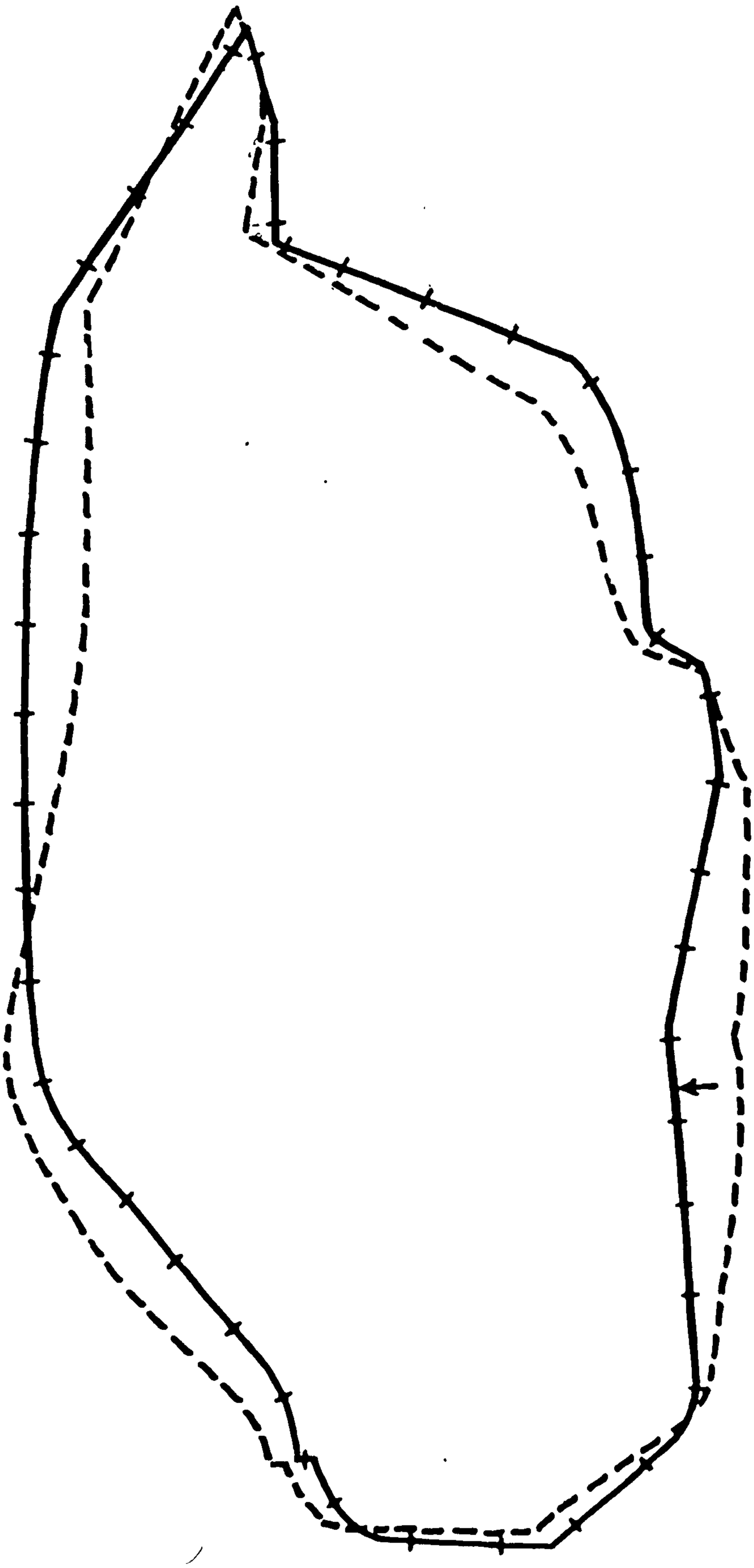

Fig. 4.5a Measured Mode at 20.7 Hz

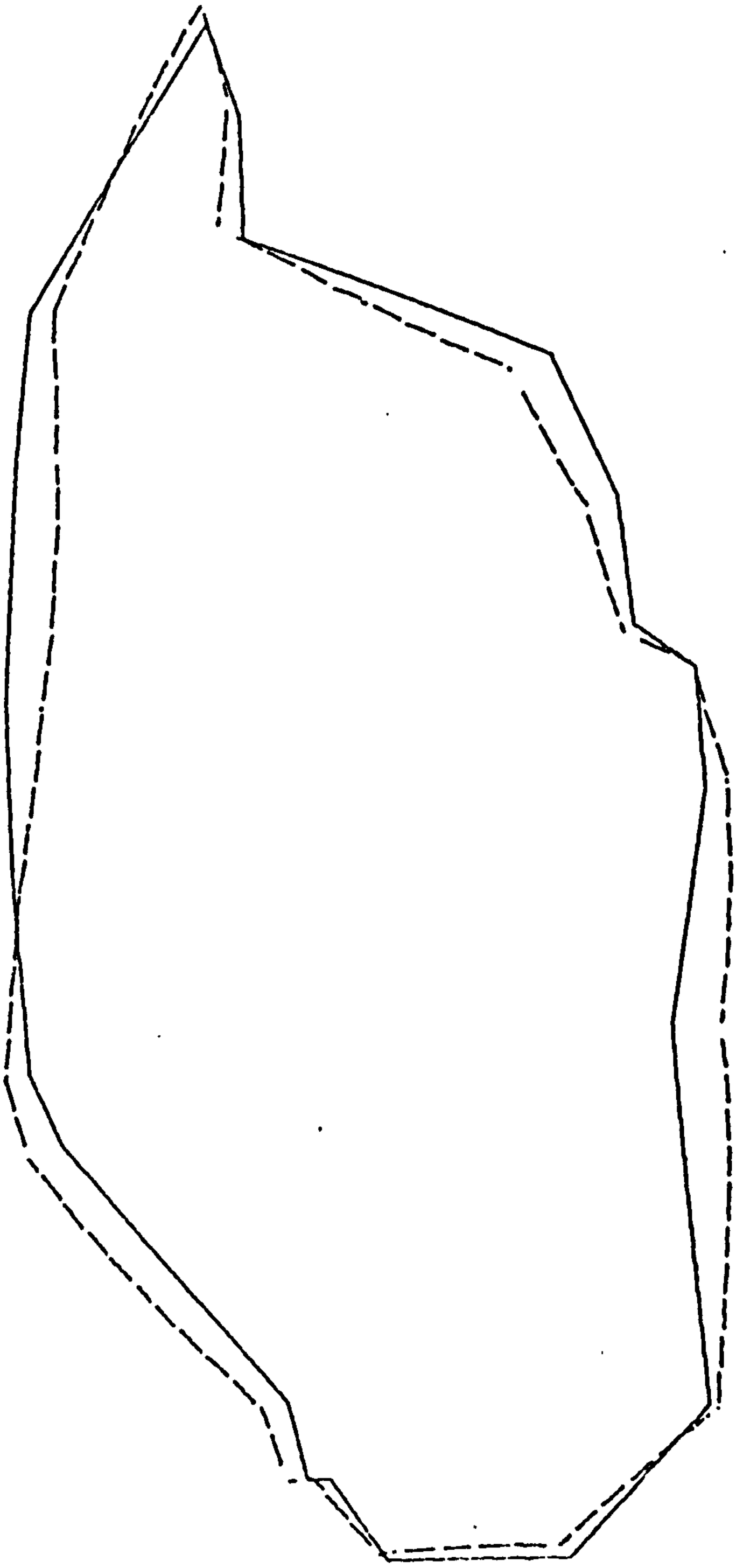

Fig. 4.5b Calculated Mode at 19.4 Hz

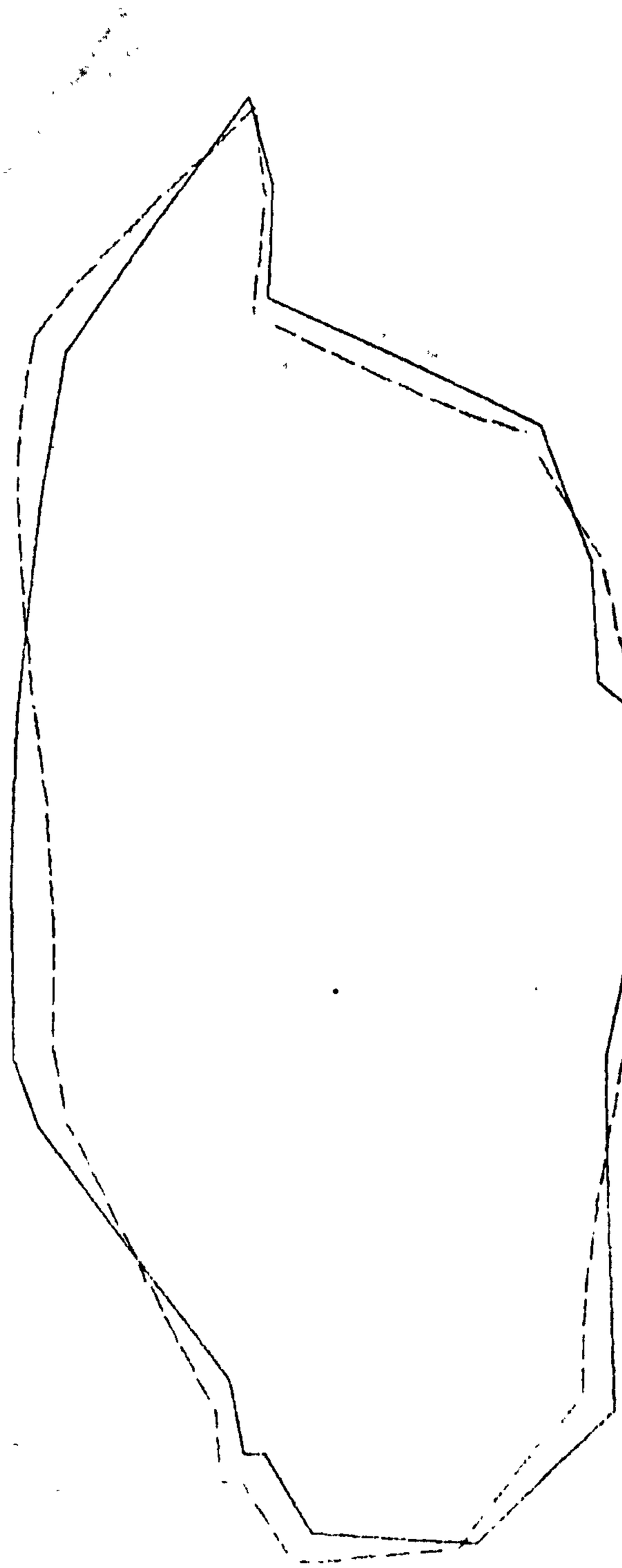

Fig. 4.6 Calculated Mode at 22.9 Hz

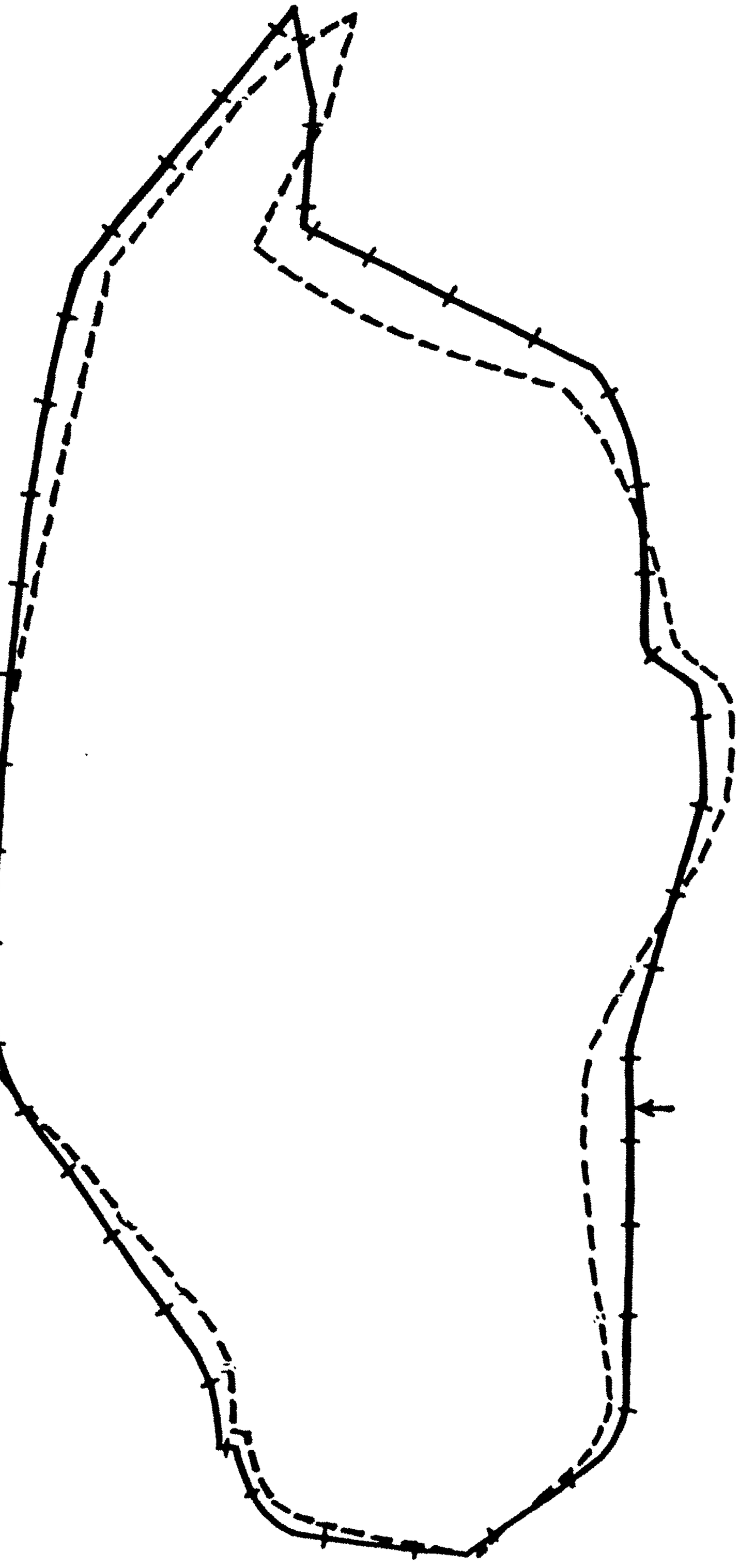

Fig. 4.7a Measured Mode at 36.6 Hz

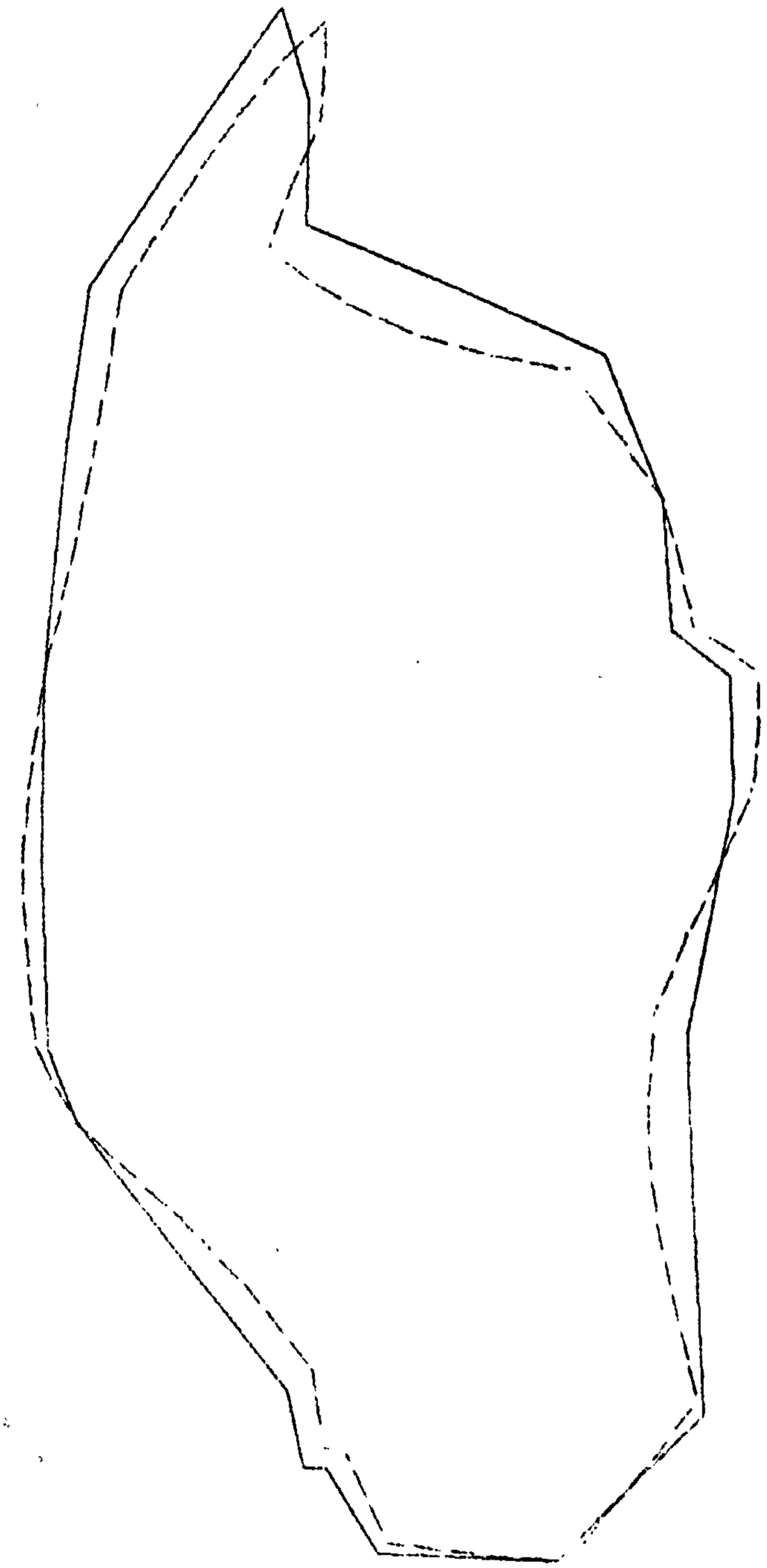

Fig. 4.7b Calculated Mode at 34.3 Hz

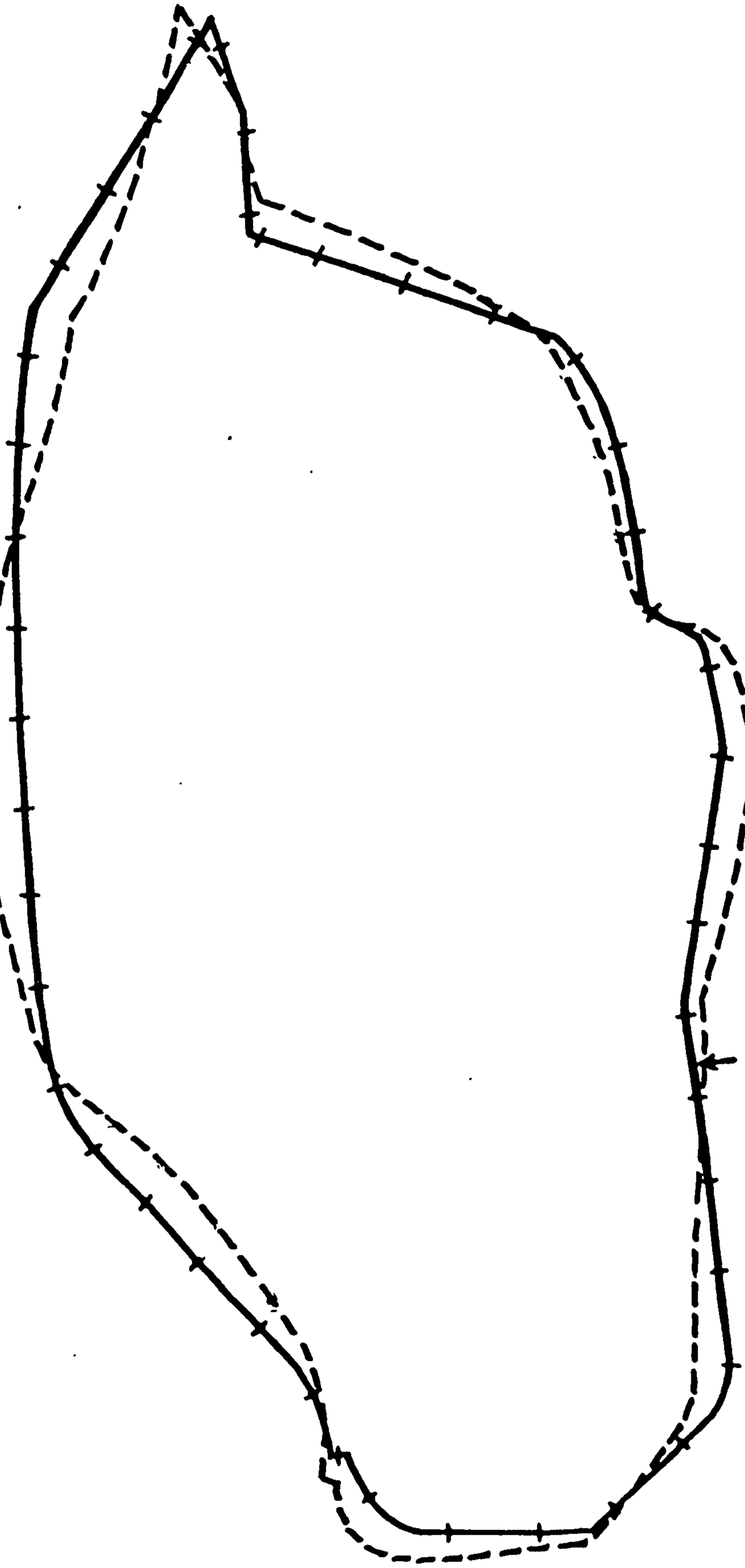

Fig. 4.8a Measured Mode at 42.1 Hz

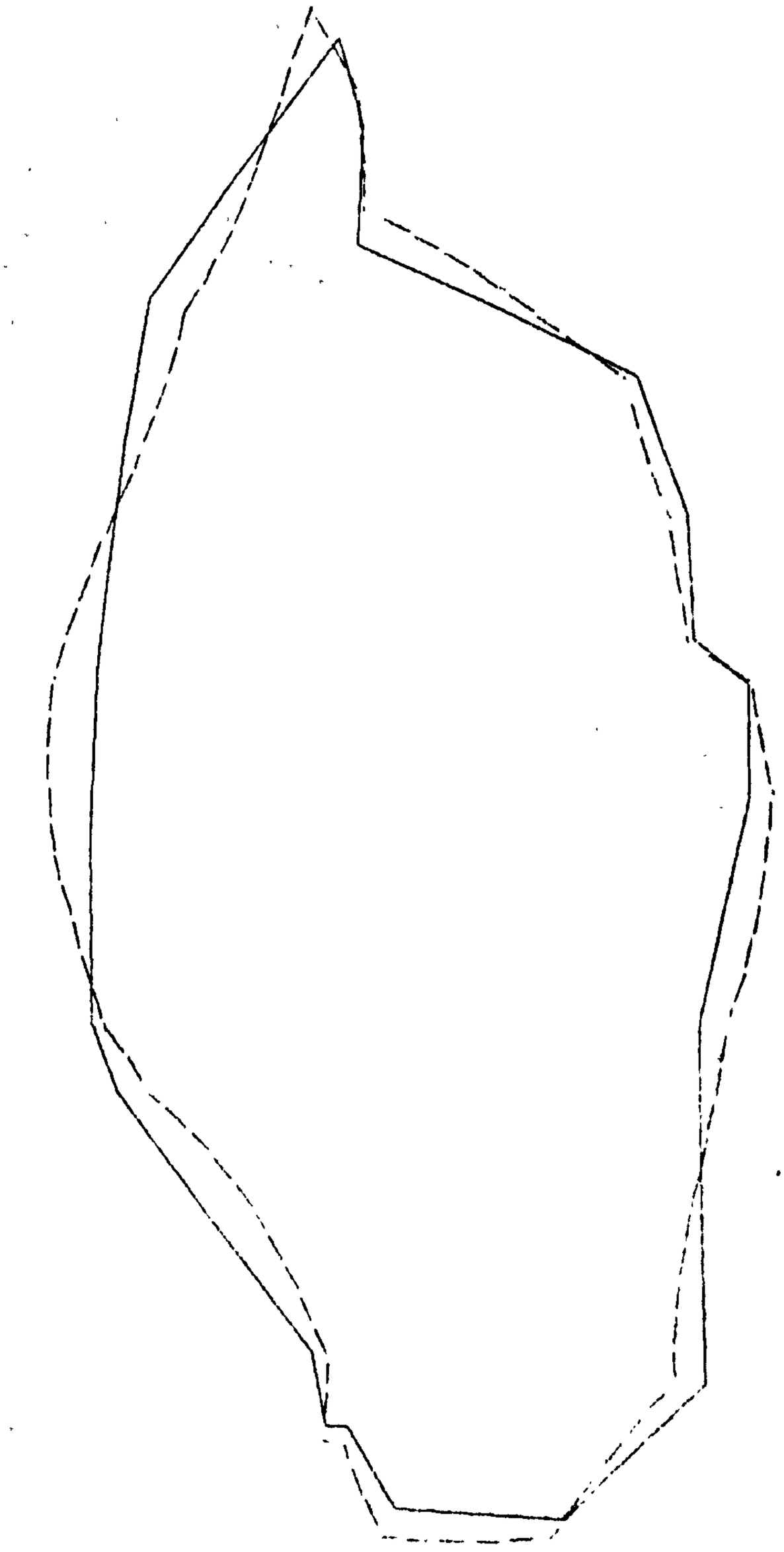

Fig. 4.8b Calculated Mode at 40.0 Hz

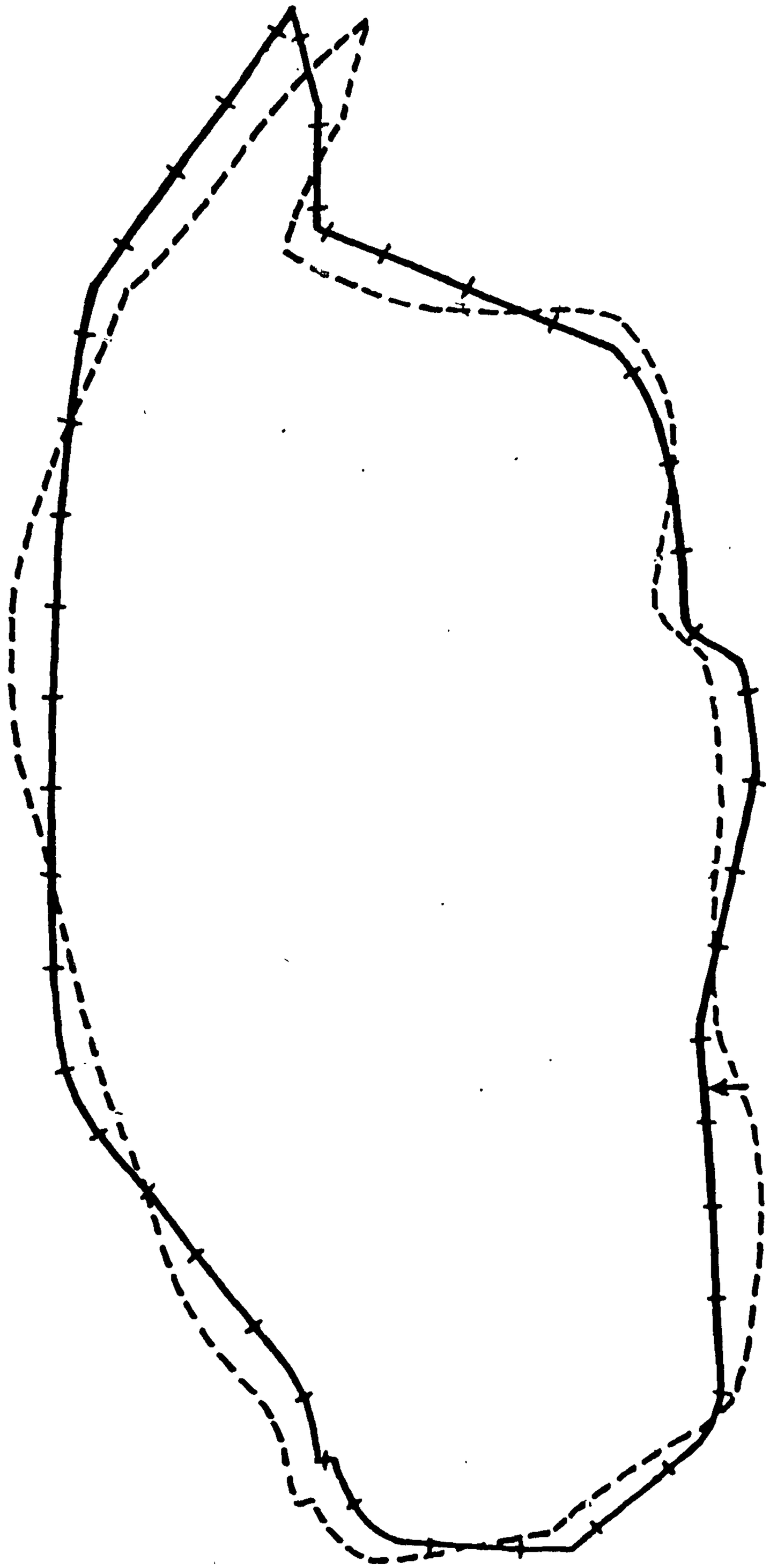

Fig. 4.9a Measured Mode at 52.0 Hz

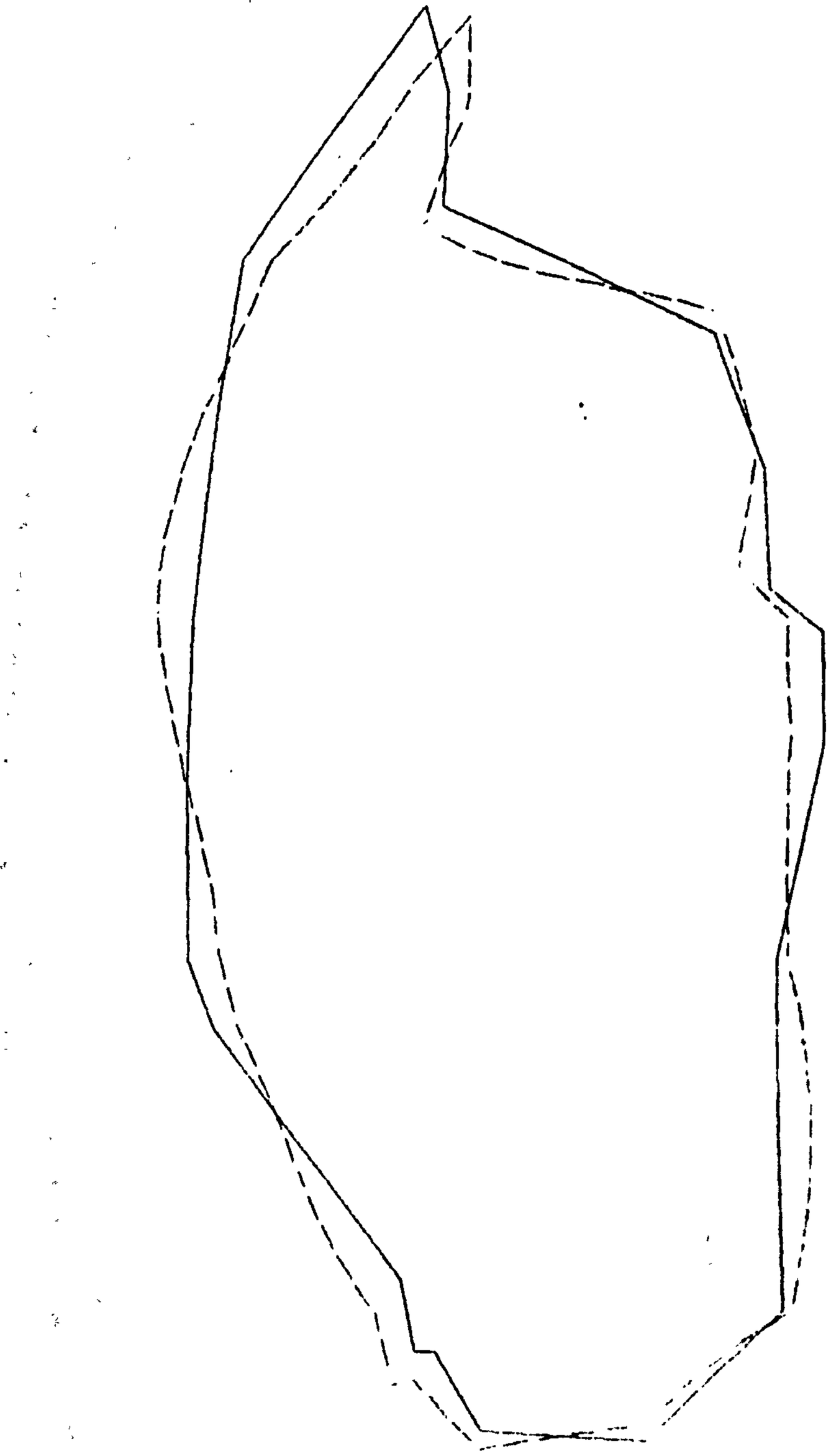

Fig. 4.9b Calculated Mode at 49.1 Hz

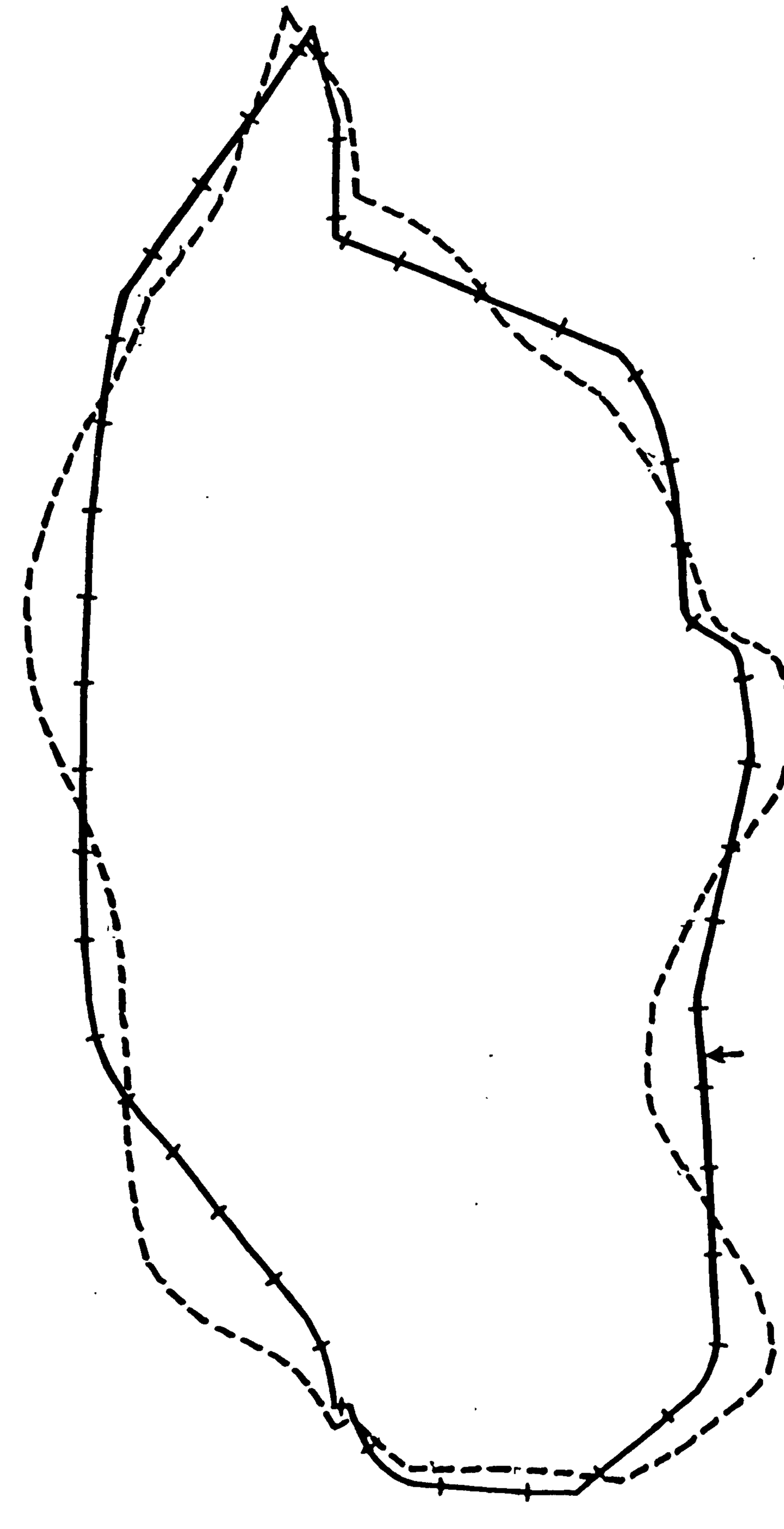

Fig. 4.10a Measured Mode at 62.3 Hz

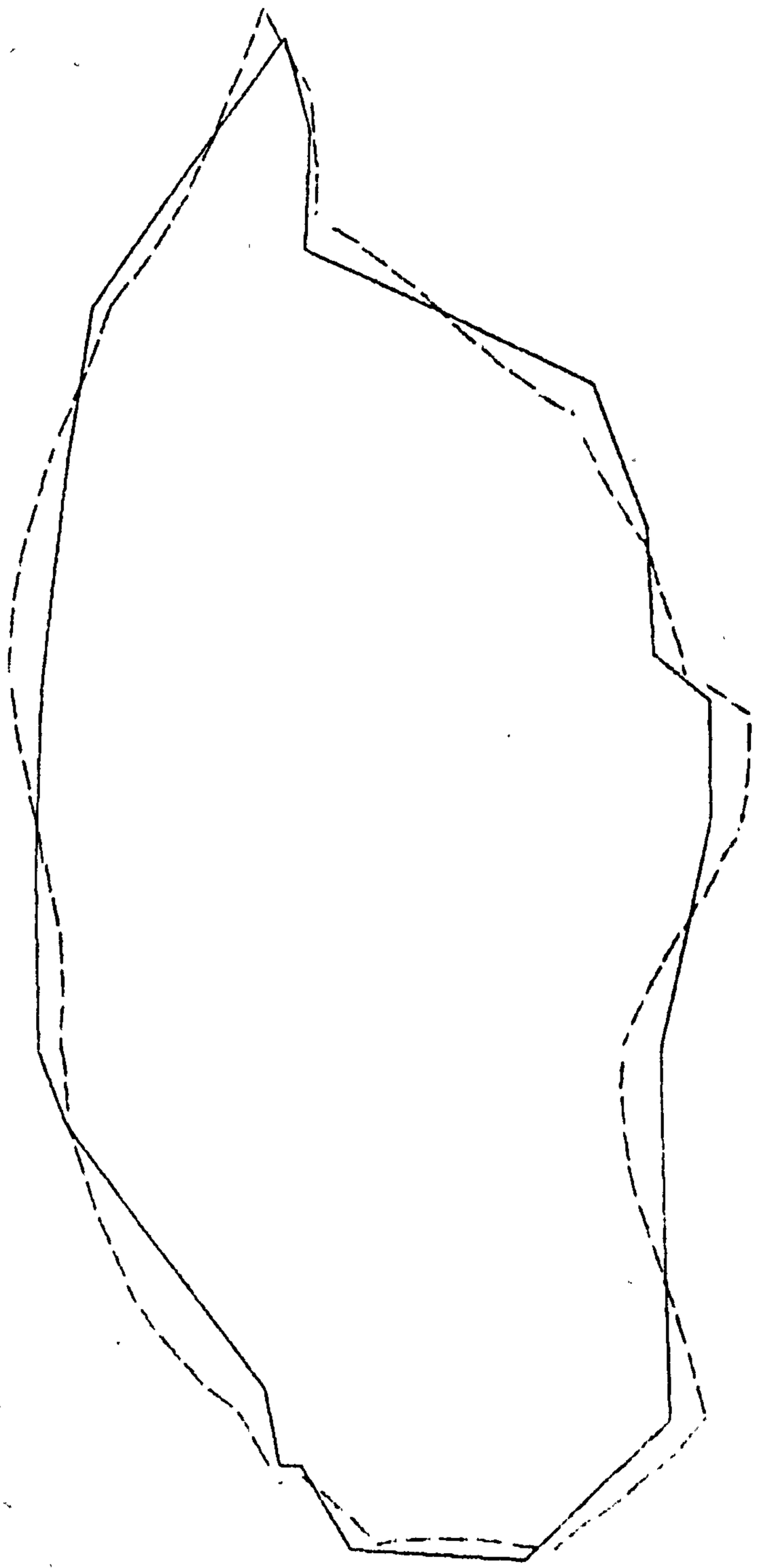

Fig. 4.10b Calculated Mode at 59.0 Hz

Fig. 4.11a Measured Mode at 82.6 Hz

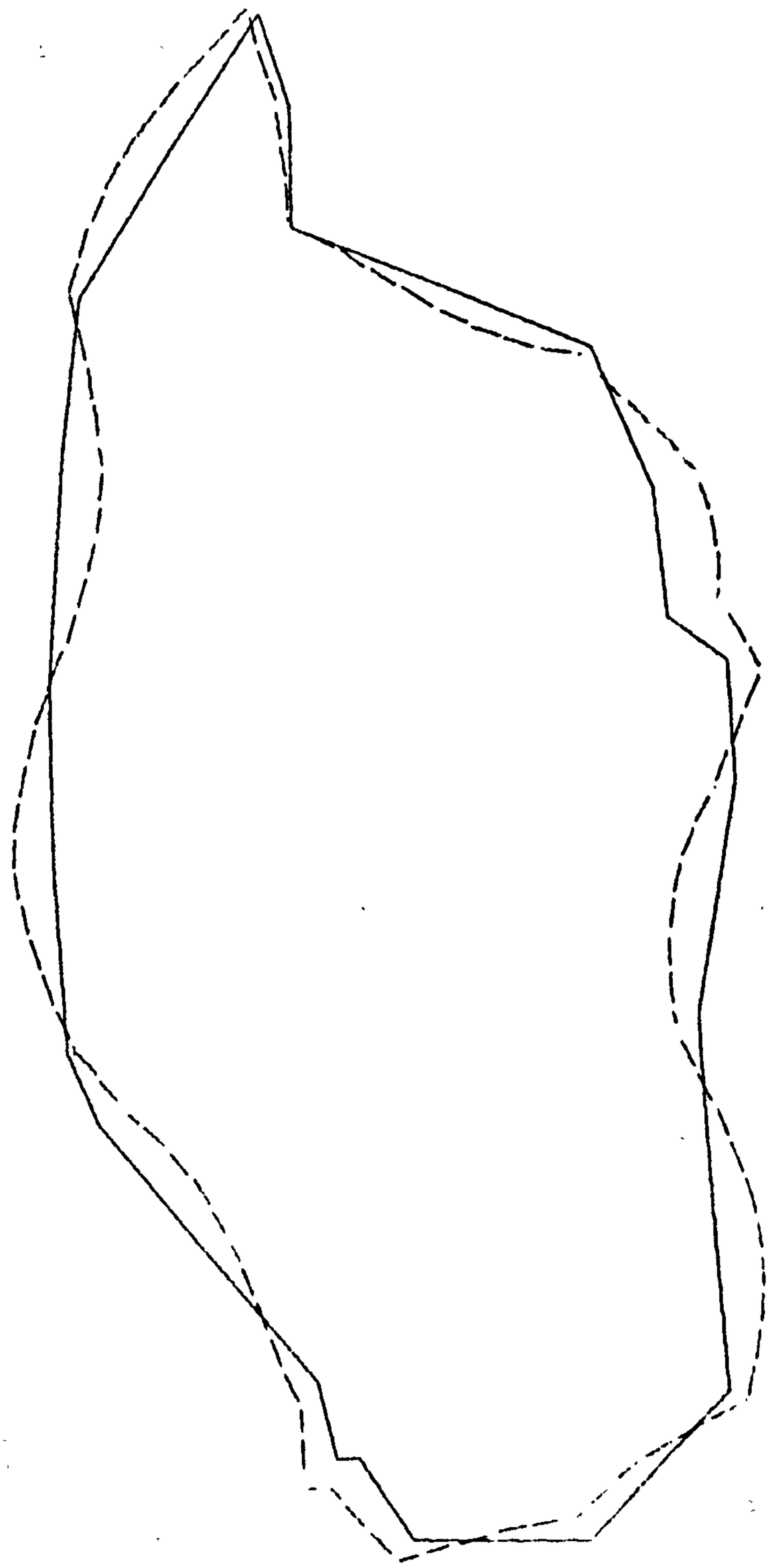

Fig. 4.11b Calculated Mode at 78.0 Hz

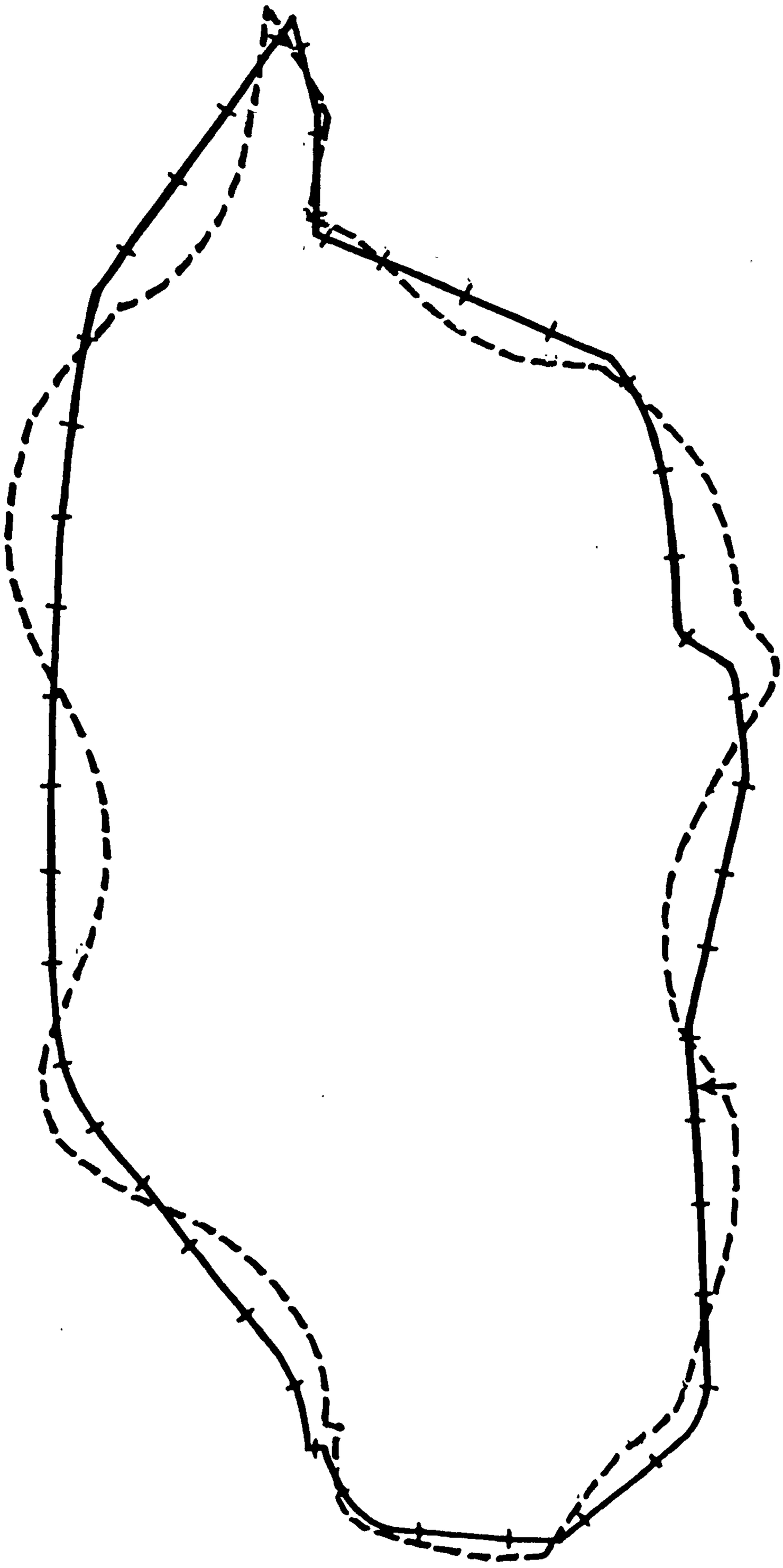

Fig. 4.12a Measured Mode at 95.8 Hz

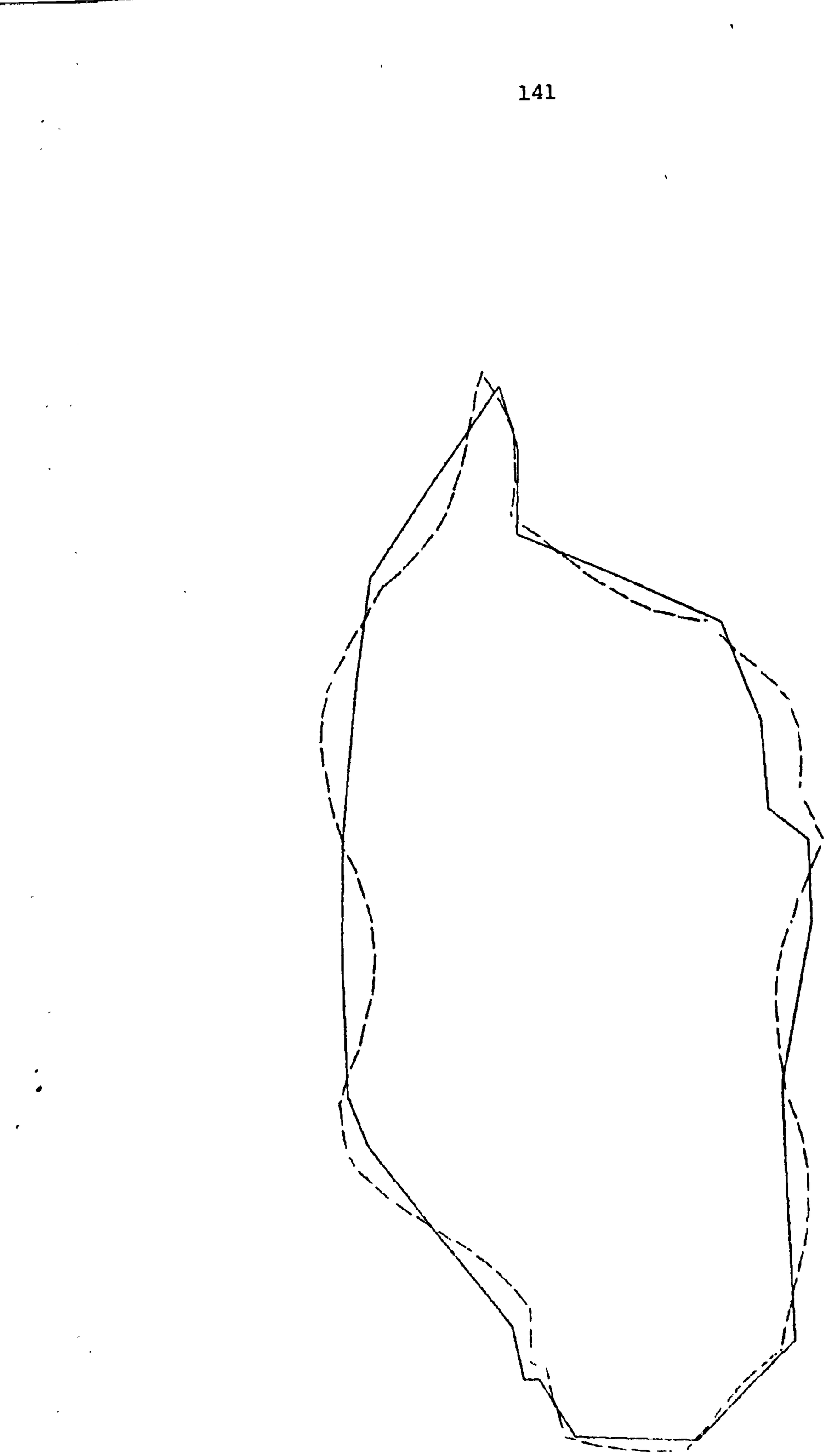

Fig. 4.12b Calculated Mode at 91.2 Hz

# Appendix 4.I Stiffness and Mass Matrices for Two-Dimensional Beam Elements; The Finite Element Computer Program.

## 1. Shape Functions for the Two-Dimensional Beam Element

The beam element is assumed to lie along the local x-axis, and all displacements are a function of x. Node 1 lies at x = 0 and node 2 lies at x = L, where L is the length of the element.

The longitudinal displacement u in the x direction is a linear function of x which is determined by the nodal values $u_1$ and $u_2$. Thus:

$$u = \left(1 - \frac{x}{L}\right) u_1 + \frac{x}{L} u_2 \qquad (4.I.1)$$

The transverse displacement v is assumed to be independent of the longitudinal displacement, and is a cubic function of x determined by the nodal displacements $v_1$, $v_2$ and rotations $\theta_1$, $\theta_2$ where:

$$\theta_1 = v'(0)$$

$$\theta_2 = v'(L)$$

Expressed in terms of the nodal displacements, v is given by:

$$v = \left[1 - 3(x/L)^2 + 2(x/L)^3\right] v_1$$
$$+ L\left[x/L - 2(x/L)^2 + (x/L)^3\right]\theta_1$$
$$+ \left[3(x/L)^2 - 2(x/L)^3\right] v_2$$
$$+ L\left[-(x/L)^2 + (x/L)^3\right]\theta_2 \qquad (4.I.2)$$

Equations 4.I.1 and 4.I.2 can be combined to form a single matrix equation:

$$\begin{Bmatrix} u \\ v \end{Bmatrix} = [N]\ \{a\} \qquad (4.I.3)$$

where:

$$\{a\} = \begin{Bmatrix} u_1 \\ v_1 \\ \theta_1 \\ u_2 \\ v_2 \\ \theta_2 \end{Bmatrix} \qquad (4.I.4)$$

$[N]$ is a 2 x 6 matrix whose elements are functions of x.

## 2. The Stiffness Matrix

Two components of strain exist within the element. In the longitudinal direction:

$$\varepsilon_L = \frac{du}{dx}$$

and for transverse deformation the strain is the curvature, that is:

$$\varepsilon_T = -\frac{d^2v}{dx^2}$$

In matrix form we can write:

$$\{\varepsilon\} = \begin{Bmatrix} \varepsilon_L \\ \varepsilon_T \end{Bmatrix} = \begin{bmatrix} d/dx & 0 \\ 0 & -d^2/dx^2 \end{bmatrix} \begin{Bmatrix} u \\ v \end{Bmatrix}$$

and using equation 4.I.3 this gives:

$$\{\varepsilon\} = [B]\{a\} \qquad (4.I.5)$$

where

$$[B] = \begin{bmatrix} d/dx & 0 \\ 0 & -d^2/dx^2 \end{bmatrix} [N] \qquad (4.I.6)$$

The corresponding stresses are related to the strains by:

$$\{\sigma\} = \begin{Bmatrix} \sigma_L \\ \sigma_T \end{Bmatrix} = \begin{bmatrix} EA & 0 \\ 0 & EI \end{bmatrix} \begin{Bmatrix} \varepsilon_L \\ \varepsilon_T \end{Bmatrix}$$

where E is Young's modulus, A is the cross-sectional area of the beam, and I is the second moment of area of the cross-section.

If:

$$[D] = \begin{bmatrix} EA & 0 \\ 0 & EI \end{bmatrix}$$

we can follow Zienkiewicz (29) and write the element stiffness matrix as:

$$[k]_e = \int_0^L [B]^T [D] [B] \, dx \qquad (4.I.8)$$

Carrying out the matrix multiplications and integrations in equation 4.I.8 results in:

$$[K]_e = \begin{bmatrix} \frac{EA}{L} & 0 & 0 & \frac{EA}{L} & 0 & 0 \\ & \frac{12EI}{L^3} & \frac{6EI}{L^2} & 0 & \frac{-12EI}{L^3} & \frac{6EI}{L^2} \\ & & \frac{4EI}{L} & 0 & \frac{-6EI}{L^2} & \frac{2EI}{L} \\ & & & \frac{EA}{L} & 0 & 0 \\ & \text{Sym.} & & & \frac{12EI}{L^3} & \frac{-6EI}{L^2} \\ & & & & & \frac{4EI}{L} \end{bmatrix} \qquad (4.I.9)$$

### 3. The Mass Matrix

Zienkiewicz (29) discusses the general formulation of mass matrices for any kind of element and shows that:

$$[m]_e = \int_{V_e} [N]^T \rho [N] \, dV, \qquad (4.I.10)$$

where $\rho$ is the density of the material and $[N]$ relates the displacements throughout the element to the nodal values.

If we neglect the variation of displacement across the thickness of the element, then we can write:

$$[m]_e = \int_0^L [N]^T \mu [N] \, dx \qquad (4.I.11)$$

where $\mu = \rho A$, the mass/unit length of the element, and the matrix $[N]$ is that given in equation 4.I.3. Making this approximation is in fact tantamount to ignoring the rotary inertia of the small volume element $Adx$.

Using equation 4.I.11, the mass matrix is obtained explicitly as:

$$[m]_e = \frac{\mu L}{420} \begin{bmatrix} 140 & 0 & 0 & 70 & 0 & 0 \\ & 156 & 22L & 0 & 54 & -13L \\ & & 4L^2 & 0 & 13L & -3L^2 \\ & & & 140 & 0 & 0 \\ & \text{Sym.} & & & 156 & -22L \\ & & & & & 4L^2 \end{bmatrix} \qquad (4.I.12)$$

## 4. Transformation to the Global System

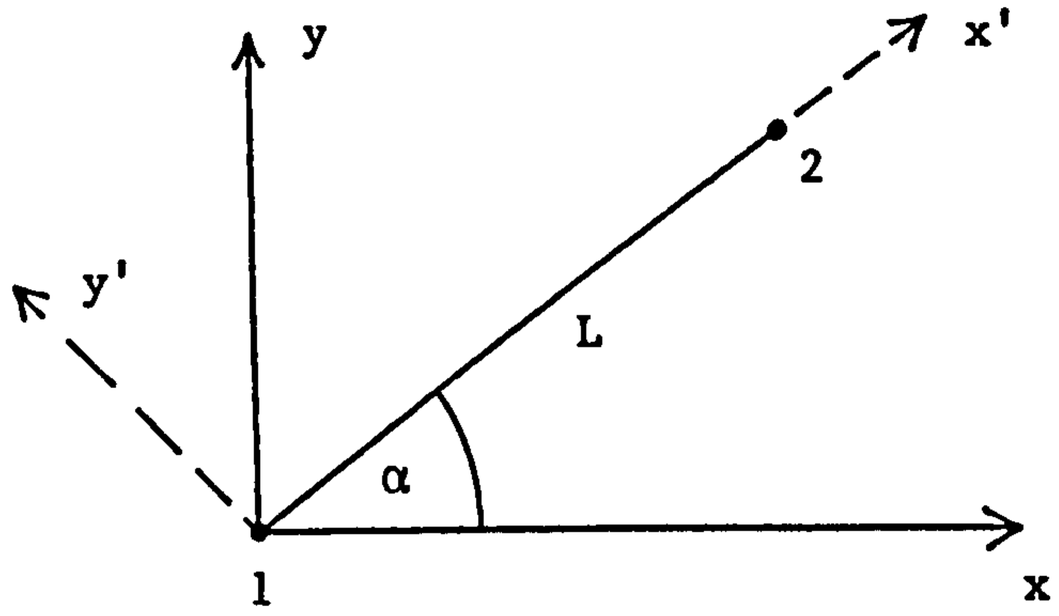


Having calculated the element matrices in the local co-ordinate system (denoted by a prime in the diagram) it is now necessary to transform them to the global system before assembly into the overall equations. If $\alpha$ is the angle between the global x-axis and the local x-axis, then the displacement u' in the local system is related to those in the global system by:

$$u' = u\cos\alpha + v\sin\alpha$$

In a similar manner:

$$v' = v\cos\alpha - u\sin\alpha$$

Rotations are identical in either co-ordinate system, that is:

$$\theta' = \theta$$

Combining these equations in matrix form allows us to express the local element nodal displacements as follows:

$$\begin{Bmatrix} u_1' \\ v_1' \\ \theta_1' \\ u_2' \\ v_2' \\ \theta_2' \end{Bmatrix} = \begin{bmatrix} \cos\alpha & \sin\alpha & 0 & 0 & 0 & 0 \\ -\sin\alpha & \cos\alpha & 0 & 0 & 0 & 0 \\ 0 & 0 & 1 & 0 & 0 & 0 \\ 0 & 0 & 0 & \cos\alpha & \sin\alpha & 0 \\ 0 & 0 & 0 & -\sin\alpha & \cos\alpha & 0 \\ 0 & 0 & 0 & 0 & 0 & 1 \end{bmatrix} \begin{Bmatrix} u_1 \\ v_1 \\ \theta_1 \\ u_2 \\ v_2 \\ \theta_2 \end{Bmatrix}$$

or

$$\{a'\} = [T]\ \{a\} \qquad (4.I.13)$$

It can be easily verified that $[T]^{-1} = [T]^T$, so that:

$$\{a\} = [T]^T\{a'\} \qquad (4.I.14)$$

The work done on the element giving the displacement must be equal in both systems, that is:

$$\{a\}^T[K]_e\{a\} = \{a'\}^T[K]_e'\{a'\}$$

Substituting 4.I.13 gives:

$$\{a\}^T[K]_e\{a\} = \{a\}^T[T]^T[k]'_e\ [T]\ \{a\}^T$$

and since this must be true for any vector {a},

$$[k]_e = [T]^T[k]'_e[T] \qquad (4.I.15)$$

Equation 4.I.15 thus relates the global stiffness matrix $[k]_e$ to the local matrix $[k]'_e$.

A similar argument, equating the element kinetic energy in both systems, gives the relation between the local and global mass matrices:

$$[m]_e = [T]^T[m]'_e\ [T] \qquad (4.I.16)$$

## 5. The Computer Program

The computer program, written in FORTRAN, follows essentially the same procedure of assembly by elements used in the acoustic problem, and uses identical NAG subroutines to solve the resulting equations. It requires as input:

a) The x and y co-ordinates of each node.

b) The nodal numbering of each element in the overall system.

c) The material properties of each element, namely the longitudinal stiffness (EA), the bending stiffness (EI), and the mass per unit length.

For each element in turn the transformation matrix T and the local stiffness and mass matrices are computed. The matrix multiplications transforming these to the global system are then carried out and the resulting element matrices are then added to the overall equations. On completion of assembly these equations are solved and the required number of modes are output to the lineprinter.

Appendix 4.II. Degeneracy in Symmetric Structures.

Thomas (44) gives an account of degeneracy in rotationally periodic structures. If the structure remains unchanged after rotation, then the same rotation of any mode shape must result in an equally valid mode having the same resonant frequency. In general this can only be achieved if the new mode is a linear combination of the original mode and an orthogonal degenerate mode. Thomas expresses this in the following way:

$$\begin{Bmatrix} u' \\ \bar{u}' \end{Bmatrix} = \begin{bmatrix} c[I] & s[I] \\ -s[I] & c[I] \end{bmatrix} \begin{Bmatrix} u \\ \bar{u} \end{Bmatrix} = [R] \begin{Bmatrix} u \\ \bar{u} \end{Bmatrix}$$

This degeneracy is unnecessary only if rotation of the mode results in no change, or merely a change in sign (i.e $u' = u$, or $u' = -u$ ).

If the structure consists of N identical substructures, then

$$[R]^N = [I] ,$$

as rotation through $2\pi$ leaves any mode unchanged. In the case of the ellipse

$$[R]^2 = [I]$$

and this is possible only if $s = 0$ and $c = \pm 1$. This means that the modes are either symmetric or antisymmetric on rotation through $\pi$ , and are therefore not degenerate unless accidentally so.

The ellipse is also symmetric with respect to reflections about the major axis and minor axis. These operations can be treated in exactly the same way as the rotations, and for these too

$$[R]^2 = [I]$$

because two reflections about the same axis must give an

unchanged mode. This leads to the conclusion that all modes are either symmetric or antisymmetric with respect to both reflections ( a well-known result for structures having this symmetry ).

The symmetry of the ellipse therefore does not require any degeneracy, and it is concluded that the small splitting of the odd order resonances is purely accidental.

The actual order of the modes can be related to the nature of their symmetry with respect to the reflections ( rotation through $\pi$ is in fact equivalent to a combination of the two reflections).

For each even n

(a) There is a mode symmetric with respect to reflection about about both axes, and

(b) an orthogonal mode which is antisymmetric with respect to these reflections.

For each odd n

(a) There is a mode symmetric with respect to reflection about the major axis and antisymmetric with respect to reflection about the minor axis, and

(b) an orthogonal mode antisymmetric with respect to reflection about the major axis and symmetric with respect to reflection about the minor axis.

In the special case of the circle these mode pairs are degenerate.

# 5. REDUCTION OF STRUCTURAL-ACOUSTIC COUPLING

## 5.1 Calculation of Structural-Acoustic Coupling using Finite Element Modal Data

The expressions given in Chapter 2 for the acoustic response due to structural vibration require calculation of the coefficients

$$C_{ij} = \int_S \phi_i(r)\, X_j(r)\, dS \qquad (5.1)$$

While exact solutions for the acoustic modes $\phi_i$ and the normal structural displacements $X_j$ may be available for simple cases, most practical problems will require a numerical approach such as the finite element method. Such solutions will consist of a vector of nodal values, from which intermediate values may be calculated using the appropriate element shape functions.

The evaluation of the surface integrals may conveniently be approached in a similar manner to that used in 'Boundary Solution' processes (29). The surface itself is divided into a number of boundary elements, and the variation of the unknown quantities within each is assumed to depend on the nodal values. The integral is then carried out over each element in turn, and summation of these contributions gives the complete surface integral.

Clearly the problem of obtaining the values at the nodes of the boundary elements is greatly facilitated if they coincide with nodes of the original structural and acoustic

finite element meshes. Furthermore the boundary elements may coincide exactly with the surfaces of the exterior acoustic elements and the interior structural elements; in such cases the same interpolations will be possible in the boundary element as in the structural and acoustic elements.

In general the normal structural displacement will not be directly available from the finite element solution, which gives the nodal displacements in the global co-ordinate system. For many types of beam, plate, and shell elements, however, the derivation of the element matrices will have at some stage required a description of the displacement in a local co-ordinate system, one of whose axes lies in the normal direction. Thus the transformation from the local system to the global system may be inverted and used to obtain the normal displacements from the solution vector. Clearly such a procedure could also be adopted at the surface of any three-dimensional structural element.

The pressure amplitude, $\phi$ , of a given acoustic mode within the boundary element is given by:

$$\phi = [N]_a \{\phi\} \qquad (5.2)$$

where $[N]_a$ is a matrix of shape functions which depend on the position within the element, and $\{\phi\}$ is the vector of nodal pressure amplitudes. Similarly the normal structural displacement, X, is given by:

$$X = [N]_s \{u\} \qquad (5.3)$$

The vector {u} may contain the values of normal displacement at the nodes of the boundary element, these having been obtained previously by the appropriate transformation from the global system. Alternatively this transformation can be incorporated in $[N]_s$, in which case {u} contains the nodal displacements in the global system.

Integrating the product of $\phi$ and X over the boundary element gives:

$$\int_s \phi \, X \, dS = \int_s [N]_A \{\phi\} \cdot [N]_s \{u\} \, dS \qquad (5.4)$$

This integration may be performed explicitly, if possible, or evaluated numerically using the appropriate number of Gauss points.

In this application the integral in equation 5.4 will usually be evaluated a number of times over the same boundary element for different combinations of structural and acoustic modes.

If

$$[A] = \int_s [N]_A^T \, [N]_s \, dS \qquad (5.5)$$

then

$$\int_s \phi X \, dS = \{\phi\}^T [A] \{u\} \qquad (5.6)$$

Thus preliminary calculation of the matrix [A] avoids the need for repeated numerical integrations.

## 5.2 Structural Modification as a Perturbation of the Finite Element Matrices

Having calculated the coefficients $C'_{ij}$ using structural and acoustic modal data, the acoustic response for any force input may be determined. Excessive responses may be a result of particularly large values of $C'_{ij}$, and it may be possible to reduce these by making structural modifications.

The effect of structural modifications may be assessed simply by repeating the finite element analysis, but since the nature of desirable modifications will not in general be apparent, a trial and error approach will usually be necessary. Thus a large number of eigenvalue solutions may be required before a satisfactory structure is achieved, and this may prove prohibitively expensive, especially for a structure as complex as a car body.

The approach taken here has been to consider small structural changes as perturbations of the original finite element matrices. In this way an approximation to the modified resonances may be obtained.

Suppose the unmodified finite element equations have eigensolutions $\{U_i\}$, $p_i$ obeying

$$[K]\ \{U_i\} - p_i\ [M]\ \{U_i\} = 0 \qquad (5.7)$$

where $p_i = \omega_i^2$, and the eigenvectors are normalised in the usual way such that

$$\{U_i\}^T[K]\{U_j\} = 0 \qquad i \neq j \tag{5.8}$$

$$= p_i \qquad i = j \tag{5.9}$$

$$\{U_i\}^T[M]\{U_j\} = 0 \qquad i \neq j \tag{5.10}$$

$$= 1 \qquad i = j \tag{5.11}$$

If a structural modification is made which results in a change in the stiffness matrix, that is

$$[K] \rightarrow [K] + \lambda[L] , \tag{5.12}$$

then the new eigensolutions $V_i$ , $q_i$ will obey

$$[K]\{V_i\} + \lambda[L]\{V_i\} - q_i[M]\{V_i\} = 0 \tag{5.13}$$

As $\lambda$ approaches zero $\{V_i\}$ and $q_i$ must approach the original eigensolution, and this is achieved if they are expressed as a power series in $\lambda$ as follows:

$$\{V_i\} = \{U_i\} + \lambda \sum_j a_{ij} \{U_j\} + \lambda^2 \sum_j b_{ij}\{U_j\} + \ldots \tag{5.14}$$

$$q_i = p_i + \lambda p_i' + \lambda^2 p_i'' + \ldots \tag{5.15}$$

Note that the unmodified modes have been used as generalised co-ordinates for the modified solution. For small $\lambda$ these series will converge rapidly, and a first or second order approximation may be sufficiently accurate, although it is perhaps necessary to place some restrictions on the nature of the change $\lambda[L]$ to the stiffness matrix. For example, the

original stiffness matrix will have a sparsity pattern which depends on the element connections and the nodal numbering, and for $\lambda[L]$ to be much smaller than $[K]$ in any strict sense means that this sparsity must be preserved. Thus any modification should not include a change of nodal numbering, nor the addition of elements between previously unconnected nodes.

When equations 5.14 and 5.15 are substituted into equation 5.13 the resulting left-hand side consists of terms in ascending powers of $\lambda$. This must be equal to zero for all $\lambda$, so the coefficients of each power are individually equal to zero. Equation 5.7 ensures this for the zeroth power, while equating coefficients of $\lambda$ gives

$$[L]\{U_i\} + \sum_j a_{ij}[K]\{U_j\}$$

$$- p_i' [M]\{U_i\} - p_i \sum_j a_{ij} [M]\{U_j\} = 0 \qquad (5.16)$$

and for $\lambda^2$:

$$\sum_j b_{ij} [K]\{U_j\} + \sum_j a_{ij}[L]\{U_j\}$$

$$-p_i \sum_j b_{ij} [M]\{U_j\} - p_i' \sum_j a_{ij} [M]\{U_j\} - p_i'' [M]\{U_i\}$$

$$= 0 \qquad (5.17)$$

Premultiplying equation 5.16 by $\{U_j\}^T$ with $j \neq i$ gives (using equations 5.8 - 5.11)

$$\{U_j\}^T [L]\{U_i\} + a_{ij}\, p_j - p_i\, a_{ij} = 0$$

and if

$$A_{ij} = \{U_j\}^T [L]\{U_i\} \tag{5.18}$$

rearrangement with $p_i = \omega_i^2$ gives

$$a_{ij} = \frac{A_{ij}}{\omega_i^2 - \omega_j^2} \qquad j \neq i \tag{5.19}$$

Premultiplication of 5.16 by $\{U_i\}^T$ gives

$$p_i' = A_{ii} \tag{5.20}$$

At this stage $a_{ii}$ has not yet been determined, but this can be done by requiring that the new mode $\{V_i\}$ is normalised in the usual way, that is:

$$\{V_i\}^T [M]\{V_i\} = 1 \tag{5.21}$$

The left-hand side of this equation is a power series in $\lambda$, with the first term equal to unity. The coefficients of higher powers must therefore be equal to zero, and it is fairly straightforward to show that:

$$a_{ii} = 0 \tag{5.22}$$

Having obtained the modified solution to first order in $\lambda$, we can, if desired, proceed to successively higher orders of approximation. Premultiplying equation 5.17 by $\{U\}_i^T$, and noting that for symmetric $[L]$, $A_{ji} = A_{ij}$, gives after some manipulation

$$P_i'' = \sum_{j \neq i} \frac{A_{ij}^2}{\omega_i^2 - \omega_j^2} \qquad (5.23)$$

while premultiplication by $\{U_j\}^T$ allows the $b_{ij}$ to be determined.

Although the calculation of these higher order approximations in principle present no difficulty, we will subsequently confine our attention to the first-order approximation because it posesses the useful property that the combined effect of a number of separate changes is additive. In the example given in the next section this aids the search for a desirable structural modification.

Degeneracy (when two or more modes have equal resonant frequencies) presents a problem in this application as the corresponding terms $a_{ij}$ in equation 5.19 will be infinite unless special precautions are taken. In the case of two-fold degeneracy, any linear combination of the two modes is itself a valid mode, so we can construct two 'replacement' modes which can be specified freely to the extent of four arbitrary coefficients. There will usually be three constraints on this choice, namely, that each mode should be normalised, and that they are orthogonal. If in addition we require that $A_{ij} = 0$ then the four coefficients are fully specified, and the offending term in equation 5.19 drops out. A similar argument can be extended to higher levels of degeneracy.

The denominator in equation 5.19 ensures that a given mode will be affected chiefly by the nearest resonances of the unmodified structure. This is a desirable feature since most practical finite element analyses will be limited to the frequency range of interest, rather than providing a complete solution for all resonances.

In Chapter 2 it was shown how the acoustic response to structural vibration could be expressed in terms of the coefficients $C_{ij}$ (equation 2.41) or $C'_{ij}$ (equation 2.43), these representing the coupling between the ith acoustic mode and the jth structural mode. Since the modified structural mode has been obtained as a sum of the unmodified modes, the modified $C_{ij}$ can be expressed as a sum over the unmodified values as follows:

$$C_{ij} \rightarrow C_{ij} + \lambda \sum_{k \neq j} a_{jk} C_{ik} \qquad (5.24)$$

where $a_{jk}$ is given by equation 5.19. Using equation 2.42 and noting that:

$$\omega_j^2 \rightarrow \omega_j^2 + \lambda A_{jj},$$

where $A_{ii}$ is given by equation 5.18, results in the expression for the modified value of $C'_{ij}$, that is

$$C'_{ij} = \frac{C_{ij}}{\omega_j^2 + \lambda A_{jj} - \Omega_i^2} \qquad (5.25)$$

Thus there is no need to calculate the new structural mode using equation 5.14, nor do the boundary integrals of the previous section require re-evaluation.

The first-order change to the structural modes for a change in the mass matrix can be treated in a similar manner. If

$$[M] \rightarrow [M] + \lambda[N]$$

and the modified modes $\{V_i\}$ and frequencies $q_i$ are as defined by equations 5.14 and 5.15, we obtain

$$a_{ij} = \frac{-\omega_i^2 B_{ij}}{\omega_i^2 - \omega_j^2} \qquad (5.26)$$

where

$$B_{ij} = \{U_j\}^T [N]\{U_i\} , \qquad (5.27)$$

and

$$P_i' = - \omega_i^2 B_{ii} \qquad (5.28)$$

## 5.3 An Idealised Model of Ring Mode Excitation of Sound

The case of structurally excited sound considered in this section consists of the car-shaped acoustic cavity described in Chapter 3 surrounded on its periphery by a simple ring. The analysis was performed in two dimensions only, but this apparent simplification can be justified because the cavity is prismatic and structural ring modes are anyway predominantly two-dimensional (that is, there is little variation of vibration amplitude across the width of the structure). The form of the three-dimensional acoustic modes in a prismatic cavity is given by equation 3.7, and it is clear that the integral across the cavity of the product of pressure amplitude and any constant vibration amplitude is zero. Thus the structural-acoustic coupling will be zero for all but the two-dimensional acoustic modes.

The finite element analysis of the acoustic cavity has already been described in Chapter 3, where the two-dimensional resonances are tabulated.

The two-dimensional ring structure surrounding the cavity was assumed to be made of material of thickness 4 cm, width 15 cm, Young's modulus $3 \times 10^{12}$ dyne $cm^{-2}$ and density 27.7 g $cm^{-3}$. These figures have no significance other than to ensure that the structural resonances are rather more numerous than acoustic resonances, a situation encountered in actual car body structures. The resonant frequencies and modes were calculated using the finite element program described in Chapter 4. The element subdivision and numbering are shown in figure 5.1, and these coincide with edges of the quadratic triangular elements used for the acoustic finite element analysis (figure 3.7).

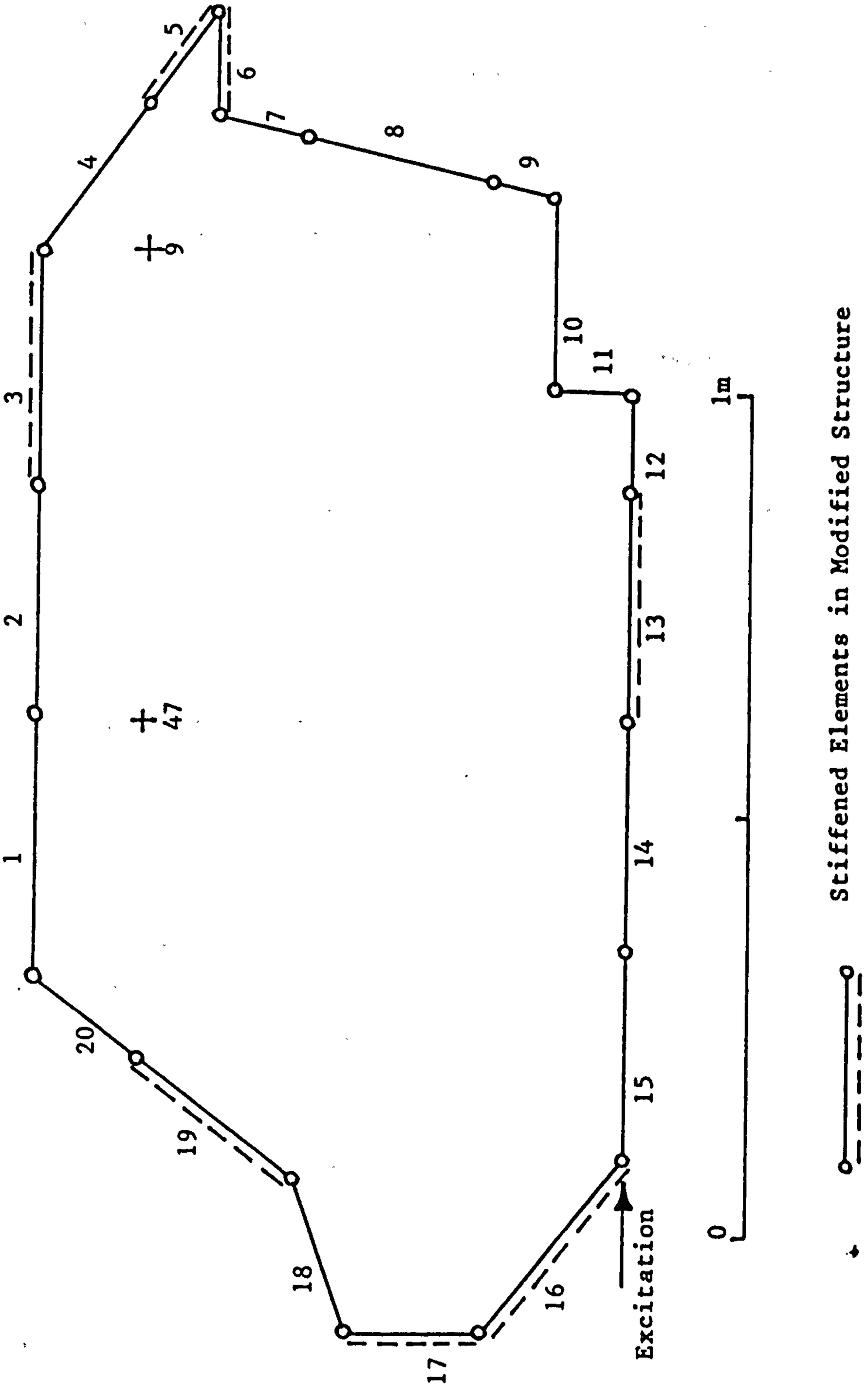


Figure 5.1 Element Subdivision of the Ring Structure

The boundary elements also coincide with the structural elements, and the following numbering scheme is used:

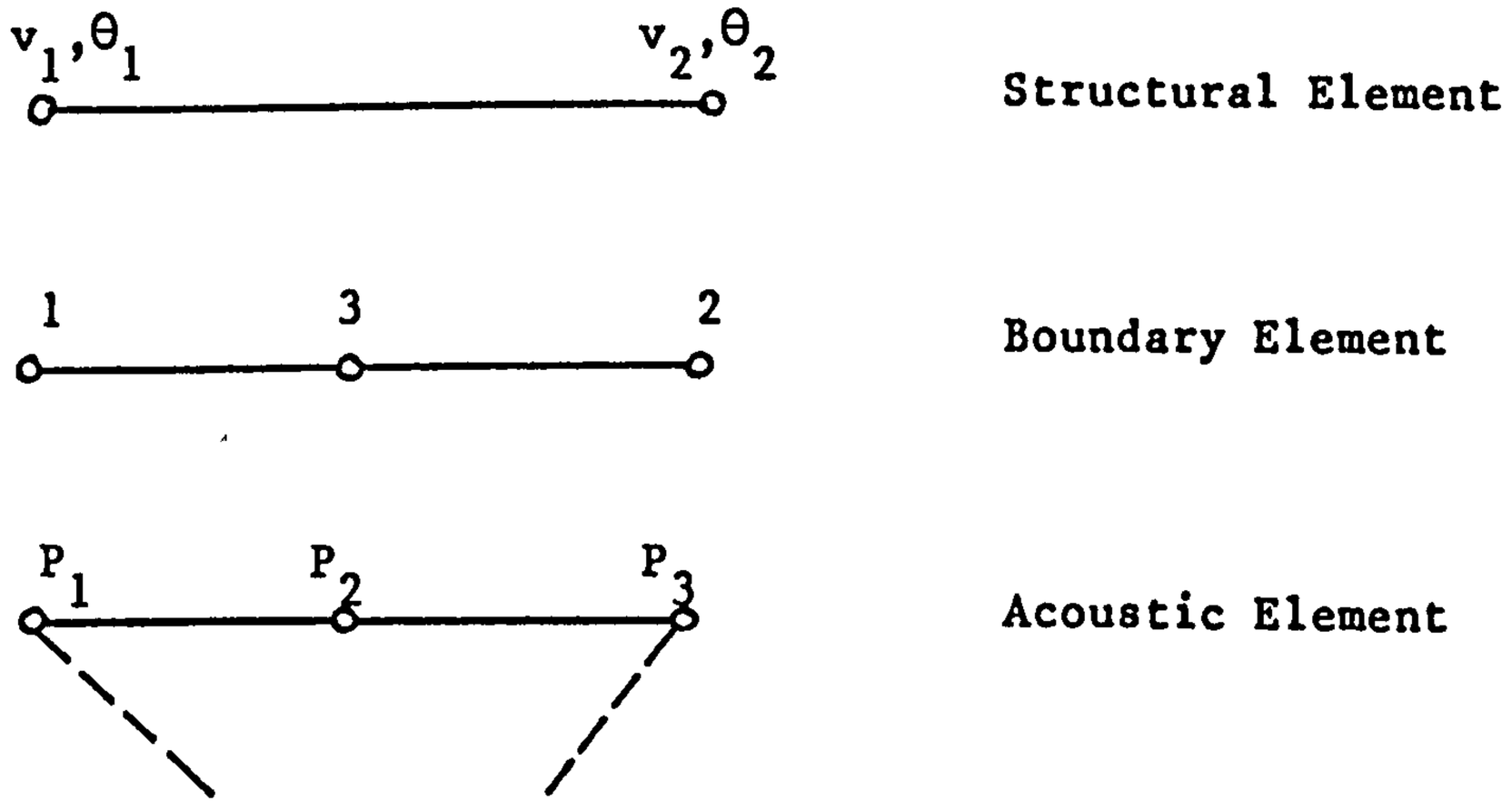


The normal structural displacement is completely specified by the four values $v_1$, $\theta_1$, $v_2$, $\theta_2$. These are obtained from the finite element modes (expressed in the global co-ordinate system) using the transformation given by equation 4.I.14. It is essential to adhere to the numbering scheme shown, that is with node 1 on the left and node 2 on the right when viewed from inside the acoustic cavity, as reversal changes the sign of the normal displacement.

Using equation 4.I.2 the normal displacement X can be expressed in the manner of equation 5.3, that is

$$X = [N]_s \{u\}$$

where

$$\{u\} = \begin{Bmatrix} v_1 \\ \theta_1 \\ v_2 \\ \theta_2 \end{Bmatrix} \qquad (5.29)$$

and

$$[N]_s^T = \begin{bmatrix} 1 - 3(x/L)^2 + 2(x/L)^3 \\ L\left(x/L - 2(x/L)^2 + 3(x/L)^3\right) \\ 3(x/L)^2 - 2(x/L)^3 \\ L\left(-(x/L)^2 + (x/L)^3\right) \end{bmatrix} \quad (5.30)$$

with $x = 0$ at node 1 and $x = L$ at node 2 (L being the length of the element).

The variation of $\phi$, the acoustic pressure amplitude, is quadratic in x and can be expressed in terms of the nodal values $P_1$, $P_2$, $P_3$ as in equation 5.2, that is

$$\phi = [N]_A \{\phi\}$$

where

$$\{\phi\} = \begin{Bmatrix} P_1 \\ P_2 \\ P_3 \end{Bmatrix} \quad (5.31)$$

and

$$[N]_A^T = \begin{bmatrix} 1 - 3(x/L) + 2(x/L)^2 \\ -(x/L) + 2(x/L)^2 \\ 4(x/L) - 4(x/L)^2 \end{bmatrix} \quad (5.32)$$

Integration of the product of X and $\phi$ over each boundary element implies a double integration both over the length of the element in x and across the width of the cavity. There is no variation in the latter direction so the final result will depend on a constant factor which is assumed here to be unity. The integration in equation 5.5 is thus carried out in x only, that is:

$$[A] = \int_0^L [N]_A^T [N]_s \, dx \qquad (5.31)$$

This integration was carried out numerically using the Gauss quadrature scheme (33). This method approximates the integral of a function as a sum of weighted samples of that function as follows:

$$I = \int_{-1}^{+1} f(a)da \approx \sum_1^n H_i \, f(a_i)$$

The accuracy depends in general on the number of sample points n, but if the function is a polynomial of order 2n-1 or less, it is integrated exactly.

Since we know that the structural displacement is cubic and the acoustic pressure amplitude is quadratic in x, the product must be of order five. Thus three sampling points are sufficient to obtain an exact integration, and the appropriate abcissae and weights are:

$a_1 = -0.77459$

$a_2 = 0.0$

$a_3 = 0.77459$

$H_1 = 0.55556$

$H_2 = 0.88889$

$H_3 = 0.55556$

Expressing the abcissae in the coordinate x to take into account the integration limits in equation 5.31 results in

$$x_i = \frac{L}{2}(a_i + 1) ,$$

and equation 5.31 becomes

$$[A] = \frac{L}{2} \sum_{i=1}^{3} H_i \left[N(x_i)\right]_A^T \left[N(x_i)\right]_s \qquad (5.32)$$

which is readily computed.

Equation 5.2 is now used to obtain the element contribution to $C_{ij}$ for the required number of combinations of structural and acoustic modes. The coefficients $C'_{ij}$ can now be calculated using the $C_{ij}$ and the known structural and acoustic resonant frequencies according to equation 2.43, and the acoustic response to a given force input can be obtained using equation 2.42.

When considering the effect of structural modifications, attention was confined to changes in the stiffness of individual elements. Any change in mass will, in addition to altering the shape of a mode and shifting its resonant frequency, affect the normalisation conditions and thus the response. It was considered desirable, in this exercise at least, to eliminate the relatively obvious effects of any such overall change in mass in favour of those due solely to changes in structural mode shape and frequency. In any case the change in mass due to a structural modification will usually in practice be somewhat less marked than the accompanying change in stiffness. For example, a change in the thickness of a simple beam element has a greater effect on the bending stiffness (proportional to the cube of the thickness) than on the mass (proportional to the thickness).

The change in element stiffness was treated simply by adding a small proportion of the element stiffness matrix (transformed to the global coordinate system) to the overall equations. In terms of the analysis of small changes given in the previous section, equation 5.18 becomes:

$$A_{ij} = \{U_j\}_e^T [k]_e \{U_i\}_e \qquad (5.33)$$

where $[k]_e$ is the element stiffness matrix and $\{U_i\}_e$ and $\{U_j\}_e$ contain the six displacements of the ith and jth modes at the nodes of the element in question. Using equations 5.19 and 5.24 and specifying $\lambda$ thus allows the changes in the coefficients $C_{ij}$ to be calculated.

Using $\lambda = 0.01$, the changes in the $C_{ij}$ were tabulated for each of the twenty structural elements in turn. Using the first order approximation the effects of changes to more than one element can thus be obtained simply by addition. The corresponding changes in the $C'_{ij}$ depends also on the change in structural resonant frequency, and these can be calculated using equation 5.25.

## 5.4 Results

The non-zero frequencies (unbracketted) and modes of the ring structure are shown in figures 5.2(a) - 5.2(l). The first three rigid body modes (translation and rotation of the structure as a whole) occurring at zero frequency are not shown, but of course must be included in the subsequent calculations. As in the structure analysed in Chapter 4, the resonances occur in pairs with the modes having the same number of wavelengths around the periphery of the ring.

The coefficients $C_{ij}$ and $C'_{ij}$ were calculated for all structural and acoustic modes up to a frequency of 500 Hz. The six values of $C'_{ij}$ having the greatest magnitude are given in table 5.1(a), along with the associated values of $C_{ij}$ and the structural and acoustic resonant frequencies. As expected, these occur only when the structural and acoustic resonant frequencies are reasonably close together, although the two largest $C'_{ij}$ are also associated with the largest values of $C_{ij}$.

The approach taken to structural modification was to stiffen selected elements in an effort to reduce these values of $C'_{ij}$. The first step was to attempt a reduction in the associated values of $C_{ij}$. Using the tabulated changes (calculated to first order as described in section 5.2) resulting from the changes in element stiffness, it was possible to pick a number of elements for which an increase in stiffness had the effect of reducing most of the $C_{ij}$ in question. This procedure was carried out simply by visual inspection. It is also necessary to take into account changes in the structural resonant frequencies resulting from the

combined increase in stiffness. It is apparent, in this case, that an appreciable increase in the structural resonant frequencies will have a beneficial effect on all the $C'_{ij}$ involved.

The elements selected for stiffening were numbered 3, 5, 6, 13, 16, 17 and 19 in the finite element subdivision, and these are shown in figure 5.1. In each case the stiffness was increased by 50%. The finite element analysis was repeated for the modified structure, and the new $C_{ij}$ and $C'_{ij}$ were calculated. These are shown in table 5.1(b) with the modified resonant frequencies, and in all cases but one there is an improvement on the original structure. The exception is the coupling between the zero frequency acoustic mode and the structural mode at 85.9 Hz (90.4 Hz in the modified structure), where there is an increase in $C_{ij}$. The shift in resonant frequency, however, results in a minimal increase in the corresponding value of $C'_{ij}$.

The modified resonant frequencies are shown bracketted in figures 5.2(a) - 5.2(1). The modified modes are not shown, as, perhaps surprisingly, the difference between these and the unmodified modes was found to be almost imperceptible on a plot of this sort.

In table 5.2 the changes in the first eight non-zero resonant frequencies are compared with the first-order approximations, and the agreement is fair given the extent of the structural modifications.

The changes in the coefficients $C_{ij}$ are shown in table 5.3, where they are compared with the first-order predictions. The agreement is not good, indicating that the change in the structure was rather too large for the first-

order approximation to be accurate. This view is confirmed by the relatively good agreement for the first two $C_{ij}$, where the changes are quite small. However, used as it was as a rough indication of the effects of structural change, the first-order approximation appears valuable for quite large modifications.

The acoustic response for a sinusoidal force of 1 newton r.m.s. applied to the structure was calculated using equation 2.42. The position and direction of the exciting force is shown in figure 5.1, and the calculation was performed for the frequency range 40-400 Hz, using all structural and acoustic modes up to 500 Hz. In order to limit the response at resonance, the acoustic and structural resonant frequencies were given a small imaginary component such that:

$$\omega_i \rightarrow \omega_i + i\omega\gamma \ ,$$

$$\Omega_i \rightarrow \Omega_i + i\omega\gamma$$

where $\omega$ is the frequency of excitation, and $\gamma = 5 \times 10^{-3}$. Multiplying the imaginary component by $\omega$ in this way has the effect of cancelling the factor $\omega^2$ in equation 2.42 at resonance. This prevents an undesirable, and probably physically unrealistic, increase in the height of the resonant peaks with increasing frequency.

The acoustic response (in db referred to $2 \times 10^{-5}$ $Nm^{-2}$) was calculated for the unmodified and modified structures at two positions (nodes 9 and 47 in the acoustic F.E. mesh) which are indicated in figure 5.1. These responses are shown in

figures 5.3 and 5.4. The most drastic reduction occurs at 175.1 Hz, where the structural and acoustic resonances were extremely close in the unmodified structure. In addition there are useful reductions of a few db in a number of other resonances, and at no point does the response of the modified structure significantly exceed that of the initial structure.

In order to to investigate the accuracy of the approximate methods, the eigenvalue solution was repeated fully for values of $\lambda$ increasing to 0.5 in increments of 0.05. The fractional changes in resonant frequency are shown in Figs. 5.5(a) - (h) and are compared with the linear and second order perturbation approximations. As expected, the second order approximation gives a considerable improvement in most cases.

Table 5.1(a) Structural-Acoustic Coupling Coefficients of the Unmodified Structure

| Acoustic Resonant Frequency $\Omega_i$ (Hz) | Structural Resonant Frequency $\omega_j$ (Hz) | $C_{ij}/10^{-4}$ | $C'_{ij}/10^{-10}$ |
|---|---|---|---|
| 175.1 | 174.2 | 3.29 | 256.34 |
| 0.0 | 64.3 | 3.37 | 20.65 |
| 330.2 | 335.2 | -2.10 | -16.04 |
| 0.0 | 85.9 | -1.51 | -5.18 |
| 455.1 | 442.8 | 1.98 | -4.52 |
| 309.6 | 335.2 | 2.64 | 4.05 |

Table 5.1(b) Structural-Acoustic Coupling Coefficients of the Modified Structure

| Acoustic Resonant Frequency $\Omega_i$ (Hz) | Structural Resonant Frequency $\omega_j$ (Hz) | $C_{ij}/10^{-4}$ | $C'_{ij}/10^{-10}$ |
|---|---|---|---|
| 175.1 | 190.0 | 3.11 | 14.52 |
| 0.0 | 70.4 | 3.23 | 16.51 |
| 330.2 | 354.8 | -1.23 | -1.85 |
| 0.0 | 90.4 | -1.68 | -5.20 |
| 455.1 | 480.5 | 1.48 | -1.58 |
| 309.6 | 354.8 | 1.40 | 1.19 |

Table 5.2 Comparison of the Exact Changes in Structural Resonant Frequency with the First-Order Approximation

| Unmodified Resonant Frequency (Hz) | Modified Resonant Frequency (Hz) | Actual Change | 1st Order Approximation |
|---|---|---|---|
| 64.3 | 70.4 | 6.1 | 7.9 |
| 85.9 | 90.4 | 4.5 | 6.2 |
| 174.2 | 190.0 | 15.8 | 20.0 |
| 202.4 | 216.4 | 14.0 | 18.3 |
| 335.2 | 354.8 | 19.6 | 35.5 |
| 347.6 | 381.6 | 34.0 | 31.1 |
| 442.8 | 480.5 | 37.7 | 45.7 |
| 552.3 | 578.2 | 25.9 | 32.2 |

Table 5.3 Comparison of the Actual Changes in $C_{ij}$ with the First-Order Approximation

| $C_{ij}/10^{-4}$ Unmodified | $C_{ij}/10^{-4}$ Modified | Actual Change % | 1st Order Approximation % |
|---|---|---|---|
| 3.29 | 3.11 | -5.5 | -6.6 |
| 3.37 | 3.23 | -4.2 | -4.7 |
| -2.10 | -1.23 | -20.7 | -40.2 |
| -1.51 | -1.68 | +5.6 | +14.0 |
| 1.98 | 1.48 | -12.6 | -25.5 |
| 2.64 | 1.40 | -23.5 | -57.0 |

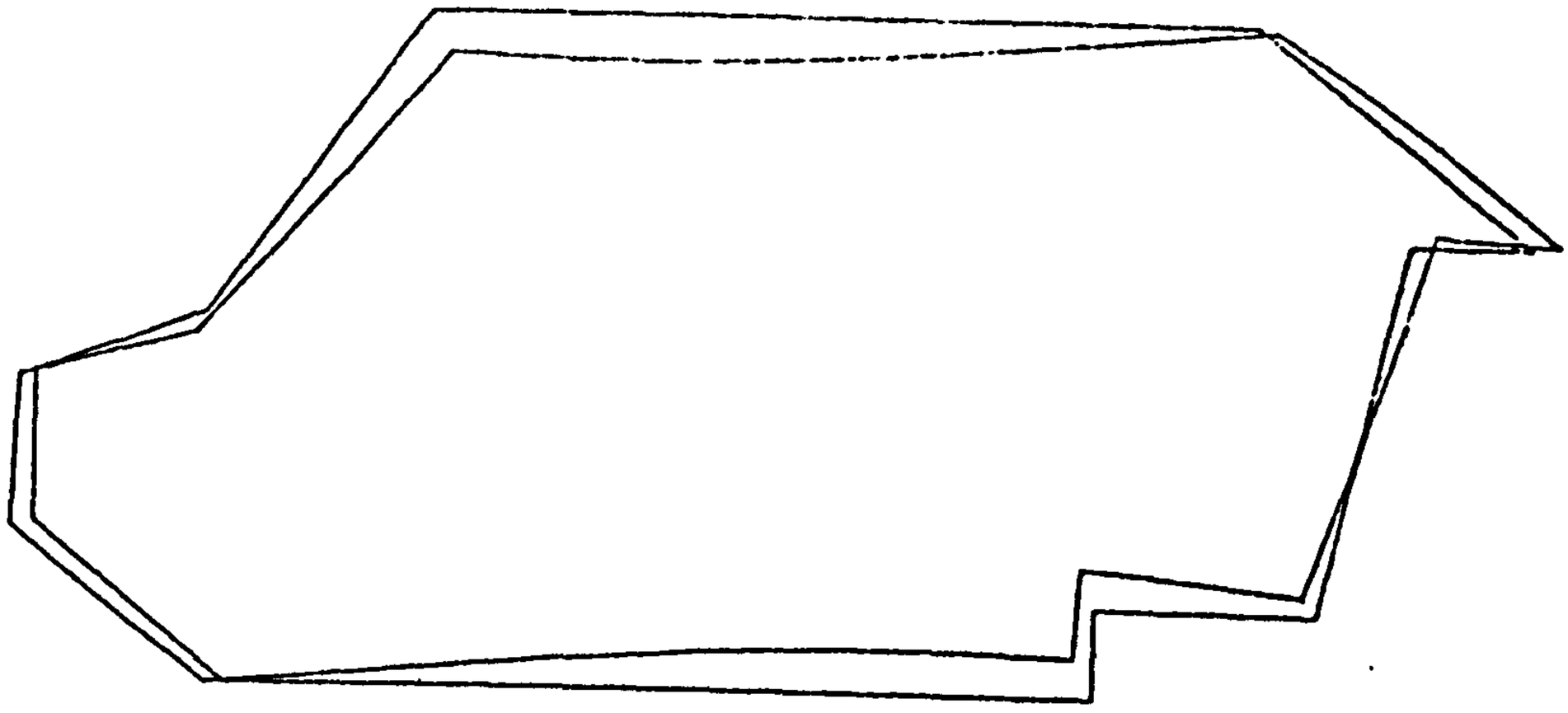

FIG. 5.2 (a) MODE AT 64.3 (70.4) HZ

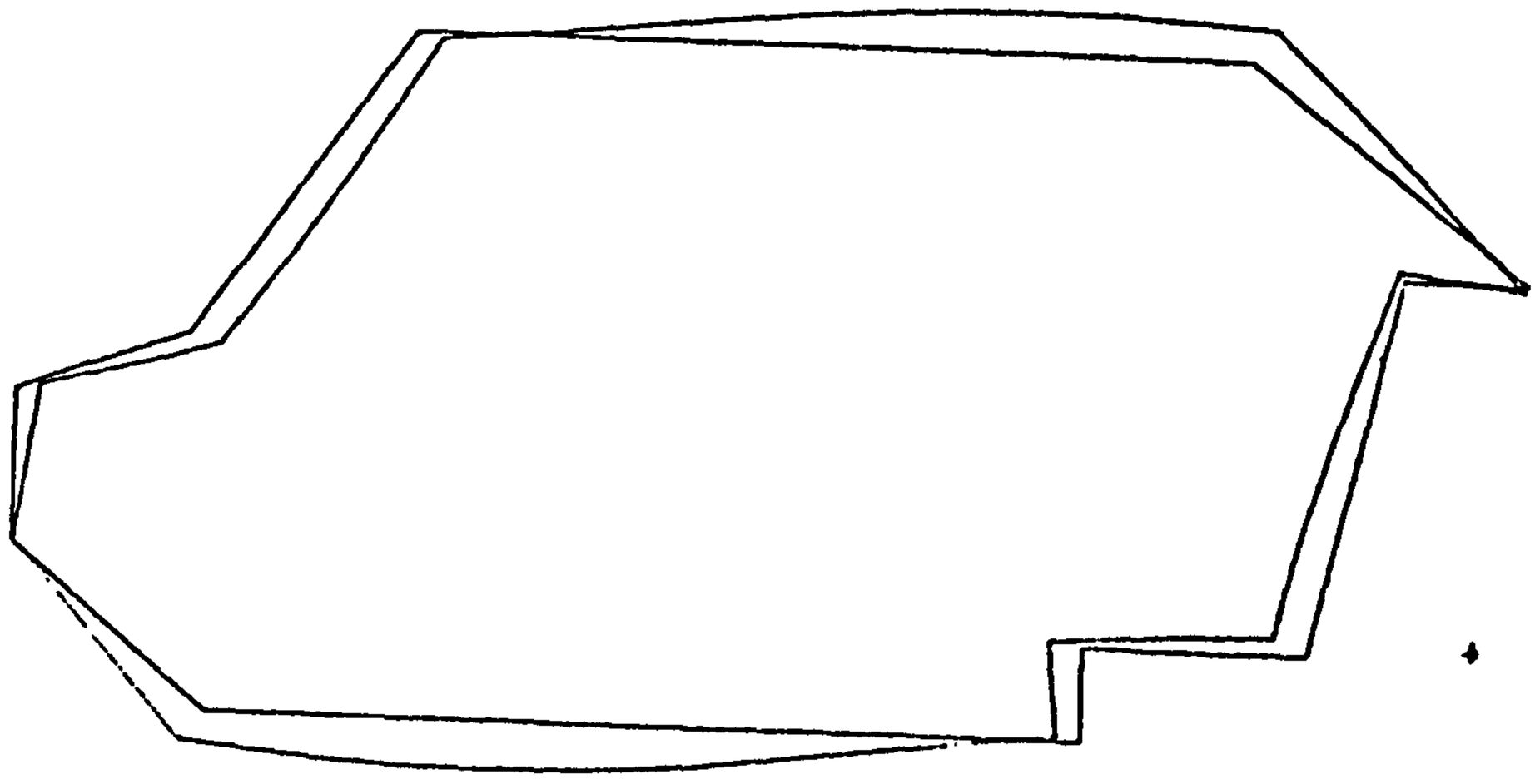

FIG. 5.2 (b) MODE AT 85.9 (90.4) HZ

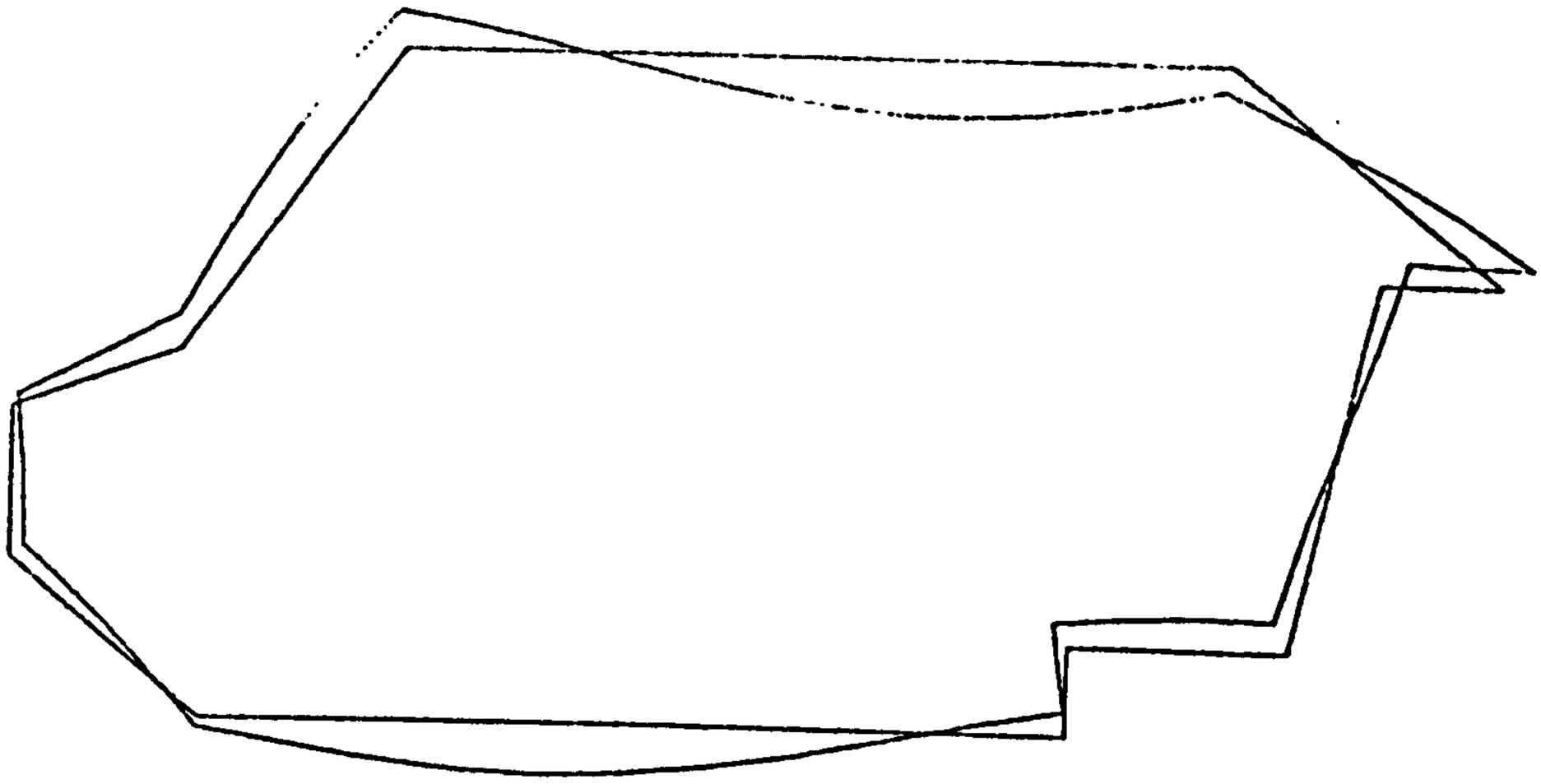

FIG. 5.2 (c) MODE AT 174.2 (190.0) HZ

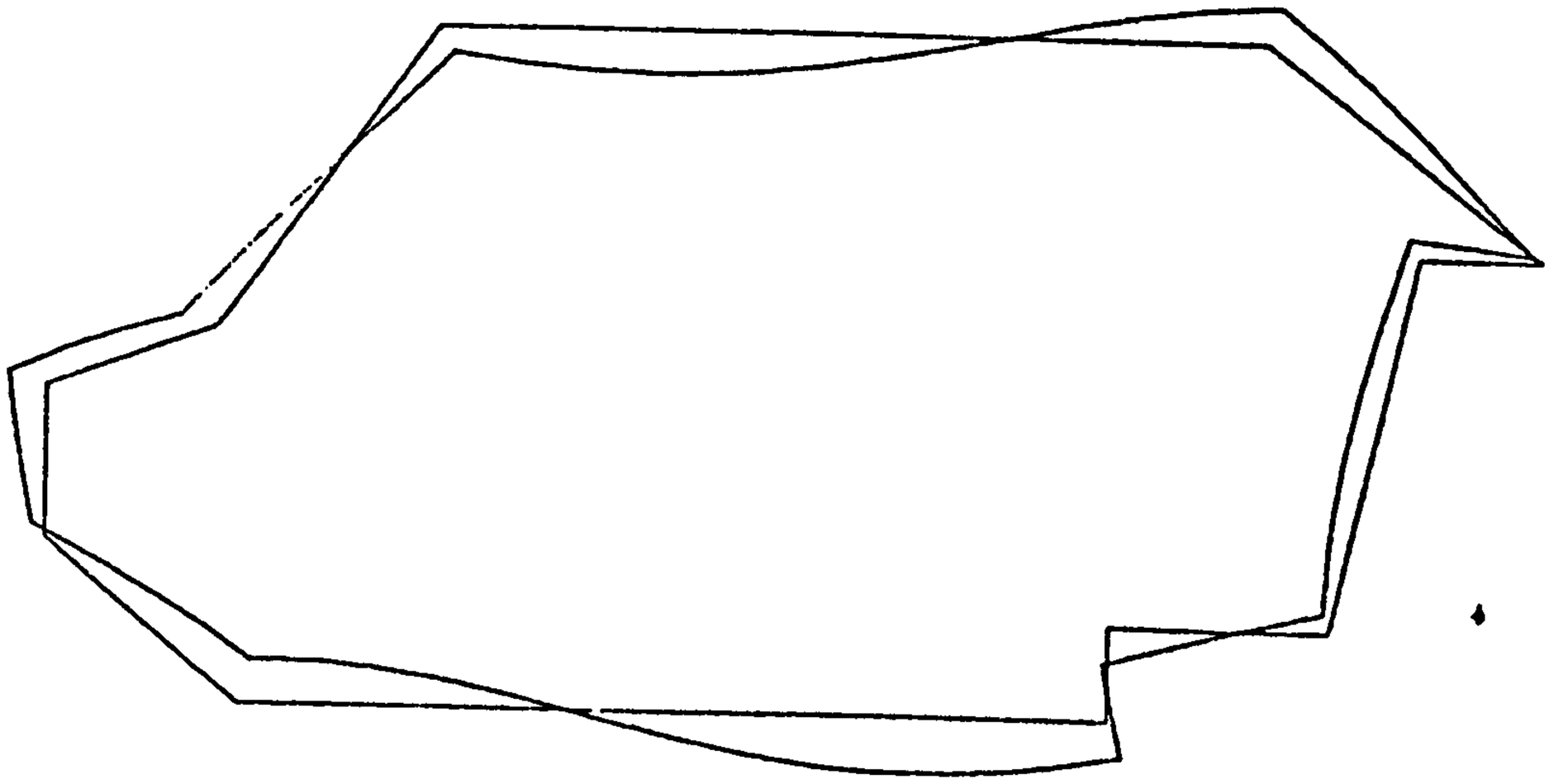

FIG. 5.2 (d) MODE AT 202.4 (216.4) HZ

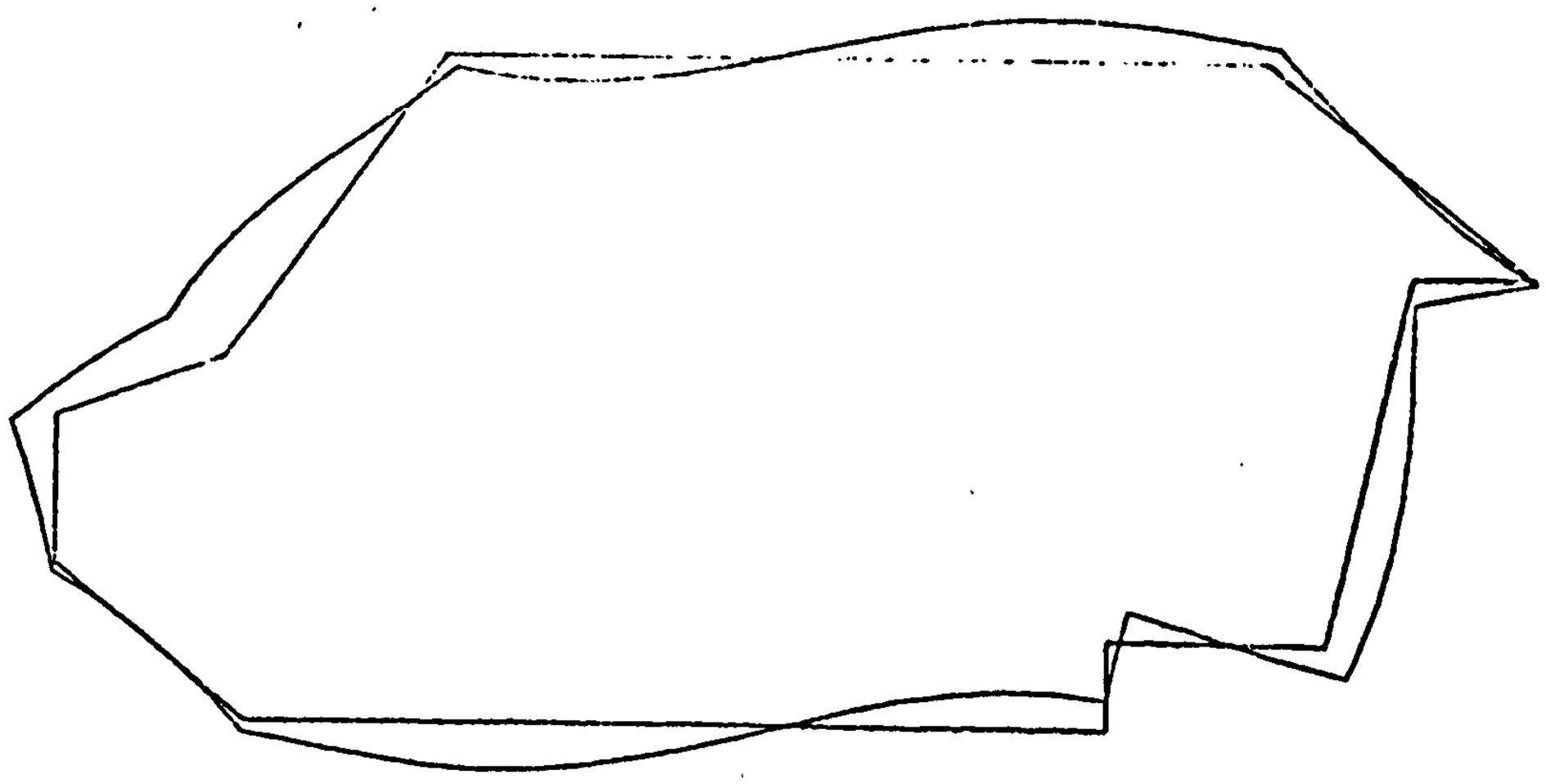

FIG. 5.2 (e) MODE AT 335.2 (354.8) HZ

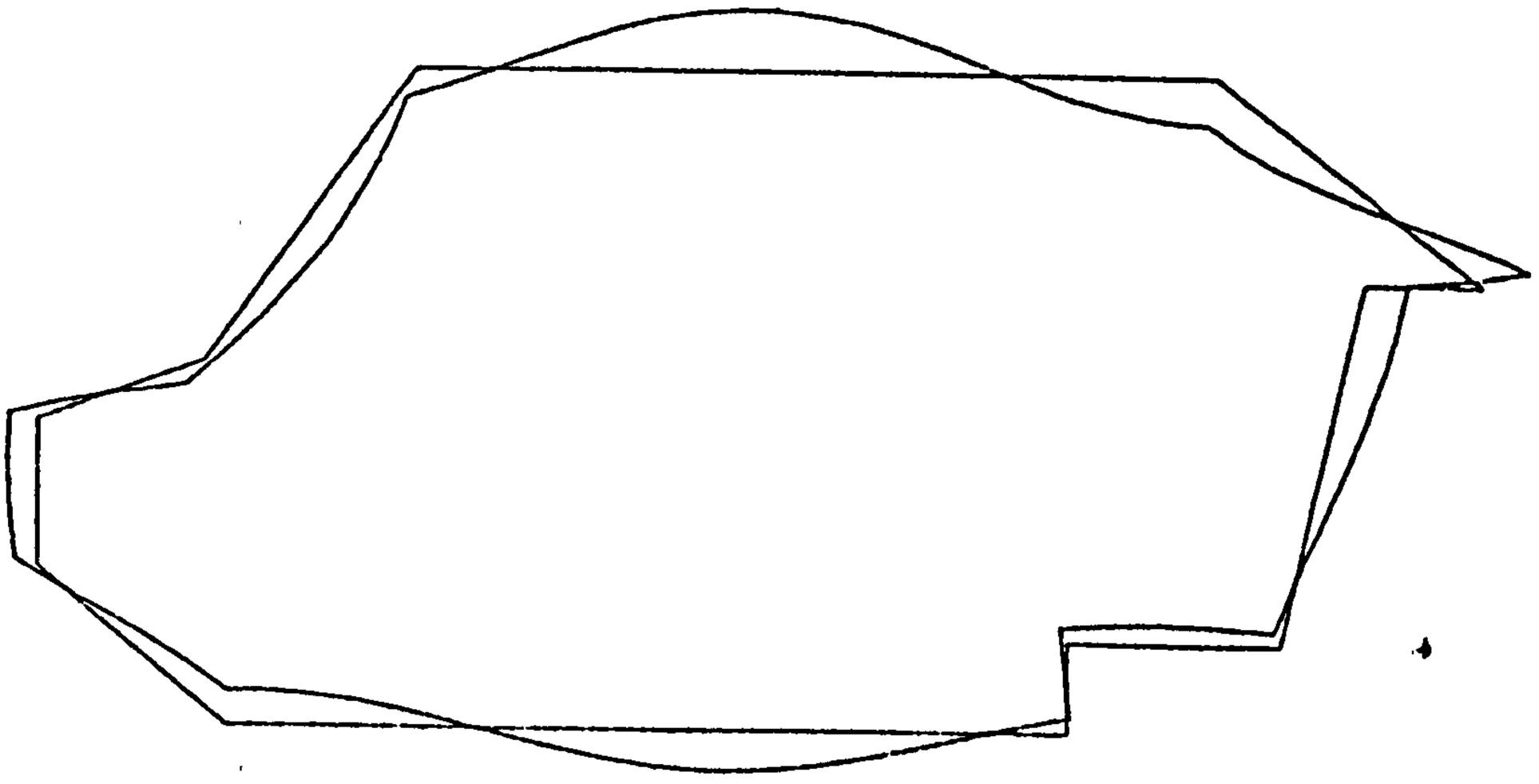

FIG. 5.2 (f) MODE AT 347.6 (381.6) HZ

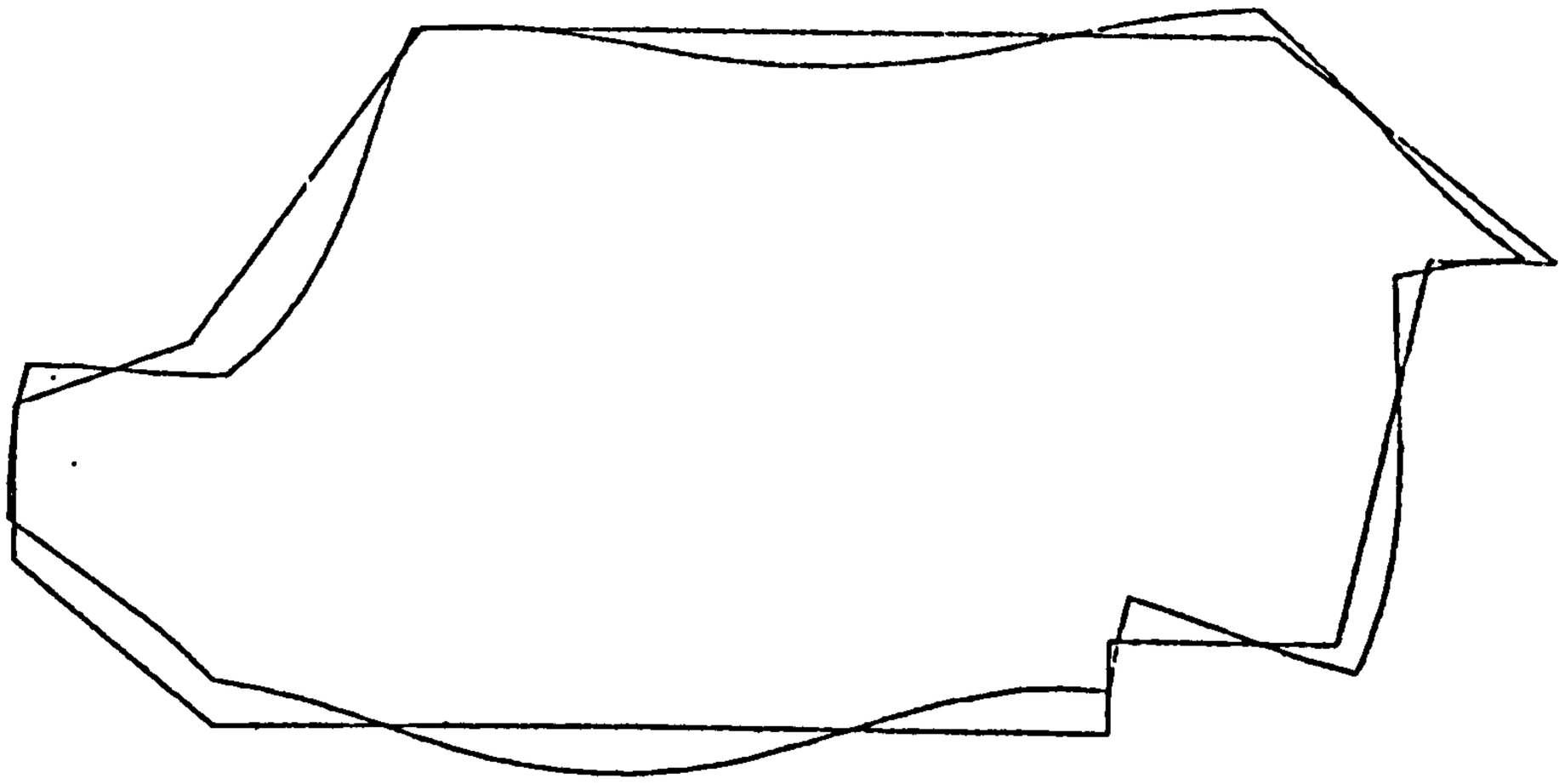

FIG. 5.2 (g) MODE AT 442.8 (480.5) HZ

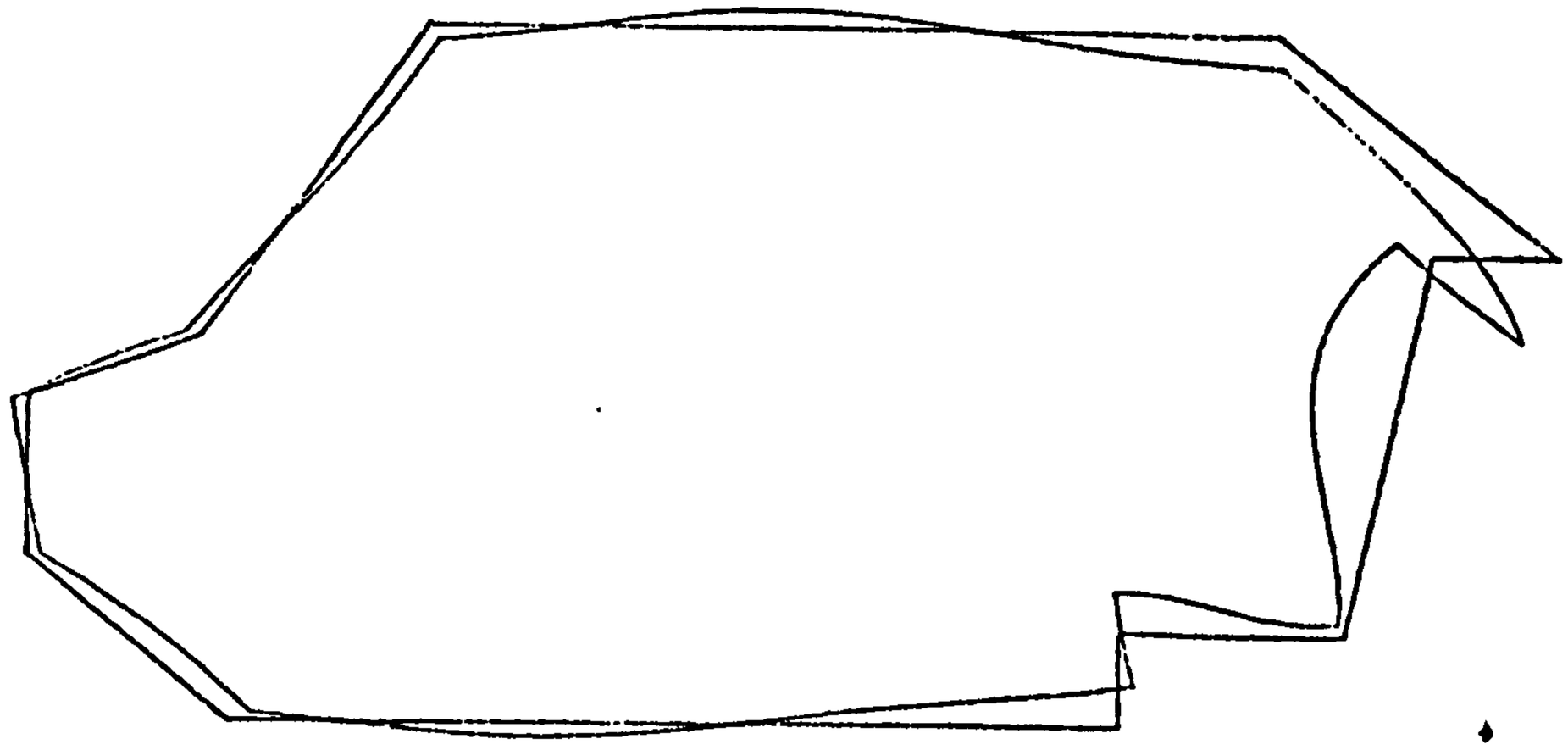

FIG. 5.2 (h) MODE AT 552.3 (578.2) HZ

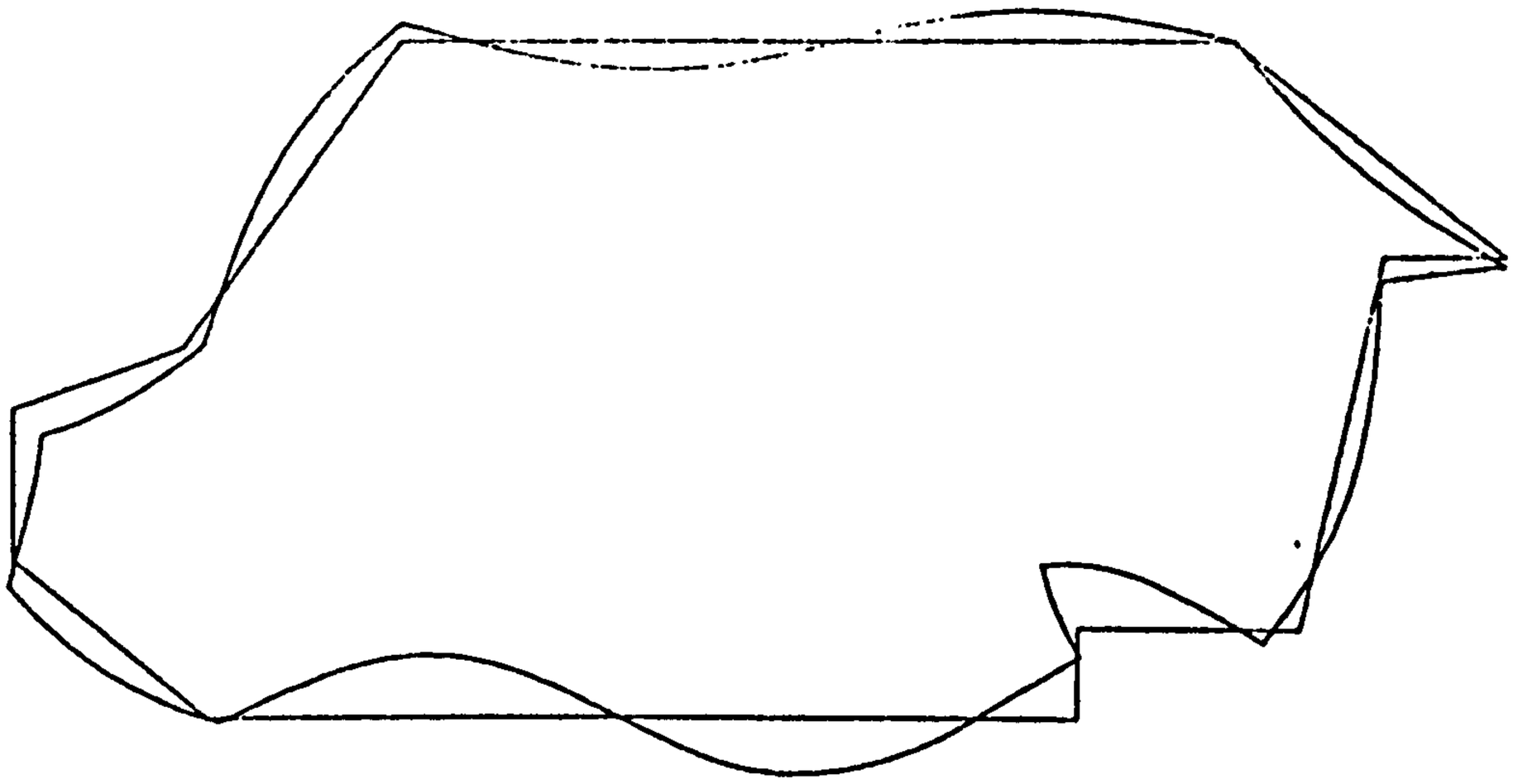

FIG. 5.2 (i) MODE AT 627.2 (670.4) HZ

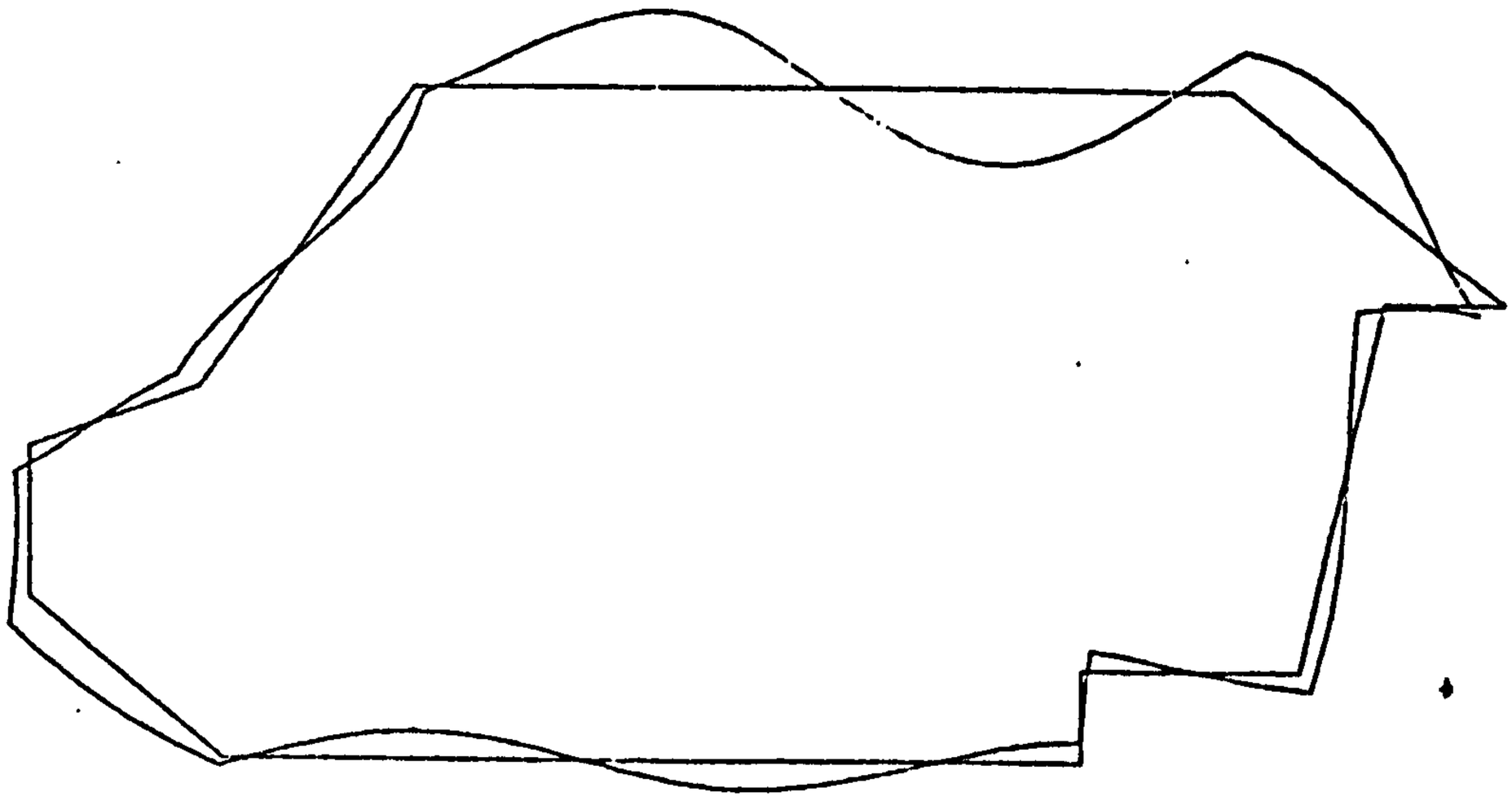

FIG. 5.2 (j) MODE AT 735.9 (786.2) HZ

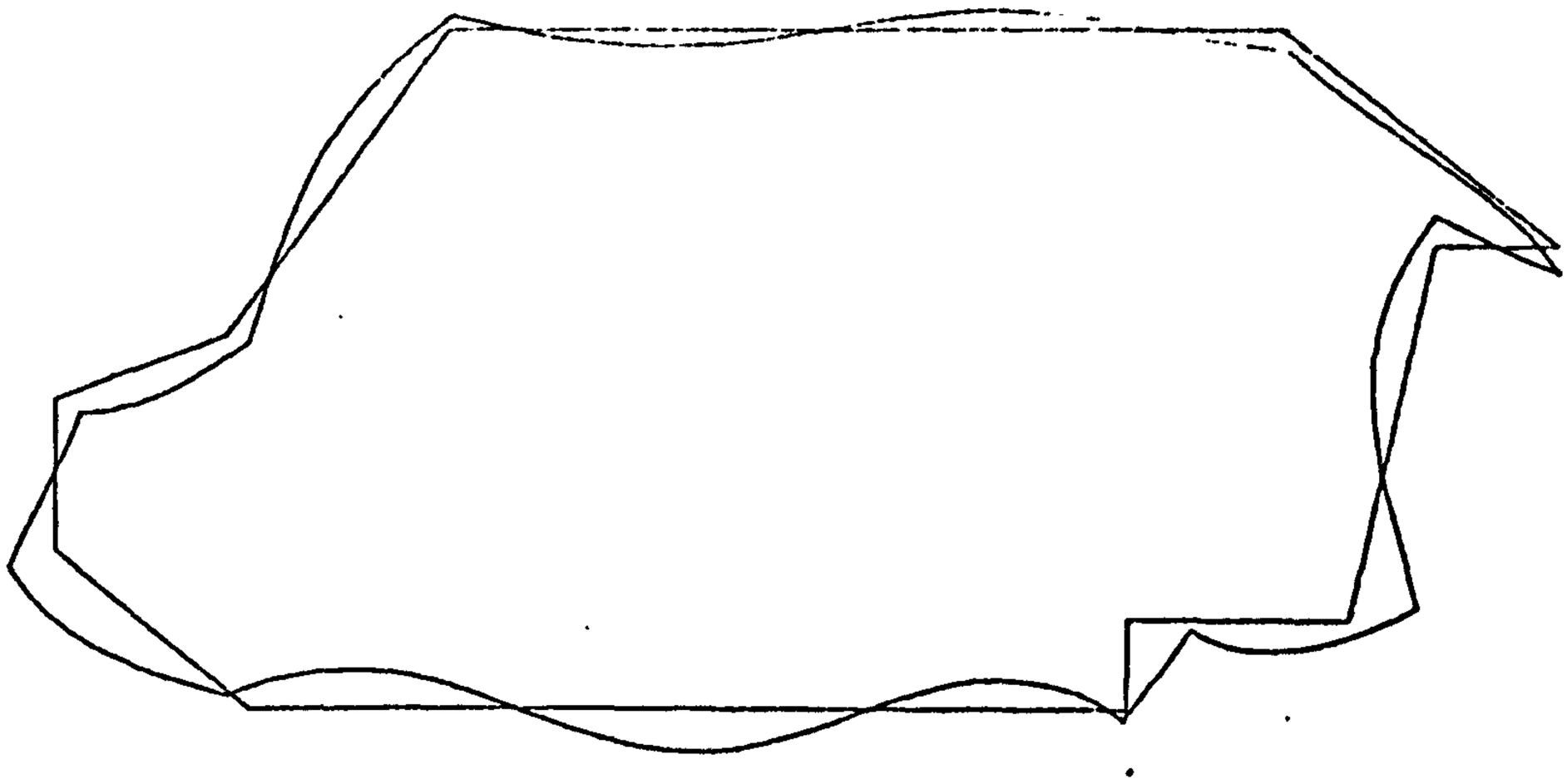

FIG. 5.2 (k) MODE AT 819.7 (867.8) HZ

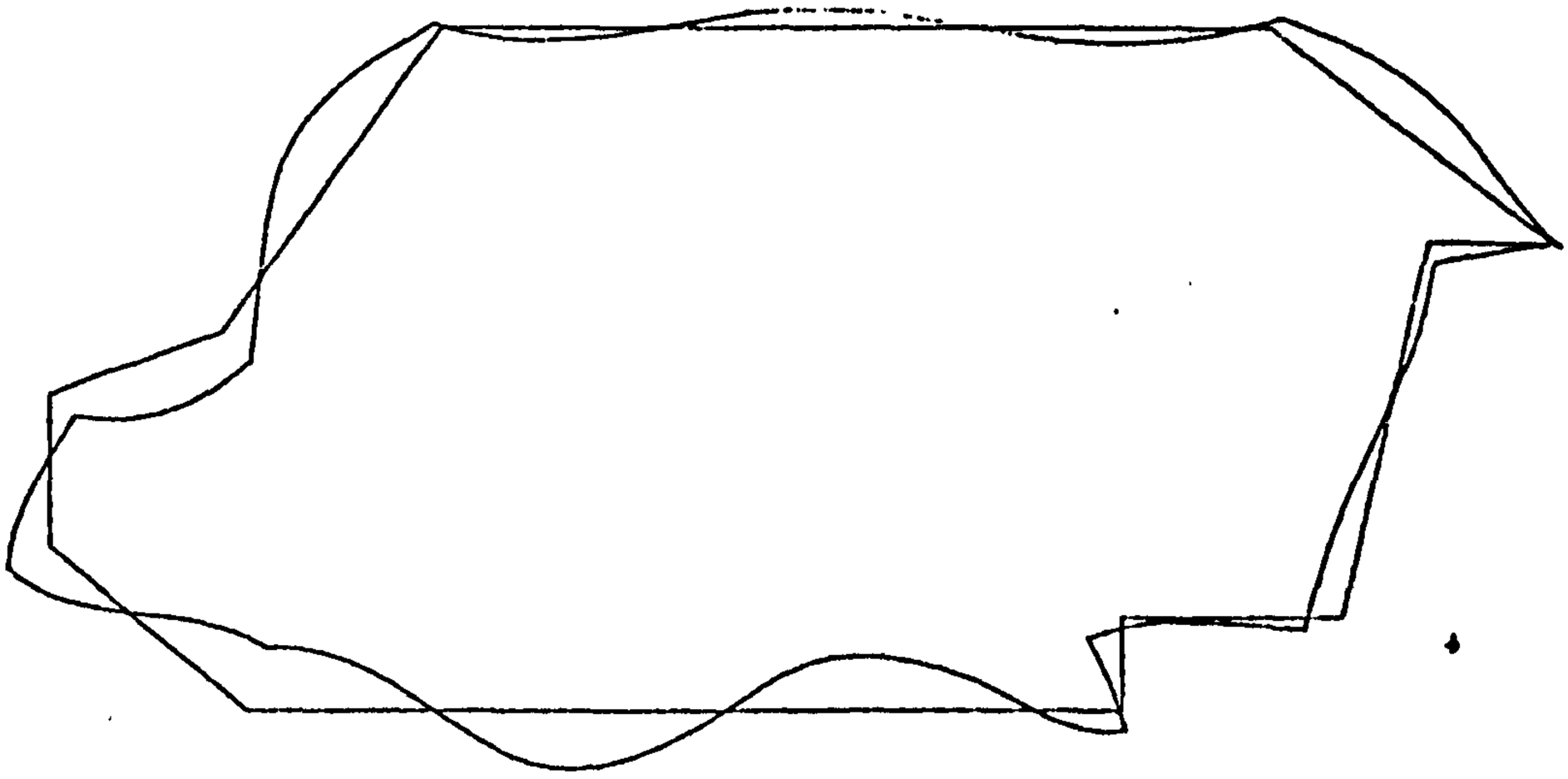

FIG. 5.2 (L) MODE AT 1056.4 (1144.5) HZ

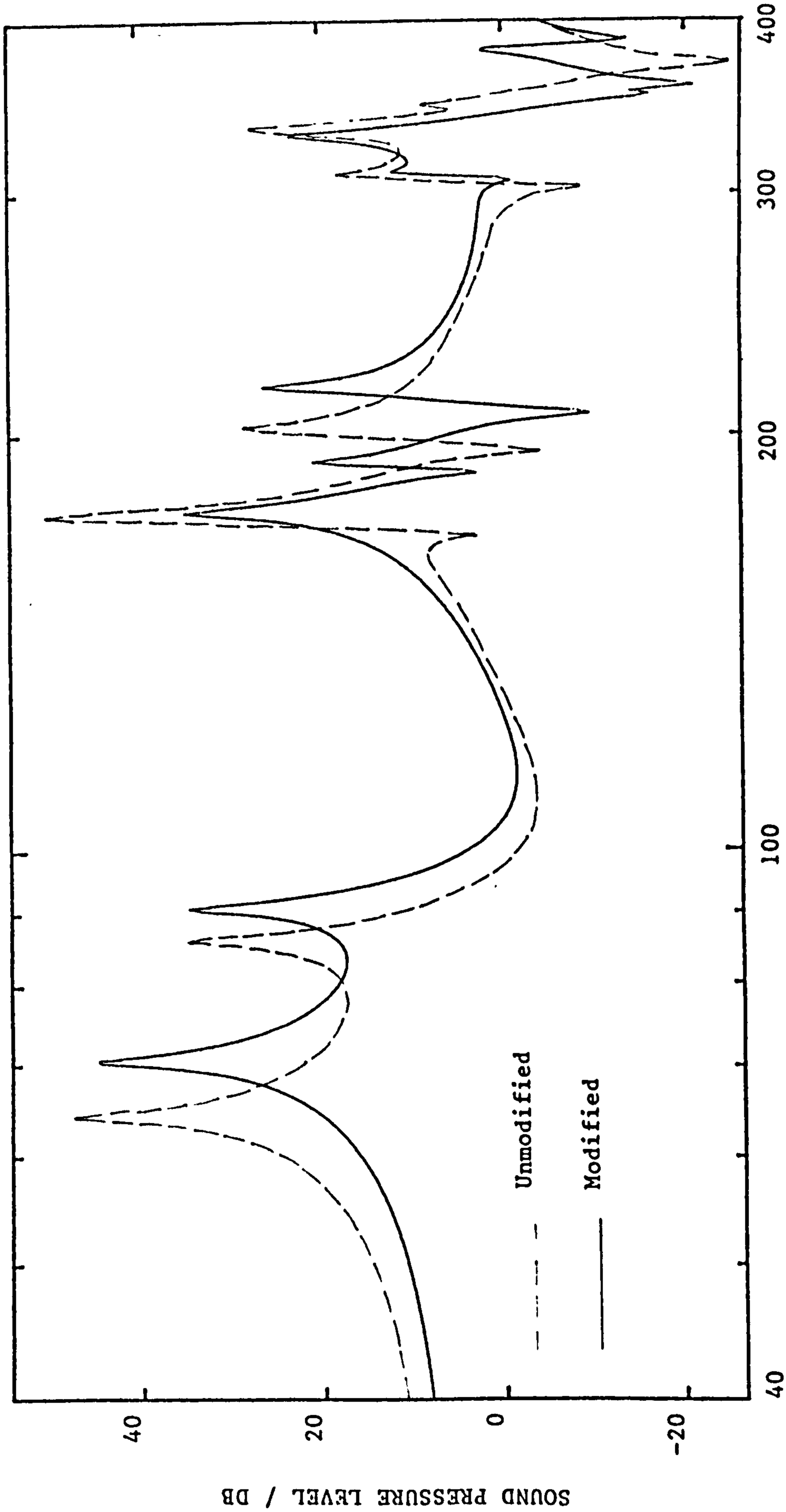


FIG. 5.3 ACOUST

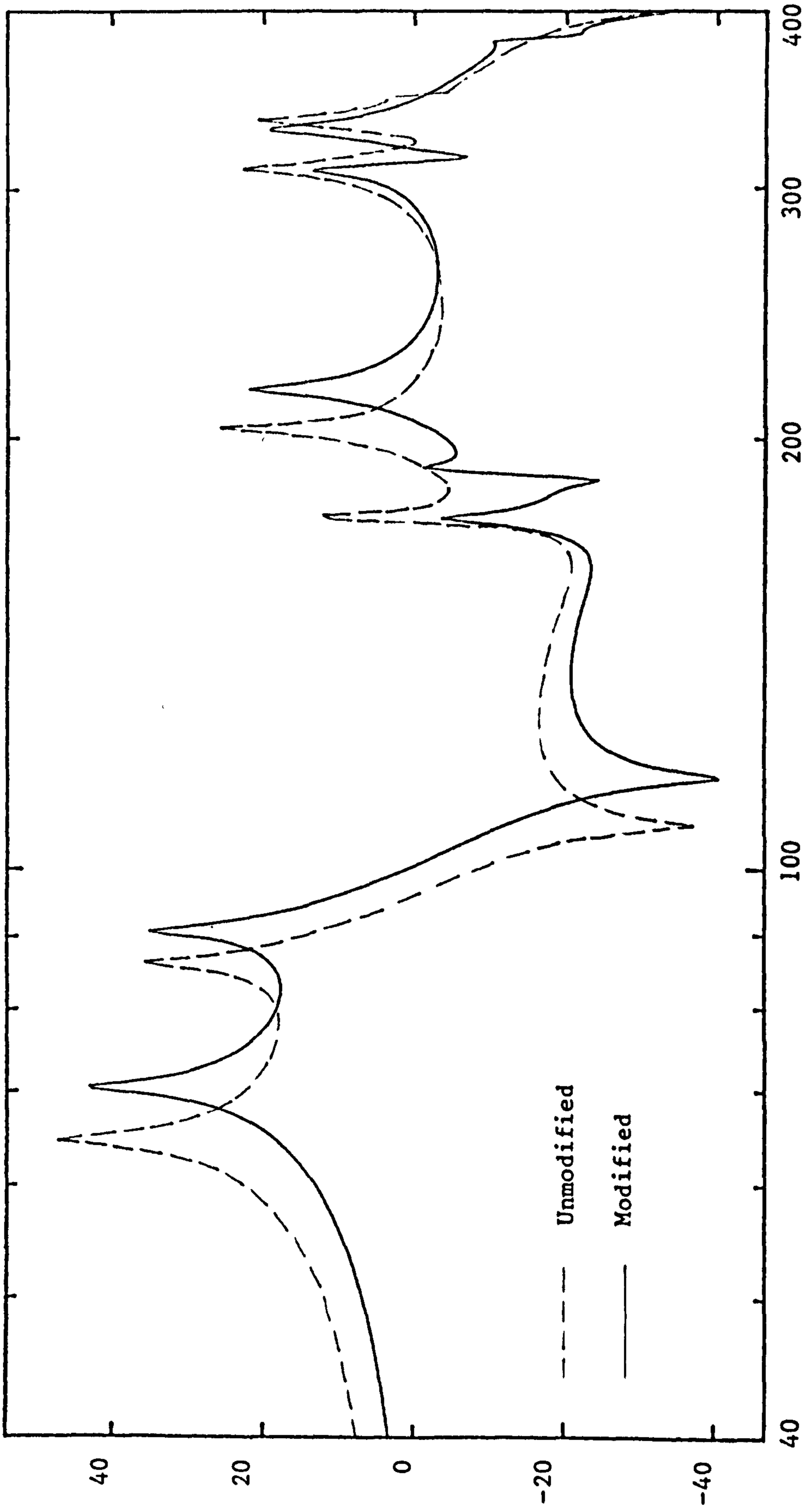


FIG. 5.4 ACOUSTIC RESPONSE TO STRUCTURAL EXCITATION

Figs. 5.5(a) - 5.5(h)

Fractional change in structural resonant frequency.

Actual change X X

Linear approximation — — — — —

Second order approximation —.—.—.—

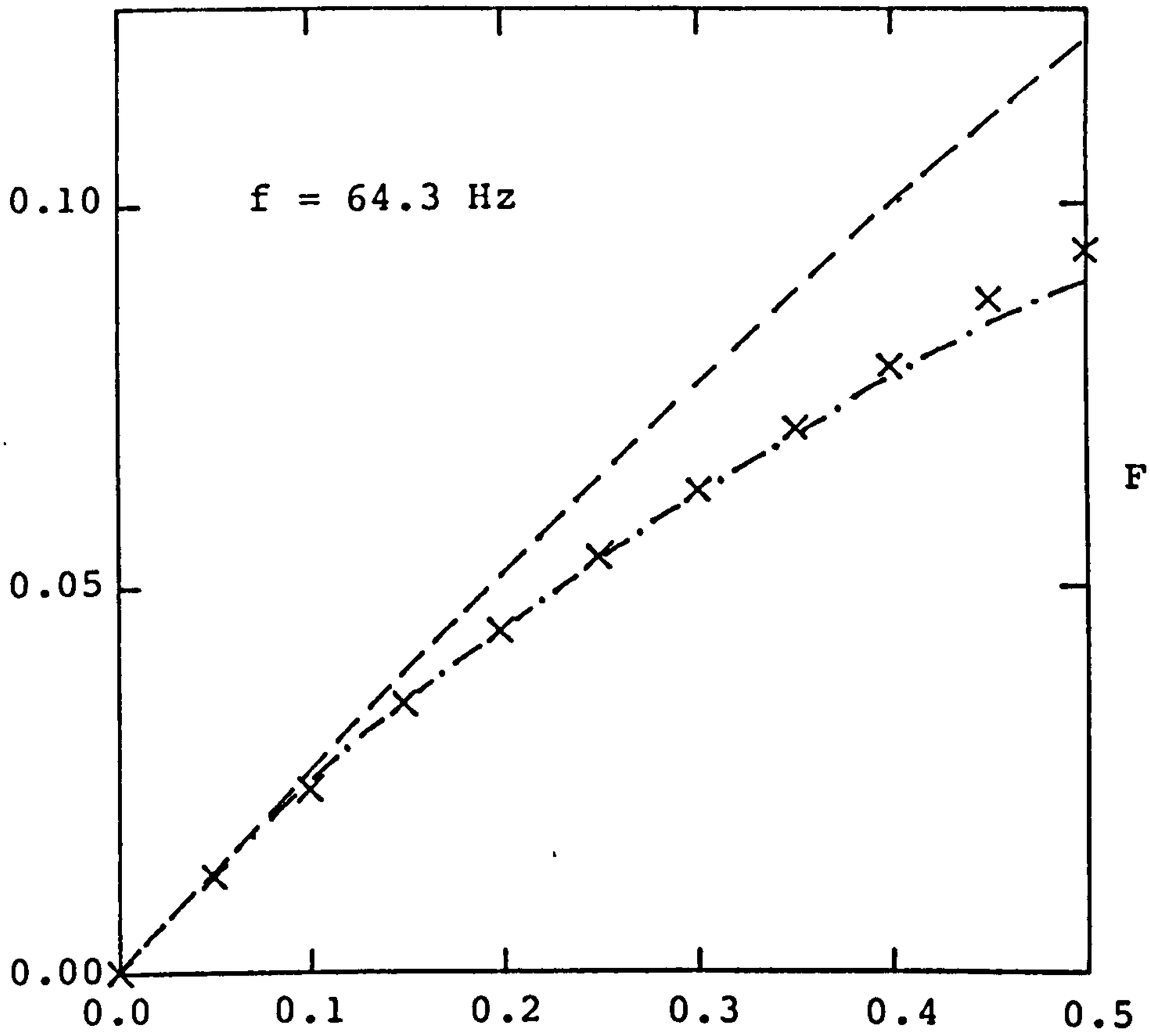


Fig. 5.5(a)

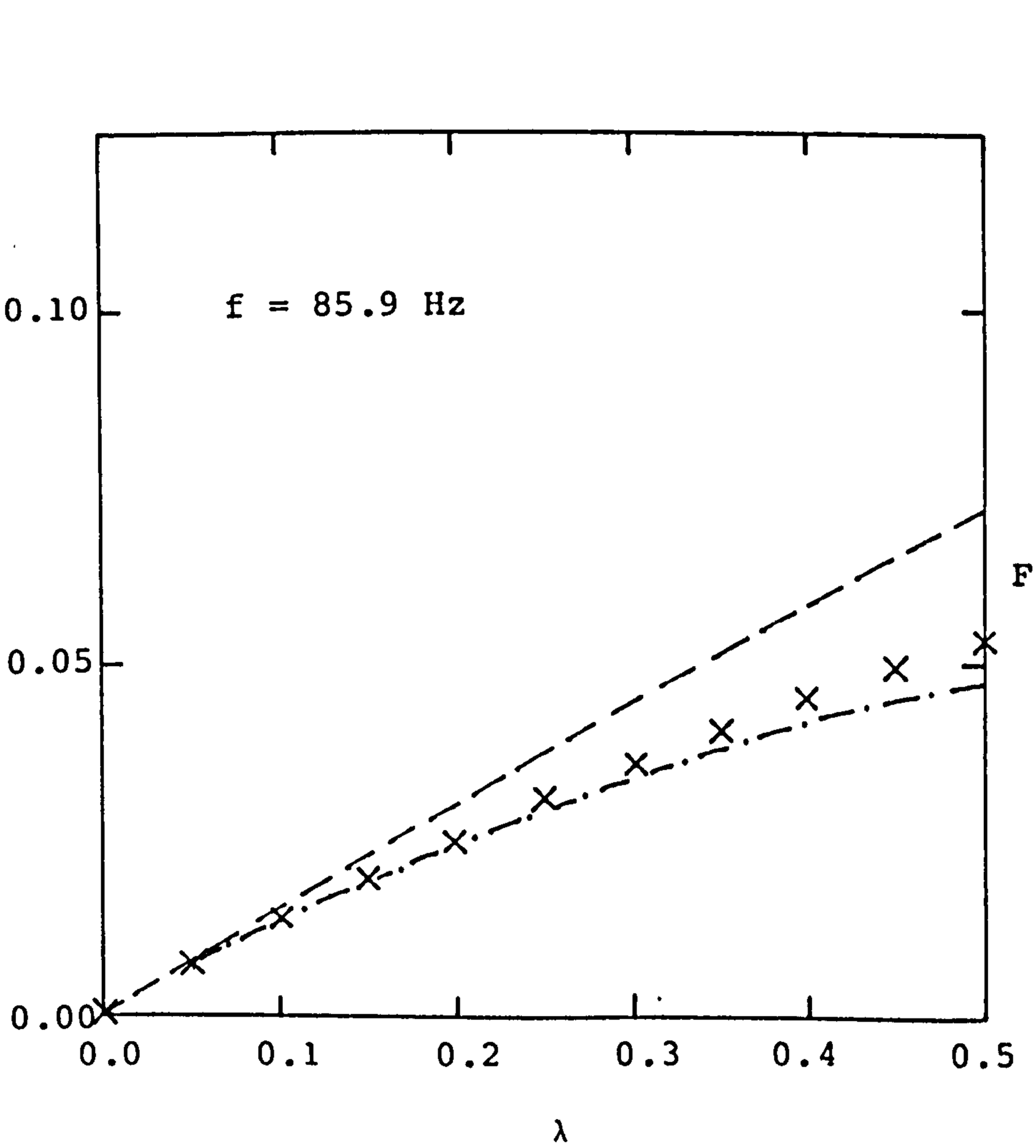


Fig. 5.5(b)

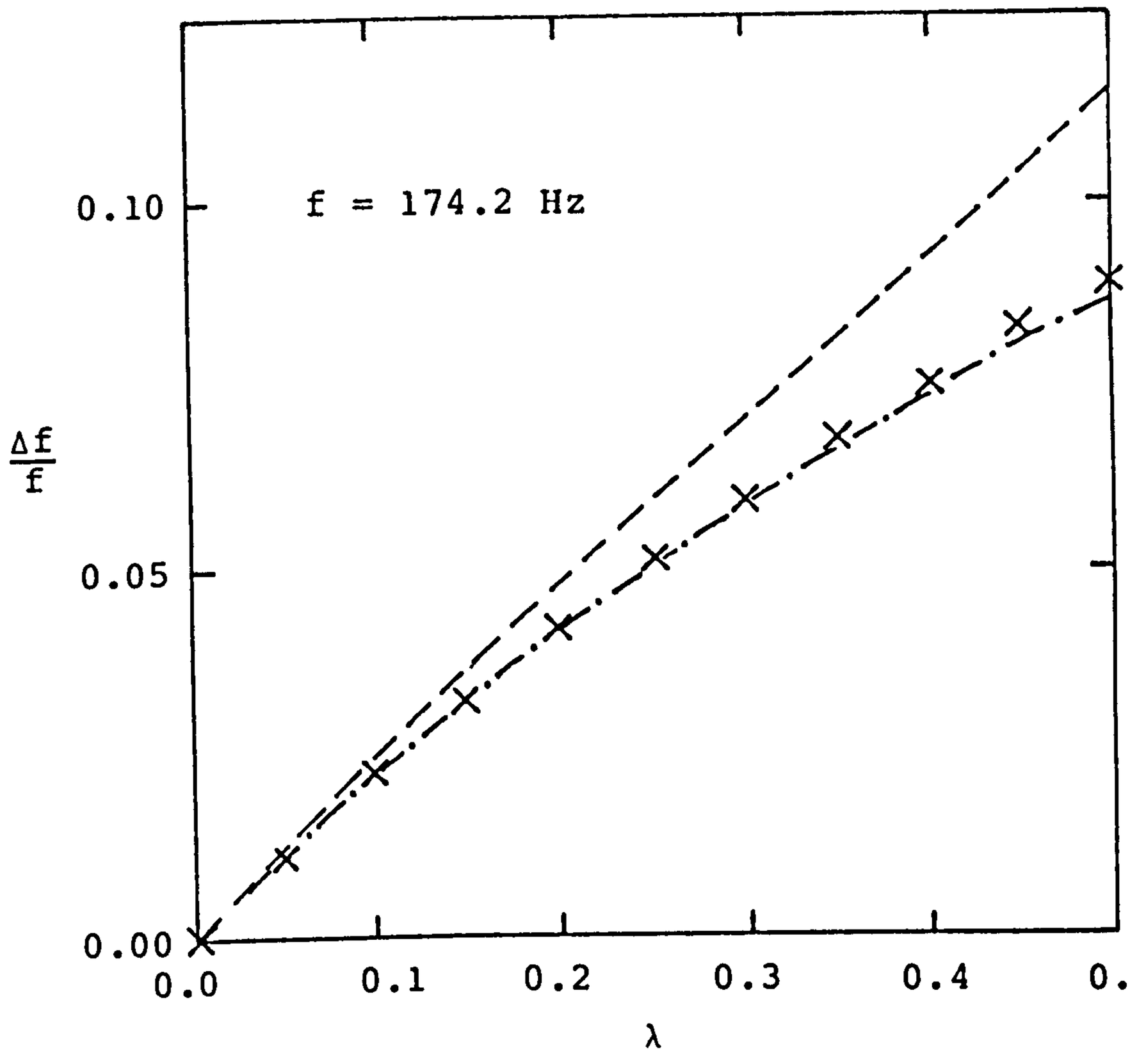


Fig. 5.5(c)

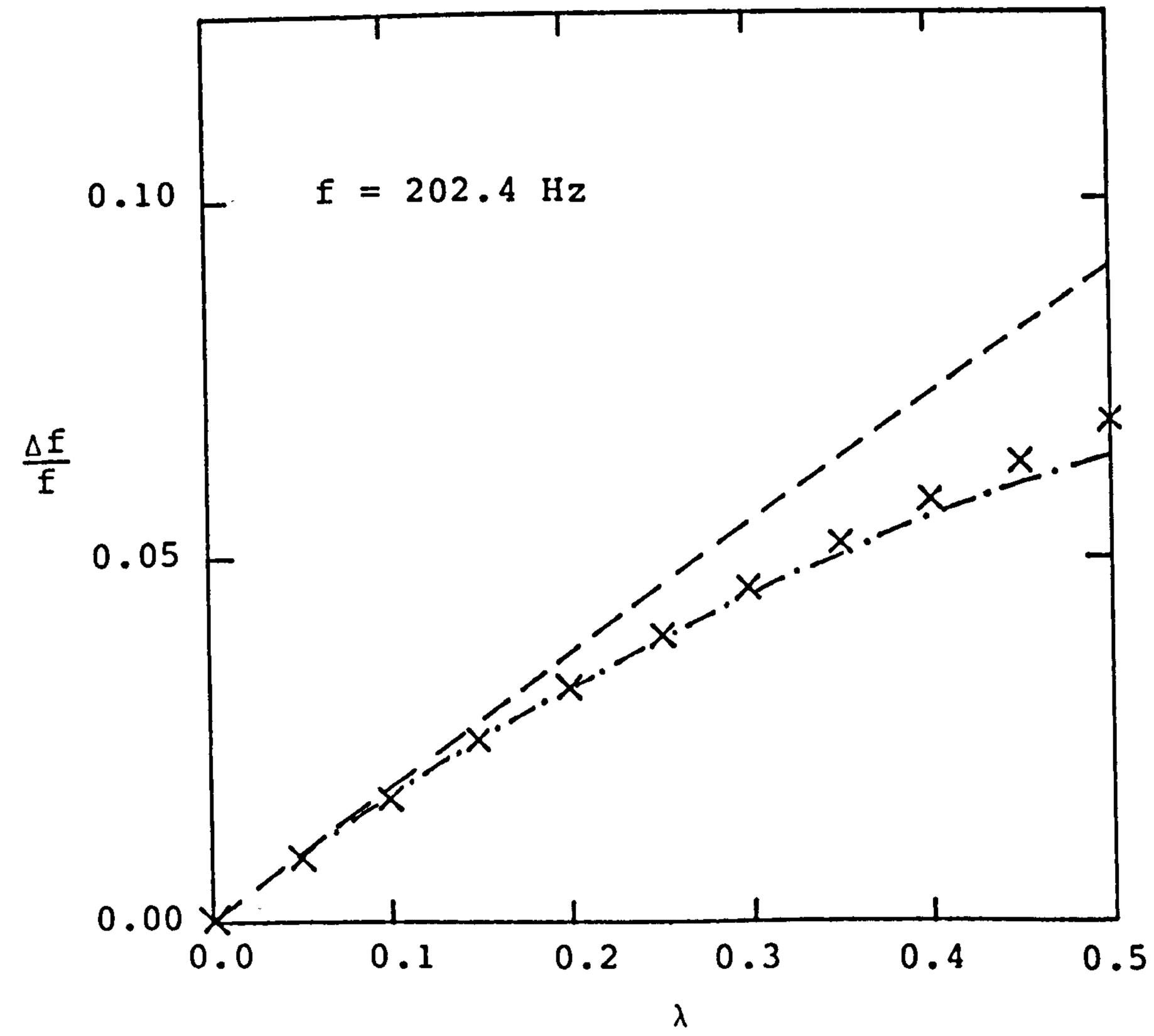


Fig. 5.5(d)

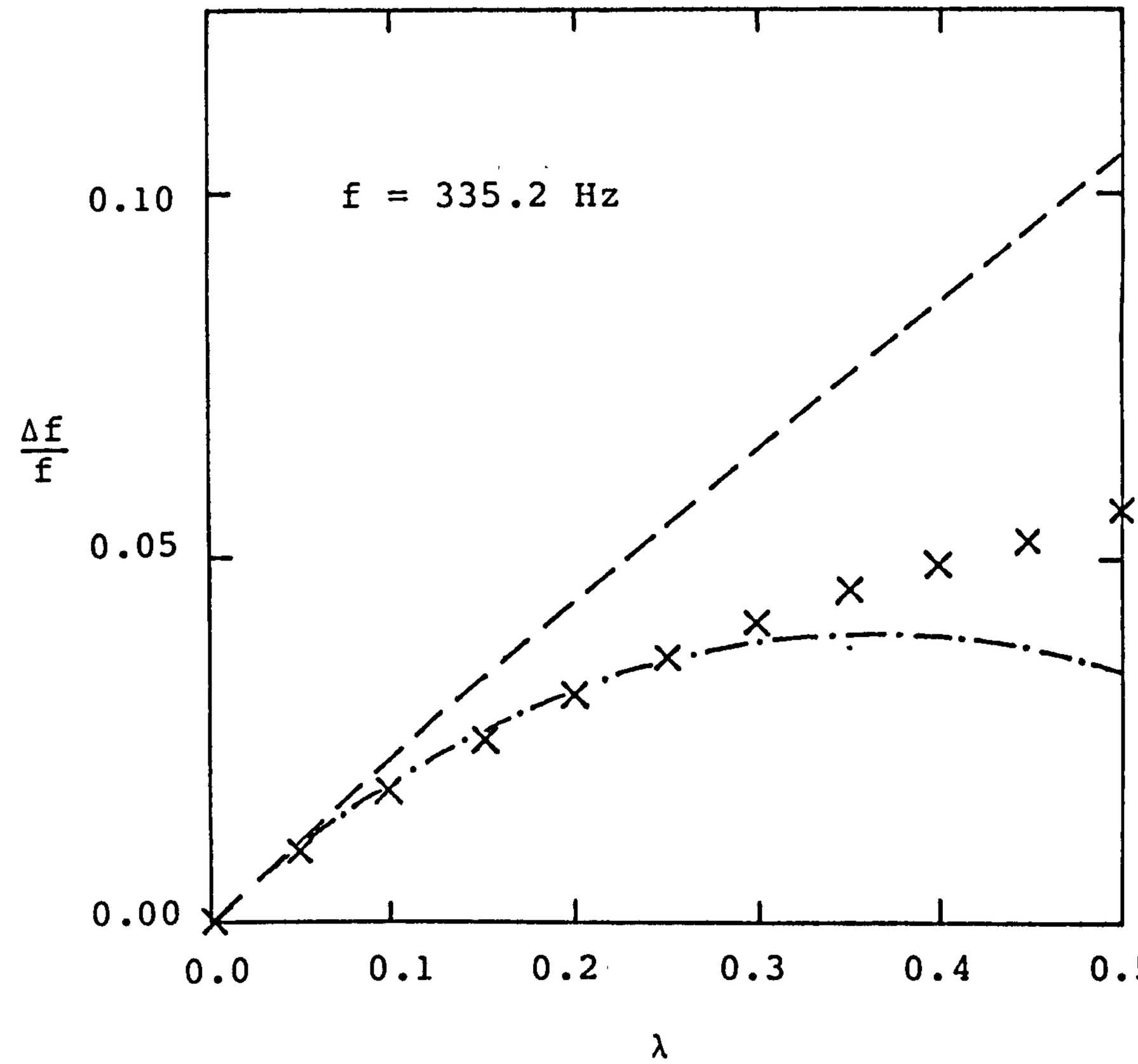


Fig. 5.5(e)

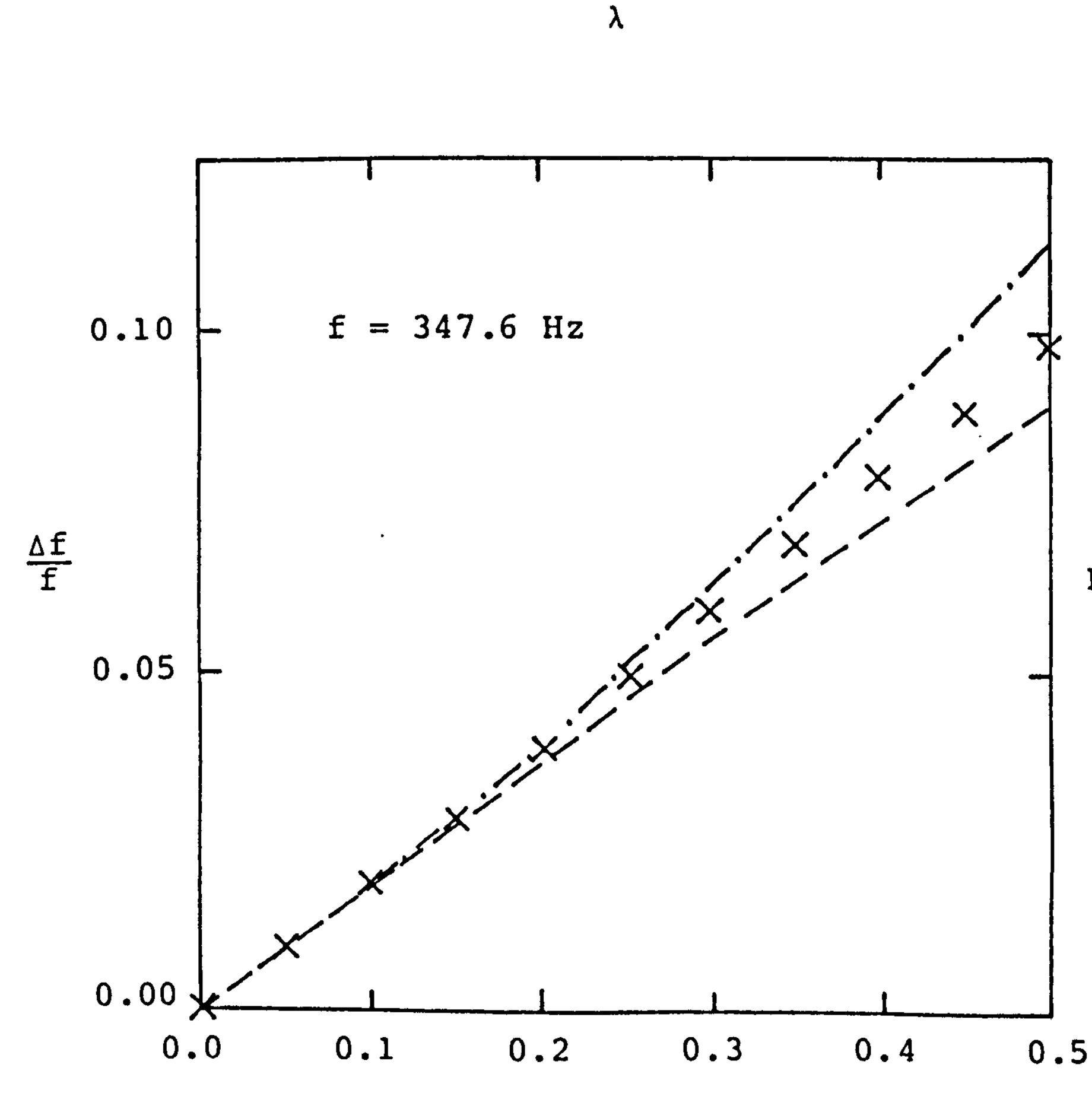


Fig. 5.5(f)

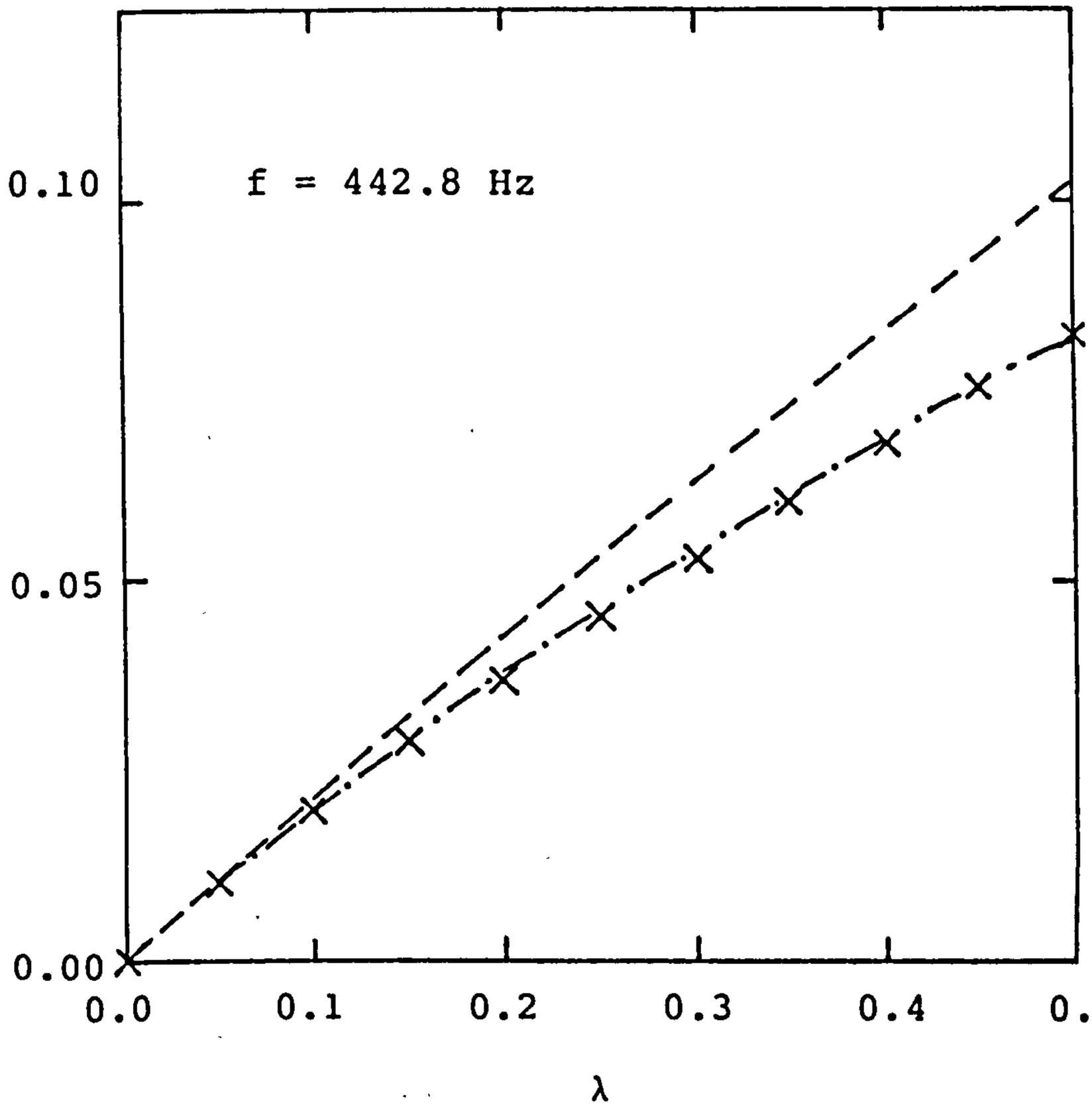


Fig. 5.5(g)

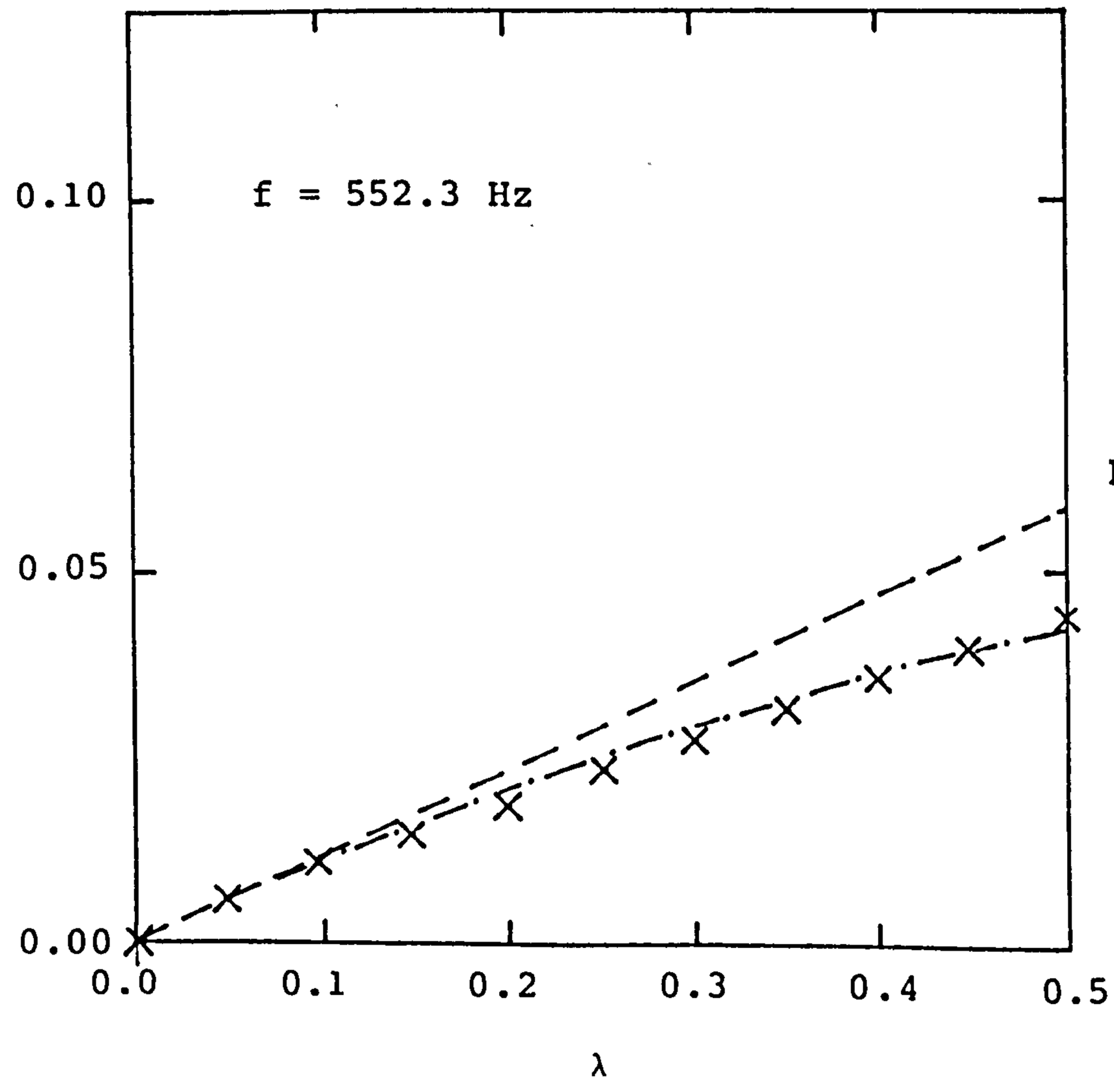


Fig. 5.5(h)

# 6 DISCUSSION

In Chapter 2 the acoustic response to structural vibration was expressed in terms of the undamped structural modes and the rigid-wall acoustic cavity modes. This approach is particularly fruitful when the frequency range of interest covers a few of the lowest resonances, as the contribution of the modes at appreciably higher frequencies is small and can be ignored. Examination of the expression obtained (equation 2.42) allows us to consider the possible means by which the acoustic response may be reduced.

Conventional methods include:-

(1) Increasing structural damping and acoustic absorption. This has the effect of reducing the resonant peaks, and can be implemented without detailed knowledge of the mode involved (although such information may assist the optimal positioning of the treatment used). Unfortunately the efficacy of materials in common use invariably falls at low frequencies where vehicle interior sound levels are particularly high.

(2) Reduction of the forces acting on the structure. This is typically achieved by improving the isolation at the mountings of the engine, transmission, suspension etc. Again no knowledge of the structural modes is necessary. Increased isolation may impair other qualities, for example the handling qualities of a vehicle.

(3) Altering the position of the exciting forces. This approach can be effective when one or more inputs are responsible for a particularly large response of a single structural mode. The exciting forces should be repositioned as closely as possible to nodes of the offending resonance, which presupposes reasonably detailed quantitative knowledge of the mode involved. The effect on other modes is uncertain, so such a modification cannot be

expected to give an improvement over a frequency range covering several resonances.

(4) Increasing the mass of the structure. Apart from changing the resonant frequencies, any increase in mass will result in normalised modes of reduced magnitude, which will reduce the acoustic response. However such an approach would be considered out of the question in modern car design, where weight reduction is a priority in the interests of performance and fuel economy.

The remaining option is to reduce the values of the coefficients Cij, which represent the coupling between structural and acoustic modes, and it is this possibility that has been examined in this work as an alternative to the more established methods of noise reduction. Any improvements that might result from such reductions will arise from changes in structural mode shape and frequency, and change to the shape of the cavity if considered.

The simple model of ring-mode excitation considered can be justified to some extent because of the two-dimensional nature of ring modes in practice, and the approximate prismatic shape of car passenger compartments. The only structural modifications made were change in element stiffness, the mass and damping being kept constant. This simplification means that any change in acoustic response is due entirely to changes in mode shape and frequency, which are the only factors affecting the coupling between structural and acoustic modes.

In order to avoid the expense of complete re-solution of the finite element equations to assess the effects of structural change, the modifications were treated as small perturbations of the stiffness matrix. In this way successively higher orders of approximation to the modes of the new structure may be found using the existing solution. The first order approximation is particularly simple in that the combined effect of several changes is additive. Furthermore the modified structural-

acoustic coupling can be obtained directly, without the need for intermediate recalculation of the structural eigenvectors, nor repetition of the boundary integrations over the surface of the acoustic cavity.

The derivatives of the structural-acoustic coupling coefficients with respect to the stiffness of each element were calculated and by inspection of these it was possible to establish a combination of stiffness increases which had the effect of reducing the largest values of coupling. While this approach is considerably more efficient than trial and error, there is much scope for more sophisticated methods. Perhaps the most general strategy would be to re-cast the problem as one of constrained optimisation - a method finding increased use in structural design (36) - as follows:-

(1) The aim would be the minimisation of an objective function consisting of a weighted sum of the squares of the coupling coefficients $C'_{ij}$. This weighting would reflect any overall trends with frequency in, for example, excitation levels, structural damping, acoustic absorption, and subjective human response.

(2) The optimisation parameters might include element stiffness and mass, and changes to the shape of the structure. in a realistic case these would be subject to constraints, for example a lower bound on the structural stiffness would be necessary to ensure adequate strength.

(3) The best method of solution will be influenced by some aspects peculiar to this particular problem. The calculation of the objective function from scratch represents by far the largest step in any such algorithm, entailing as it does a complete eigen solution, and the number of times this is necessary must be reduced as far as possible, especially for large and complex structures. On the other hand, derivatives of the objective

function can be subsequently obtained at very little expense using the methods outlined in the previous chapter, so maximum use of these is desirable. For instance, the first derivative of the objective function with respect to the optimisation parameters leads naturally to a steepest descent algorithm, although it would seem worthwhile to devise schemes making use of the second and higher derivatives.

The question remains as to whether the methods described here can be usefully applied to the vastly more complicated case of a real car body. An essential requirement is demonstrably accurate finite element analyses of structural and acoustic modes ultimately at frequencies up to 300 Hz. To achive this it will be necessary to take into account the fine detail of the construction. In the case of the acoustic cavity this would include the effects of trim and other absorbing materials, and the presence of objects inside the cavity - seats and even passengers. The structural problem appears even more complex; the density of modes is much greater than in the acoustic cavity, and the accurate modelling of damping, joints, and seams would undoubtedly require many more degrees of freedom. Clearly just to quantify these effects would require an exhaustive experimental programme, and a comparable numerical effort would be necessary to incorporate them in any predictive scheme.

Although this presents a formidable task, most major motor manufacturers have already embarked upon this route. In view of the increasing availability of more and more powerful computing machinery, there is every reason to believe that progress in this area will continue unabated into the foreseeable future.

# 7. CONCLUSIONS

1. Previous experimental work on car noise has studied the nature of the interior sound levels, and the mechanisms by which they are generated. The dominant components lie at frequencies below 300 Hz, and despite the reduced sensitivity of the human ear at low frequencies there is little evidence of significant noise contributions above this range.

For a given force input, the acoustic response inside the body structure depends on its resonances, both structural and acoustic, and the degree of structural damping and sound absorption. The low-frequency structural modes (25 - 40 Hz) consist of bending and torsional vibration of the body as a whole, while at higher frequencies (50 - 150 Hz) the so-called 'ring' mode vibration of the passenger compartment dominates. It has been suggested that these latter play a largepart in the noise generation process, and this is not surprising as the acoustic cavity resonances (about 90 and 150 Hz) also lie in this frequency range.

The response at resonance is limited by structural damping and acoustic absorption. A degree of both arises from the normal materials and methods of car manufacture, but additional treatments are usually added as a deliberate noise reduction measure. Unfortunately the effectiveness of such materials falls at low frequencies, precisely where sound levels are particularly high.

2. The sound field inside an enclosure was analysed theoretically in terms of the rigid-wall acoustic cavity modes. This approach is necessary because, in the case of a car passenger compartment, the wavelength of sound is comparable with the dimensions of the cavity. In this way it is possible to find the response due to vibration of the surrounding structure, and

to take into account the effect of acoustic absorption and internal objects.

By expressing the structural vibration also in terms of its resonant modes a general expression was obtained for the acoustic response to a given force input. From this it ispossible to identify a variety of factors which affect the response. Of these, the total mass, structural damping, acoustic absorption, the magnitude of the exciting forces and their distribution in relation to the structural modes represent the areas where traditional efforts at noise and vibration reduction have been made. What remains are a number of coefficients which represent the coupling between each structural and acoustic mode, the magnitudes of which depend on

(a) The shapes of the structural and acoustic modes,

and (b) The proximity of their resonant frequencies.

Since particuarly large values of this coefficient can be expected to give a correspondingly pronounced acoustic response, it is proposed that reduction of these by structural modification will have a beneficial effect more or less regardless of the nature of the exciting forces, which will anyway be extremely complex in any practical case.

The key to these methods is a detailed knowledge of the structural and acoustic modes, and since exact solutions will be unavailable for all but a few simple cases, a numerical approach is necessary. In particular, the finite element method has been used with some success for both the acoustic and structural problems.

3. A finite element computer program was written which calculated the acoustic modes of a two-dimensional cavity. The results for a rectangular and cylindrical cavity were compared

with the exact solutions and the agreement was good given a sufficiently fine mesh. The validity of any particular solution could be judged by the degree of discontinuity exhibited by the computed mode shape.

The performances of two types of element - the linear triangle and quadratic triangle - were compared. As expected, the higher order element give better results, yielding more accurate resonant frequencies in all but one case.

It was shown how the full three-dimensional solution for a prismatic cavity could be obtained simply from a single two-dimensional solution. A half-scale model of a car passenger compartment was analysed in this manner and the results gave excellent agreement with those obtained experimentally in a perspex model.

4. The ring modes of a car body are so named because of the resemblance they bear to those of simple two-dimensional ring structures. The resonant frequencies and modes of such a ring, made of steel and in the shape of a longitudinal section through a car passenger compartment, were determined experimentally. It was observed that the resonances occurred in pairs, the modes having the same number of standing waves about the periphery of the ring.

A theoretical analysis of this structure was performed using two-dimensional beam elements with distributed mass, and these results agreed well with experiment. The modes for circular and elliptical rings were also calculated, the former showing two-fold degeneracy at each resonant frequency. This degeneracy remained in the ellipses for odd-order modes, but the even-order resonances progressively split as the shape departed from that of a circle.

5. A simple theoretical model was devised in which the acoustic

response of a two-dimensinal cavity to the vibration of a surrounding ring was calculated according to the theory given in Chapter 2. The restriction to two-dimensions is justified because in practice ring-modes are themselves predominantly two-dimensional, and as such should not excite the three-dimensional acoustic modes of a near-prismatic cavity to any large extent.

The calculation of the surface integrals in the structural-acoustic coupling coefficients was approached using the concept of boundary elements. In this case the procedure was simplified by using structural beam elements which coincided with the exterior edges of the triangular acoustic elements. The integrations were carried out exactly using the Gauss quadrature scheme.

It proved virtually impossible to arrive at a beneficial combination of structural changes by trial and error even for this simple structure. However by expressing the modifications as a perturbation of the structural stiffness matrix it was possible to obtain a first-order approximation to the new solution, which could be used directly to calculate the change in structural-acoustic coupling. Using these results it was possible to find a combination of changes which had the effect of reducing the largest values of structural-acoustic coupling.

The modified acoustic response was considerably reduced at the most prominent resonances, and there was no significant increase elsewhere.

6. The application of these methods to the design of real vehicles presupposes the existence of large, sophisticated finite element programs capable of accurately computing structural and acousic resonances up to 300 Hz. Most major motor manufacturers are now actively involved in the development of such packages.

## REFERENCES


1. D. C. Apps, "Automobile Noise", Ch.31, Handbook of Noise Control, C. H. Harris, ed., McGraw-Hill, New York, 1957.

2. J. A. Raff and R. D. H. Perry, "A Review of Vehicle Noise Studies Carried out at the Institute of Sound and Vibration Research with Reference to some Recent Research on Petrol Engine Noise". Journal of Sound and Vibration 1973, 28 (3), 433-470.

3. S. K. Jha, "Characteristics and Sources of Noise and Vibration and their Control in Motor Cars". Journal of Sound and Vibration 1976, 47(4), 543-558.

4. L. L. Beranek, "Acoustics". McGraw-Hill, 1954.

5. M. E. Bryan, "A Tentative Criterion for Acceptable Noise Levels in Passenger Vehicles". Journal of Sound and Vibration 1976, 48(4), 525-535.

6. T. H. Hodgson, "Advances in Automobile Engineering Part III". G. H. Tidbury, ed., Pergamon, Oxford, 1965.

7. L. L. Beranek, "Acoustic Measurements", John Wiley & Sons, New York, 1949.

8. Handbook of Noise and Vibration Control, 3rd Ed., Trade and Technical Press.

9. M. J. Evans and W. Tempest, "Some Effects of Infrasonic Noise in Transportation". Journal of Sound and Vibration 1972, 22(1), 19-24.

10. P. M. Morse and K. U. Ingard, "Theoretical Acoustics". McGraw-Hill, New York, 1968.

11. G. Jennequin, "Is the Computation of Noise Level Inside a Car Feasible?"
1971 Proceedings of the Joint Symposium on Vibration and Noise in Motor Vehicles, London, July 1971, Paper No. C108/71, 132-137.

12. A. Craggs, "The Use of Simple Three-Dimensional Acoustic Finite Elements for Determining the Natural Modes and Frequencies of Complex Shaped Enclosures".
Journal of Sound and Vibration 1972, 23, 331-339.

13. T. Shuku and K. Ishihara, "The Analysis of the Acoustic Field in Irregularly Shaped Rooms by the Finite Element Method".
Journal of Sound and Vibration 1973, 29, 67-76.

14. M. Petyt, J. Lea, G. H. Koopman, "A Finite Element Method for Determining the Acoustic Modes of Irregular Shaped Cavities".
Journal of Sound and Vibration 1976, 45(4), 495-502.

15. J. A. Wolf, D. J. Nefske, L. J. Howell, "Structural-Acoustic Finite Element Analysis of the Automobile Passenger Compartment".
SAE Automotive Engineering Congress and Exposition, Detroit, Feb. 1976, Paper No. 760184.

16. J. A. Wolf, D. J. Nefske, L. J. Howell, "Automobile Interior Noise Reduction Using Finite Element Methods".
SAE Congress and Exposition, Detroit, Feb. 1978, Paper No. 780365.

17. T. L. Richards and S. K. Jha, "A Simplified Finite Element Method for Studying Acoustic Characteristics Inside a Car Cavity".
Journal of Sound and Vibration 1979, 63(1), 61-72.

18. S. K. Jha and N. Cheilas, "Acoustic Characteristics of a Car Cavity and Estimation of Interior Sound Field Produced by Vibrating Panel".
ASME, 1976, Paper No. 76-WA/DE-1.

19. C. W. Kosten, "Technical Aspects of Sound", Ch.4, Ed. E. G. Richardson, Elsevier, 1953.

20. L. L. Beranek, "Acoustic Impedance of Porous Materials", J.A.S.A. (1942), 13, 248-260.

21. P. M. Morse, R. H. Bolt, R. L. Brown, "Acoustic Impedance and Sound Absorption". J.A.S.A. (1940), 12, p.217.

22. E. A. G. Shaw, "The Acoustic Waveguide II" J.A.S.A. (1953), 25, 231-235.

23. M. E. Delaney, E. N. Bazley, "Acoustical Properties of Fibrous Absorbent Materials". Applied Acoustics, (1970), 3(2), 105-116.

24. R. H. Nichols, H. P. Sleeper, R. L. Wallace, H. L. Ericson, "Acoustical Materials and Acoustic Treatments for Aircraft", J.A.S.A. (1947), 19, 428-443.

25. H. P. Hsu, "Vector Analysis", Simon and Schuster, New York, 1969.

26. M. W. Zemansky, "Heat and Thermodynamics", McGraw-Hill Kogakusha, Tokyo, 1968.

27. W. T. Thomson, T. Calkins, P. Caravani, "A Numerical Study of Damping", Earthquake Engg. and Structural Dynamics (1974), 3, 97-103.

28. A. Craggs, "A Finite Element Model for Rigid Porous Absorbing Materials", Journal of Sound and Vibration (1978), 61(1), 101-111.

29. O. C. Zienkiewicz, "The Finite Element Method", McGraw-Hill, London, 1977.

30. G.H. Koopman and H.F. Pollard, "A Joint Acceptance Function for Structural-Acoustic Coupling Problems", Journal of Sound and Vibration, (1976), 46(2), 302-305.

31. L.B. Kinsler and A.R. Frey, "Fundamentals of Acoustics". John Wiley and Sons, New York, 1962.

32. N. Cheilas, "Sound Field Inside a Car Cavity Produced by Vibrating Panels" M.Sc. Thesis, School of Automotive Studies. Cranfield Institute of Technology, 1974.

33. O.C. Zienkiewicz, "The Finite Element Method in Engineering Science", McGraw-Hill, London, 1971.

34. M. Abramowitz and I.A. Stegun, "Handbook of Mathematical Functions", Dover Publications, New York, 1968.

35. R.K. Livesley, "Matrix Methods in Structural Analysis", Pergamon Press, 1975.

36. R.H. Gallagher and O.C. Zienkiewicz, "Optimum Structural Design", John Wiley, London, 1973.

37. D.J. Nefske, J.A. Wolf and L.J. Howell, "Structural-Acoustic Finite Element Analysis of the Automobile Passenger Compartment : A Review of Current Practice", Journal of Sound and Vibration, 1982, 80(2).

38. G.H. Koopman and H.F. Pollard, "A Joint Acceptance Function for Enclosed Spaces", Journal of Sound and Vibration, 1980, 73(3).

39. J.A. Wolf, "Modal Synthesis for Combined Structural-Acoustic Systems", AIAA Journal, 1977, 15(5).

40. E.H. Dowell, G.F. Gorman and D.A. Smith, "Acousto-elasticity : General Theory, Acoustic Natural Modes and Forced Response to Sinusoidal Excitation, Including Comparisons with Experiment", Journal of Sound and Vibration, 1977, 52(4).

41. A. Craggs and G. Stead, "Sound Transmission between Enclosures - A Study Using Plate and Acoustic Finite Elements", Acustica, 1976, 35(2).

42. G.J. McRae, "Finite Element Solutions of the Wave Equation", Noise, Shock and Vibration Conference, 1974, Melbourne.

43. R.N. Arnold and G.B. Warburton, "Flexural vibrations of the walls of thin cylindrical shells having freely supported ends", Proceedings of the Royal Society (A), 1949, 197.

44. D.L. Thomas, "Dynamics of Rotationally Periodic Structures", Int.J. for Numerical Methods in Engineering, 1979, 14.